THE MEASUREMENT OF LIQUID HEIGHT IN FLOTATION CELLS USING MICROWAVE TECHNIQUES

by

MICHAEL RAYMOND ARCHER.

Submitted to the UNIVERSITY of CAPE TOWN in fulfilment of the requirements for the Degree of MASTER of SCIENCE in ENGINEERING.

SEPTEMBER,1980.

SUMMARY

The flotation process is used in extractive metallurgy to concentrate the mineral contents of ores by 'floating' the mineral particles out of an ore pulp with air bubbles. The pulp consists of finely ground ore, water and reagents, whose purpose is to make the mineral particles attach themselves to the air bubbles passing through the liquid. These bubbles reach the surface of the pulp and form a layer of froth, containing the ore concentrate, which is skimmed off for further processing.

In order to optimise the process, it is necessary to have a reliable method of monitoring liquid level in the flotation cell. The presence of the flotation froth complicates this measurement as it obscures the surface from visual observation and clogs conventional mechanical level measurement systems. The presence of air bubbles in the pulp and foam, makes acoustic systems equally unsuitable due to attenuation effects [101,102].

The absence of a microwave system for level measurement in flotation cells led to the proposal of this thesis. It is therefore concerned with investigating the feasibility of using a microwave level measurement system for automatic liquid level control in flotation cells (figure 5.13).

The hostile industrial environment dictates that the final level measuring instrument be robust and of a design requiring a minimum of maintenance. The need for a great number of these units (an average mineral processing plant contains hundreds of flotation cells) means that they should be cheap to produce, using locally obtainable components. A resolution of 10 mm was regarded as being sufficient.

It is well known that a system's response time and resolution are related. The longer the time taken for a measurement, the more accurate the measurement will be. A compromise between resolution (10 mm is regarded as being adequate) and response time will have to be found for the flotation cell level control system.

This is not regarded as being too big a problem as the response time of the liquid level control mechanisms in the cell are slow in comparison to that of any electrical level-measuring system.

A survey and discussion of the various microwave level measurement systems available was carried out. Considerations of complexity (i.e. cost) and resolution led to the proposal of two systems for the liquid level measurement.

They were:

1. A multiple frequency continuous wave (MFCW) system using a carrier frequency of 9,9 GHz and a modulation frequency of 100 MHz.
2. A baseband pulse Time Domain Reflectometry (TDR) system utilizing pulses of less than 1 nS.

Experiments with froth revealed that 10 GHz radiation experienced very high attenuation ($\approx$ 400 dB/m) on passing through it. Further experiments demonstrated that this was not due to scattering or reflection of the incident radiation in the froth. The observed attenuation is far higher than is theoretically explainable using the observed froth conductivities measured at 1 kc/s. A possible cause of this high attenuation is thought to be some loss mechanism that only manifests itself at high frequencies and is therefore not detected by the low frequency conductivity measurement.

Baseband pulses are attenuated to a far lesser degree (2.5 dB/m) in the froth and this is thought to be as a result of the relatively lower frequency components in the pulse spectrum as compared to the 10 GHz radiation.

The low attenuation of baseband pulses in the froth and the fact that this attenuation effect could be compensated for, led to the adoption of Time Domain Reflectometry (TDR) techniques for the measurement system.

The theory and applications of Time Domain Reflectometry (TDR) are fully covered, special attention being given to the definition of pulse parameters and the behaviour of pulses on transmission lines. This is important, as in the case of pulses of less than 1nS duration, it is no longer possible to regard coaxial cable as a perfect transmission line.

Using the principles described above, a basic TDR system utilizing a guided-wave transmission line to minimise unwanted reflections and attenuation, is proposed. Theoretical expressions for system resolution are derived and the two detector comparison method of attenuation compensation is described in detail. The design and practical realisation of the component parts is covered and tests on the completed instrument show that the resolution criterion of 10 mm is satisfied.

Information about the use of TDR for the identification of material properties (Time Domain Spectroscopy) is given and use of the level measuring instrument for this type of work is discussed as a future development.

ACKNOWLEDGEMENTS

The author wishes to thank the following:

PROFESSOR J.L.N. BESSELING, of UCT, the thesis supervisor, for his help and guidance.

DR D.E.H. NAUDE, the NIM Research Group Leader, for his helpful suggestions and support.

The NATIONAL INSTITUTE FOR METALLURGY for their financial support in the form of a bursary and the financing of the necessary research equipment.

The staff of the DEPARTMENT OF ELECTRICAL ENGINEERING, at the UNIVERSITY OF CAPE TOWN, for making my stay there pleasant and enjoyable.

Mrs C.M. Heyns and Mrs M. Arinto for their assistance with the typing.

Mrs E. Reiser for her help with the drawings.

TERMINOLOGY

In order to facilitate the readibility of this text, a number of terms are referenced below.

"fast" pulses - pulses with fast rise and fall times (in the region of 500pS in most cases mentioned here).

Baseband pulses- carrierless pulses usually of very short duration and producing spectral components of a very high frequency.

FFT - Fast Fourier Transform

FMCW - Frequency Modulated Continuous Wave

GHz - 10^9 Hertz

HISS - Holographic Ice Survey System

MFCW - Multiple Frequency Continuous Wave

nS - 10^{-9} second

pS - 10^{-12} second

SAR - Synthetic Aperture Radar

TDR - Time Domain Reflectometry

TDS - Time Domain Spectroscopy

TWT - Travelling Wave Tube

X Band - 8 to 12 GHz

ε - permittivity (F/m)

k - dielectric constant

ρ - reflection coefficient

σ - specific conductivity (mhos/m)

μ - permeability (H/m)

Λ - equivalent conductance (mho cm^2/eq)

I N D E X

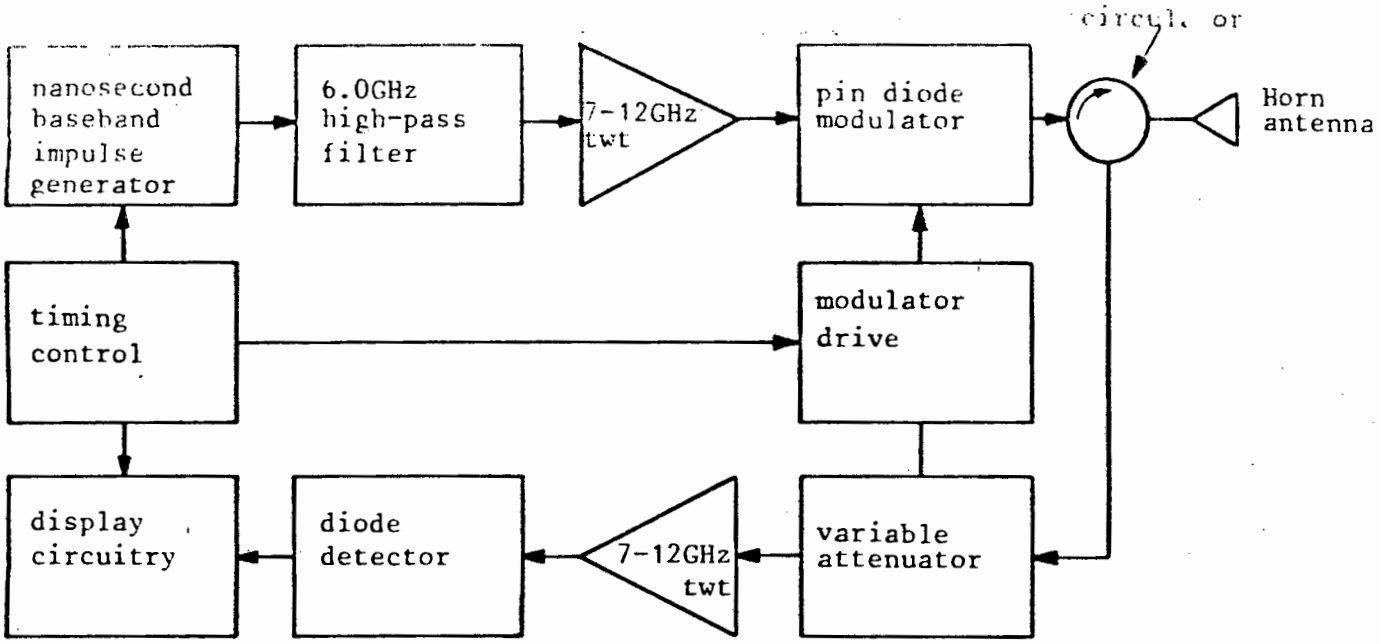

FIGURE 1.4 THE BASIC BLOCK DIAGRAM FOR AN X-BAND IMPULSE RADAR

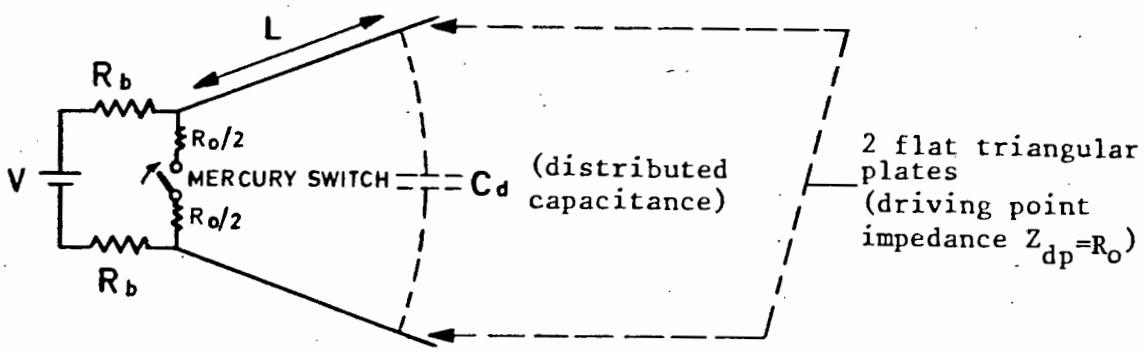

FIGURE 1.5(a) THE COMPOSITE HORN ANTENNA AND TRANSMITTER

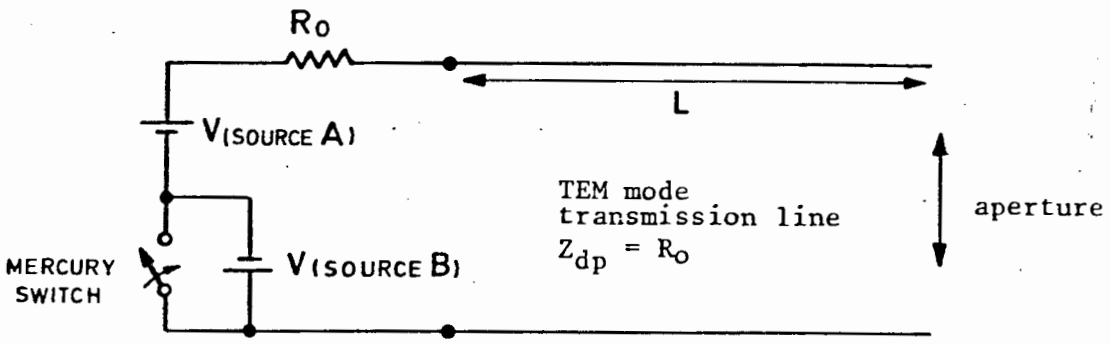

FIGURE 1.5(b) THE EQUIVALENT CIRCUIT OF THE HORN AND TRANSMITTER

1.2.1 Holographic/Imaging

Initially, the imaging method of level detection was regarded as being very promising as it related directly to the problem at hand. Furthermore, experimental verification of the feasibility of this method could easily be carried out as a similar system working on this principle had already been built as part of a research project at UCT.

The resolution of a holographic imaging system is determined primarily by the size of the sampling array of antennae and not by the bandwidth of the system. Ogura *et al*[16] obtained results with resolutions of many centimetres using an 8 m receive/transmit array, consisting of 32 transmit and 32 receive elements (Figure (1.2)). Theoretically, better results would be expected and the authors regard this as being caused by quantization errors in the instrument. The complexity and cost of this particular system at once made it impractical for the application in mind.

An experiment[44] using a monofrequency source of 9,9 Ghz and an aperture of 300 mm. (Figure (1.3)) was carried out to investigate the depth resolution of a simpler version of this system. The scattered field from a cooperative target was sampled across the antenna aperture and this data used to compute image positions for various antenna focal lengths. A complete copy of the original article describing this experiment is enclosed in Appendix B.

From the results of the experiment it was concluded that high depth resolution is not an intrinsic property of microwave imaging systems.

This conclusion along with its cost and the fact that such a system would be susceptible to interference from the stirrer and nearby objects led to its being shelved as a method of level measurement.

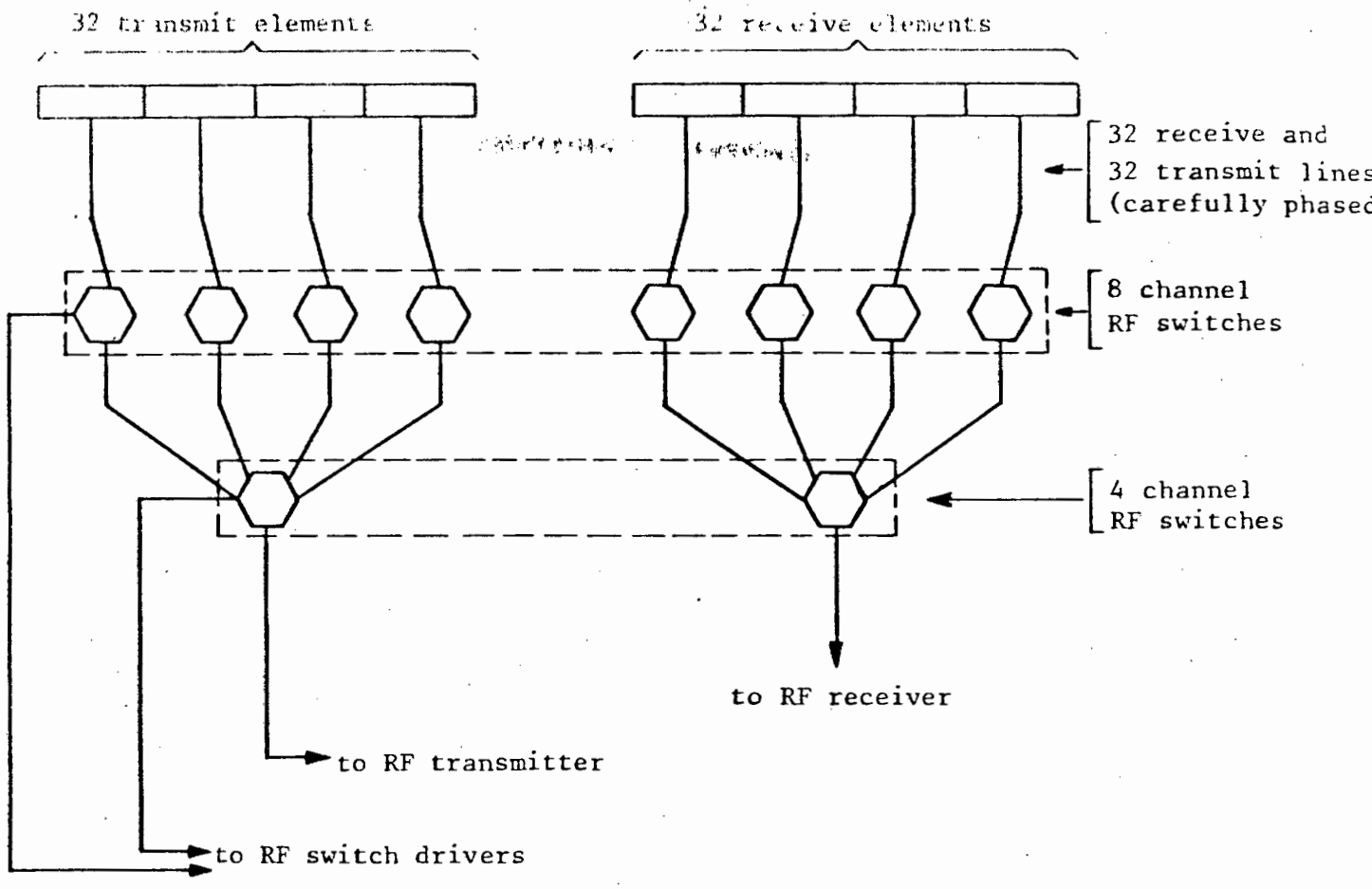

FIGURE 1.2

DEMONSTRATES THE COMPLEXITY OF THE RF SWITCHING IN A HOLOGRAPHIC/IMAGING SYSTEM FOR LEVEL MEASUREMENT

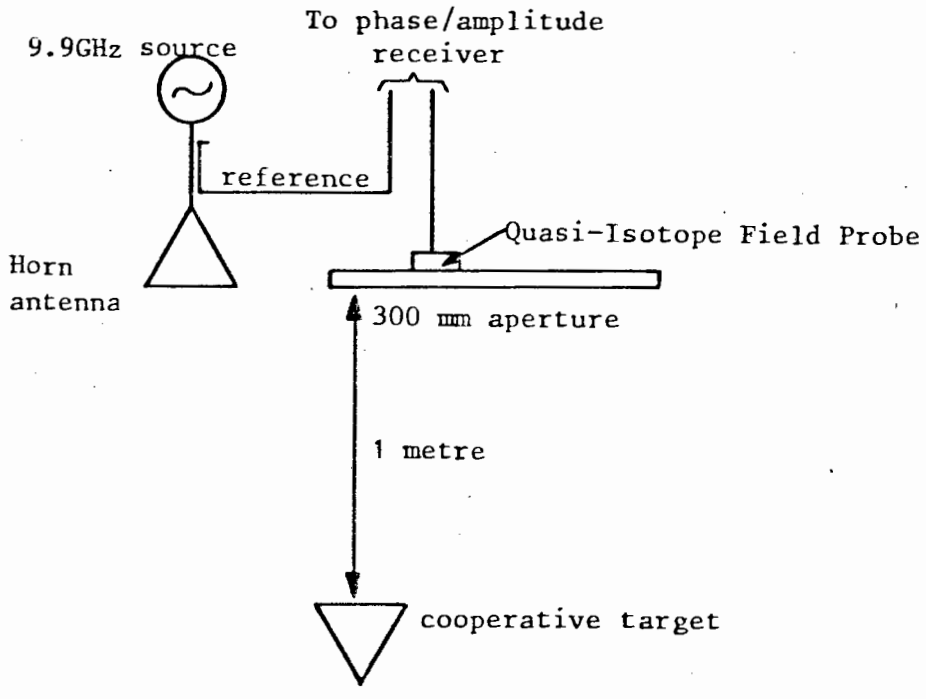

FIGURE 1.3 THE EXPERIMENTAL SETUP FOR THE INVESTIGATION OF DEPTH RESOLUTION IN AN IMAGING SYSTEM

the necessary technical and theoretical information for the construction of such a system is contained in his paper. A resolution of better than two inches in thirty miles is claimed.

Stuchley, Hamid and Andrews[42] apply the MFCW technique to the monitoring and controlling of surface levels in tanks and reservoirs. A waveguide projecting into the liquid is used as a sensing element for liquids in reservoirs while a horn antenna is used for the sensing of solid levels in tanks.

Wantenaar, Bacon and Goodhead[43] describe the use of Lecher wires to guide microwaves through regions whose dielectric properties are to be measured. This technique lends itself to the confinement of microwaves for interferometric measurement purposes as well.

1.2 A Discussion of the Proposed Systems in the Light of System Requirements

Before continuing it is necessary to define the requirements of the liquid level measuring instrument. They are:

(a) A resolution of 10 mm at a distance of two metres. Higher accuracy is unnecessary as the surface of the flotation liquid is in continuous agitation.

(b) Immunity to external disturbances such as the movement of the flotation cell stirrer and people moving nearby.

(c) Cheap to produce and maintain, using locally obtainable components. This requirement is necessary because of the great numbers of these instruments needed.

(d) Robust construction to survive in a hostile industrial environment.

The use of wire-guided transients for remote sensing is first mentioned by Danielson and Gardner[35] in 1966. They used a slotted air-dielectric coaxial line as a TDR probe for determining the thickness of various liquid layers. Gerharz[36] uses TDR in conjunction with open (unshielded) transmission lines laid alongside a road as a sensor wire to determine the position of traffic on the road. Ross and Bennett[32] mention the use of a similar but more complex system as a basis for a ground collision avoidance system at airports.

In the same article the use of a guided-wave reflectometry system for the measurement of liquid level is also described. The relative simplicity of this system when compared with the hologram matrix radar of the previous section, makes it extremely attractive.

1.1.3 Modulated Continuous Wave (CW) systems

Altimeters were the earliest and most successful form of frequency modulated continuous wave (FMCW) devices used for distance measurement. With a few exceptions most modern altimeters use wide deviation FM at low modulation frequencies with various sweep rates as a basis for operation.

Their theory and operation is fully discussed by Skolnik[37,38]. Their adaptation to shorter range work for vehicle anticollision systems is described by Zur Heiden/Oehlen[39], while their adaptation for very short range work is described by Clarricoats[40].

Wadley[41] proposed the use of a multiple frequency continuous wave (MFCW) technique to eliminate distance ambiguities in his Tellurometer. The basic idea of MFCW is that the fundamental frequency(f_1) provides the basic accuracy for distance measurement while a set of frequencies (f_2, f_3, f_4, etc.) permit the resolution of ambiguities. If more frequencies are employed, the spectrum and distance resolution approach that obtained with pulse or FMCW radar. All

This information is processed using a microcomputer implementing a Fast Fourier Transform (FFT) Algorithm[17,18,19,20] to give information about the target. The essence of the data processing is the dual focusing of the transmitter and receiver at the same location. Moving the focus downwards produces a maximum scattering intensity when an object such as the ice layer surface or bottom is encountered.

Further development on the data processing side[21] in 1977 provided a significant expansion in the radar's dynamic range, allowing the bottom of lossy ice to be detected more easily.

1.1.2 Baseband Pulse/Time Domain Reflectormetry (TDR) systems

Baseband (carrierless) pulse techniques provide an alternative solution to the measurement of target distance. The literature contains a number of applications including automobile pre-collision sensing[22,23], geophysical prospecting[24,25] and the measurement of ice thickness[26].

Time-domain techniques have been in use for more than a decade to characterise networks, materials, antennae and radar targets.

The principle involves the use of subnanosecond pulses to excite the transient (i.e. impulse) response of networks and materials. Processing of the resultant waveform provides information about the frequency response of such networks and the dielectric constants of materials over a wide frequency range.

Further details of this investigative technique, called time-domain spectroscopy, are given by Fellner-Feldegg[27,28], Nicolson and Ross[29], Cole[30] and Suggett[31].

The basic theory and applications of time domain methods are well covered by Ross and Bennett[32], while Tektronix[33,34], describe the more practical aspects of time domain reflectometry measurements.

Synthetic Aperture Radar (SAR) utilises quasi-microwave holography to form one dimensional holograms from satellite or aircraft records. Tomiyasu[4], Brooks[5], Ellis[6] and Skolnik[7] all describe applications of this technique.

In the case under consideration, it is only necessary to be concerned with true-microwave holography. De Velis and Reynolds[8] provide the necessary theoretical background for understanding the physics of holography, while Tricoles/Farhat[9] and Anderson[10] between them describe the theoretical considerations and applications of microwave holography in particular.

As far back as 1967 Deschamps[11] proposed a number of systems for recording holograms formed using radiowaves. In 1973 Ogura/Iizuka[12] defined the hologram matrix and used computer simulation to apply it to a microwave holographic radar. The development and testing of this radar is later described in 1974[13]. Although errors of between 9 and 30 per cent are reported for the hologram matrix radar, the authors still claim that it can provide better performance in the short range than conventional radars with large bandwidths or very narrow pulses. Ogura/Fukuoka[14] carried out a further computer simulation in 1976, applying the hologram matrix to the imaging of a two dimensional target using two orthogonal antenna arrays, while Nilsen/Swingler[15] used a (10 x 10) orthogonal array of helical antennae to produce a hologram of a point scatterer and demonstrated the feasibility of this method for collecting holographic information.

The culmination of the work by Ogura *et al*[16] is the incorporation of the hologram matrix radar in a Holographic Ice Surveying System (HISS) for the mapping of ice thickness profiles. The system utilizes two antenna arrays, one for transmit and one for receive. Holographic information is obtained by scanning the illuminating source, as well as the receiver, in order to acquire information about the target with every geometric configuration of source, receiver and target (Figure (1.1)).

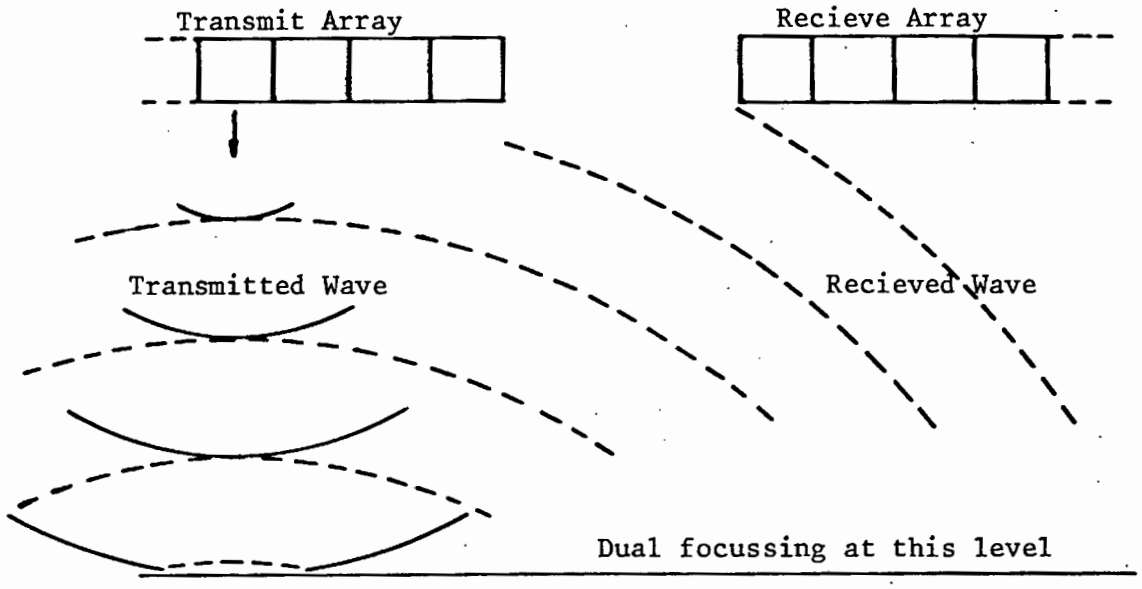

FIGURE 1.1 A HOLOGRAPHIC SYSTEM FOR DEPTH MEASUREMENT.

1. MICROWAVE SYSTEMS FOR LEVEL MEASUREMENTS

1.1 A Survey of Proposed Microwave Level-Measuring Systems

Investigation of the literature available shows that microwave distance/level measuring systems can be divided into three broad categories according to their principle of operation.

They are:

(a) Holographic/Imaging systems,

(b) Baseband Pulse/Time Domain Reflectometry (TDR) systems (including Pulse Compression systems), and

(c) Modulated Continuous Wave (CW) systems.

The last of these includes the classic pulsed carrier systems normally associated with radar.

1.1.1 Holographic or Imaging systems

During the past ten years microwave holography has been developed as an extension of optical and acoustic holography[1,2]. Unlike conventional measuring systems it determines distance by observation of the spatial distribution of the scattered wave rather than by the lapse of time and presents a means of remote imaging with unique properties.

Leith[3] defines true and quasi-microwave holography. Quasi-microwave holography utilises pulsed radiation to measure range and doppler records to measure azimuth while true holography uses measurements over a two-dimensional area to obtain holographic information. Also, in true-holography coordinates are two orthogonal distances both orthogonal to radial distance, while in quasi-holography one of the coordinates is range.

O B J E C T I V E S

To summarise then, the aim of this thesis is:

1. To conduct a survey to determine what methods of level measurement are available;

2. To carry out experiments to determine which method of level measurement is most practical for use in a flotation cell;

3. To produce a cheap, robust instrument, using this measurement technique, with the following specifications:

   Resolution:

   10 mm

   Response time:

   to be fast enough to control the level in the flotation cell effectively. As a first approximation, it was decided that it should take 20 seconds to reach 90 per cent of the final value after a step input;

4. To test the final system and see how its performance measures up to the design criteria above.

An instrument that gives information about froth characteristics as well as liquid level would help a great deal in this respect, and this consideration was also regarded as being important in the choice of the final technique used.

Further,more detailed information about the flotation process and the construction of flotation cells appears in Appendix A.

I N T R O D U C T I O N

Froth flotation is a method of concentrating finely ground ores and is one of the most widely used processes in extractive metallurgy today. Nearly all the world's supplies of copper, lead, zinc, platinum and lesser proportions of nickel, molybdenum, chromium, tungsten and titanium are obtained using froth flotation at some stage.

The process involves chemical treatment of an ore pulp to create conditions favourable for the attachment of certain mineral particles to air bubbles. These air bubbles carry selected minerals to the surface of the pulp (water and crushed ore mixture) to form a stabilised froth which is skimmed off. The other unwanted minerals and rock remain submerged in the pulp.

The height of the liquid in the tank determines the thickness of the froth layer that can form and this in turn affects the efficiency of the extractive process. A reliable method of liquid level control was therefore sought.

Experience has shown that conventional mechanical systems for level measurement are unsuitable. These problems led to an investigation into the feasibility of using a microwave-based system for level measurement and control in a flotation cell. The aim of this thesis was to investigate what microwave measurement systems are available for liquid level measurement and to decide, by experiment, if necessary, which of them is most suited to carrying out the measurement in the flotation cell. Ultimately, a working prototype was to be constructed and tested, the aim being to produce an instrument that is cheap and robust, with a resolution of 10 mm.

As the flotation process has been developed mainly by empirical methods, scientists are still trying to explain why it works so well. The stage has now been reached where any further substantial improvement in the process will demand a more profound understanding of the fundamentals involved.

1.2.2 Time Domain reflectometry (TDR)

In TDR systems, resolution is dependent on pulse risetime, which is the same as saying that it is dependent on system bandwidth.

Very promising results (resolution <10mm) are reported by Chudobaik *et al*[26] for an X-band impulse radar. This instrument is far less complex (Figure (1.4)) than the hologram matrix radar previously discussed but unfortunately uses expensive microwave components (i.e. 2 travelling-wave tubes) which are not easily obtainable locally.

An alternative baseband pulse system using a minimum of microwave hardware is described by Ross[23]. This simplification is made possible by the integration of the transmitter and transmitting antenna using distributed network theory (Figure (1.5)).

The interesting properties claimed for this system are:

(a) Good resolution (<<1 foot).

(b) Low cost (<R100) because of the use of available components.

(c) Low average radiated power, as the available power is spread over a wide frequency range, producing virtually no electromagnetic pollution.

(d) Gating to remove extraneous reflections.

The use of pulse lengths of less than a nanosecond presented special constructional (e.g. Wideband antennae) and processing (e.g. pulse detection) problems but the promise of this system warranted further investigation.

1.2.3 Continuous Wave (CW)

In an FMCW system the theoretical accuracy with which distance can be measured depends on the swept frequency bandwidth of the transmitted signal. In addition, measurement accuracy is affected by practical considera-

CARRIER FREQUENCY = 8.75 GH3	
MODULATION FREQUENCY (MH_2)	RESOLUTION(mm)
30	$\pm$ 27.6
100	$\pm$ 8.77
200	$\pm$ 4.13

FIGURE 1.6 RESOLUTION VERSUS MODULATION FREQUENCY IN A MFCW SYSTEM.

tions such as the accuracy of the frequency measuring device, errors caused by multiple reflections and transmitter leakage, and the frequency error due to the turn around of the frequency modulation.

The discreteness of the frequency measurement gives rise to an error called the fixed or step error. This quantization error limits the resolution of the system to a finite value given by ($\delta R = 76{,}3/\Delta f(MH_z)$) where Δf is the frequency deviation in megacycles and R is the resolution in metres. A frequency deviation of 2 Ghz would only give a resolution of about 4 cm which is in good agreement with the results of Clarricoats[40] who uses a swept frequency bandwidth covering 2-4 Ghz.

In order to obtain the required resolution of 10 mm it would be necessary to use a swept frequency bandwidth Δf of almost 8 Ghz. This is obviously impractical.

The alternative is to use a MFCW system as described by Wadley[41] and Stuchley *et al*[42]. As previously stated, the fundamental frequency (f_1), provides the basic distance accuracy while a further frequency or frequencies is/are used to modulate f_1, for the resolution of ambiguities.

Experimental results are given[42] for a carrier frequency of 8.75 Ghz and modulation frequencies of 30, 100 and 300 Mhz. The results (Figure (1.6)) clearly show how the measurement error decreases with increasing modulation frequency. A modulation frequency of 100 Mhz is necessary for a resolution less than 10 mm.

The use of heterodyne methods greatly simplifies phase measurement of the distance measuring pattern frequencies. This allows all amplifier, display and relaying circuits to operate at a lower comparison frequency while carrying the phase information derived from the higher frequency measuring waves.

This in turn allows the use of readily obtainable components for the major part of the instrument thus keeping construction and maintenance costs down.

1.2.4 To summarise

A number of microwave level-measuring systems have been evaluated in the light of the stated design criteria.

Two systems offering similar resolutions (10 mm) but operating on different principles are proposed:

(a) A multiple frequency continuous wave system using a carrier frequency of 9,9 Ghz and a modulation frequency of 100 Mhz.

(b) A baseband pulse system utilizing pulses of about 1nS.

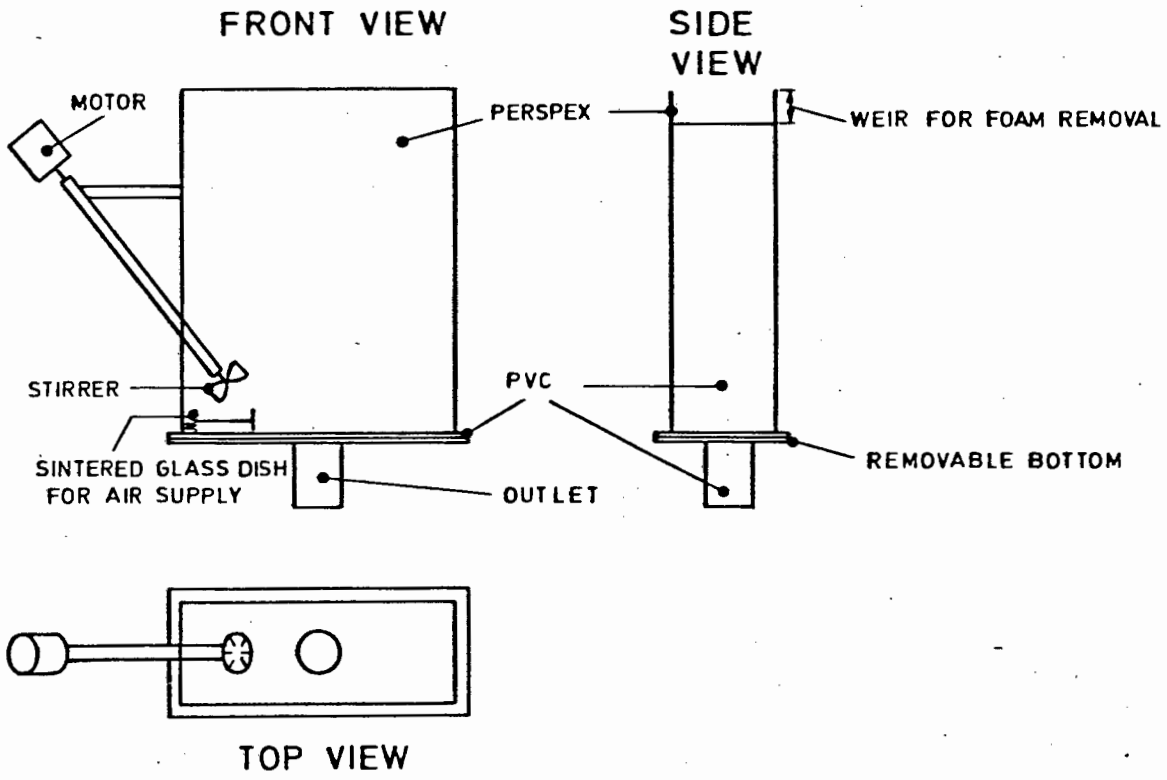

FIGURE 2.1 EXPERIMENTAL FLOTATION CELL CONSTRUCTION.

2. INVESTIGATION OF FROTH PROPERTIES

Examination of the available literature brought little information about the electrical properties (dielectric constant, conductivity and attenuation) of froth and foams, to light. This necessitated an investigation of these properties.

2.1 Experimental Apparatus, Instrumentation and Techniques

2.1.1 The Experimental Flotation Cell

The design criteria for the cell were that it should allow easy observation of, and access to the froth.

The general constructional details of the flotation cell are illustrated in (Figure (2.1)). To allow observation of the froth and pulp, 6 mm clear Perspex was used for the sides, while 6 mm PVC was used for the remainder of the cell. A pipe in the bottom facilitated emptying.

In order to ensure a good pulp/air mixture, a motor driven stirrer was installed above the sintered glass dish used to supply air to the pulp. A special stand for the cell was constructed out of Dexion angle iron sections.

2.1.2 Microwave Hardware

The energy source used for microwave measurements on the flotation froth was a Gunn diode X-band device with varactor diode tuning. The bias on the varactor was adjusted to give an operating frequency in the region of 9.9 GHz. This was chosen to be the same as the operating frequency of the MFCW system proposed in Section 1.2.4.

Other passive microwave hardware used in measurement systems for the investigation of the froth include isolators, directional couplers, power dividers, etc.

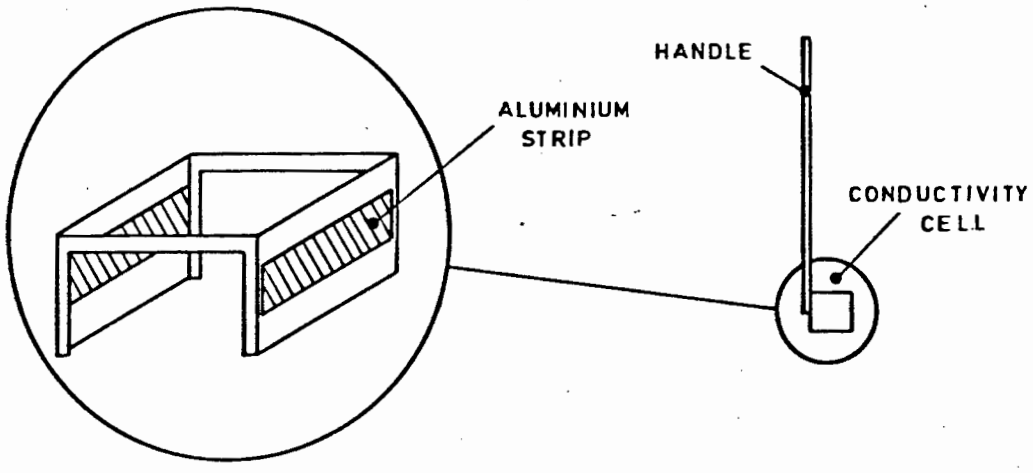

FIGURE 2.2 CONDUCTIVITY CELL CONSTRUCTION.

2.1.3 The Measurement of Microwave Power

An 8555A Hewlett Packard Spectrum Analyser was used for microwave power measurement. It is well suited to the task as it has absolute amplitude calibration from 10 dBm to -125 dBm over a 10 MHz to 18 GHz frequency range.

2.1.4 Fast rise-time short-pulse generation

In order to carry out TDR experiments on the froth it was necessary to provide a source of very short pulses with fast rise-times.

The design of a suitable unit using avalanche transistors and with 500 pS rise- and fall-times is described in Section (5.8).

2.1.5 Fast-Pulse Measurement and Display

A Tektronix 7000-Series Sampling Oscilloscope System was used to display the fast pulses used in the TDR experiments. The oscilloscope builds a composite picture of an individual pulse by sampling each identical pulse in a repetitive pulse train and displaying these samples on an expanded time scale.

Using an S-4 Sampling Head, with a 25 pS rise-time and an Equivalent Bandwidth of DC to 14 Ghz, it was possible to measure pulse risetimes of the order of 500 pS with an accuracy better than 0,5 per cent.

2.1.6 The Measurement of Conductivity

The conductivity of the froth and pulp was measured using a conductivity cell with parallel plates (Figure (2.2)). The electrolytic nature of the froth and pulp made it necessary to use an AC measurement voltage to avoid polarisation effects. It was found that using a frequency of 1 kc/s minimized these effects sufficiently for accurate measurements to be taken.

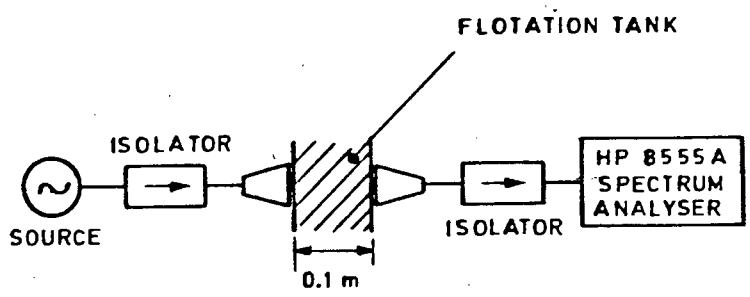

FIGURE 2.3 ATTENUATION MEASUREMENT APPARATUS

Further design information and a calibration test appear in Appendix (C).

2.1.7 The Measurement of Attenuation

The 8555A Spectrum Analyser was used to monitor the power transmission through the flotation cell with it both full of froth and empty. The power loss in the foam was found by subtracting the power transmitted with the cell full from the power transmitted with the cell empty. The attenuation per meter was found by multiplying this figure by ten (as the cell is 100 mm wide (Figure (2.3)).

2.1.8 The Measurement of Dielectric Constant

There are a number of ways normally used for the determination of dielectric constant of a material at microwave frequencies. They are:

(a) Cavity Resonance[45,46]

(b) Brewster Angle Measurement[47],

(c) Phase Variation Measurement[48,49,50], and

(d) Time Domain Techniques[27,29,30].

The fact that the froth does not support itself and must be continuously generated to prevent its dielectric properties from changing,renders a number of the above methods impractical.

(a) Cavity Resonance

This method uses a cavity of known resonant frequency. The material to be tested is placed in the cavity and its new resonant frequency measured. The materials' dielectric constant is calculated from the change in frequency caused by it.

Providing a continuous flow of foam through the cavity causes changes in the resonant frequency for geometric as well as dielectric reasons.

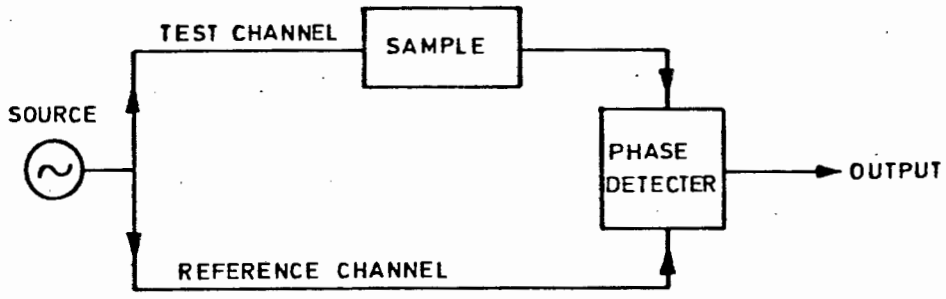

FIGURE 2.4 DIELECTRIC CONSTANT MEASUREMENT USING PHASE VARIATION.

Furthermore, any hole in the cavity wall with material flowing through it would couple energy out of the cavity and would cause erratic frequency fluctuations.

(b) Brewster Angle Measurement

The determination of the necessary formulae relating electromagnetic fields reflected from, and transmitted through a dielectric, are dealt with by Jordan/Balmain[51] and Lorrain/Corson[52]. From such analyses it may be shown that an angle θ_β (The Brewster Angle) can be found for which the reflected wave from the interface between two dielectrics is a minimum. By determining the angle that effects minimum reflection, it is possible to calculate dielectric constant for a low loss medium.

It was found, unfortunately, that flotation froth is a high-loss medium and that very little radiation is reflected from it at 10 GHz. The uneven surface of the froth also scatters what reflected energy there is, making accurate angular measurements difficult.

(c) Phase Variation Measurement

The speed with which electromagnetic radiation travels through a medium is related to the dielectric constant of that medium. Consequently, by comparing the phase of a signal passing through a sample in a test channel with the phase of the signal passing through the test channel alone, it is possible to compute the dielectric constant of the sample (Figure (2.4)).

This system was eventually chosen for the dielectric constant measurement because the test channel could be a free-space link, allowing continuous generation of froth during measurement.

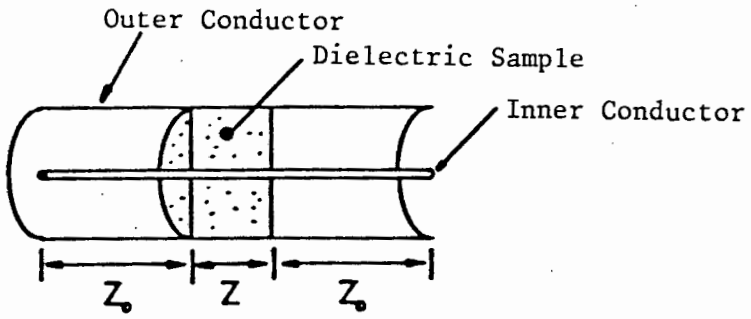

FIGURE 2.5

AIR FILLED COAXIAL LINE FOR TIME DOMAIN SPECTROSCOPY MEASUREMENTS.

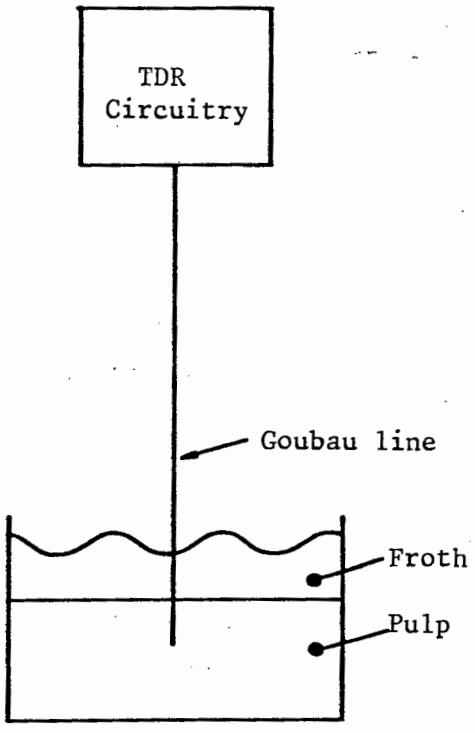

FIGURE 2.6 A TIME DOMAIN REFLECTOMETRY SYSTEM FOR INVESTIGATING FROTH PROPERTIES.

(d) Time Domain Techniques

This method normally uses the time dependence of the reflection of a step pulse from the interface between an air and dielectric medium in a coaxial line to identify dielectric constant. As in the case of the cavity resonator, introduction of froth continuously into the test apparatus (Figure (2.5)) made this method impractical at the time.

Later, after further work and development of a TDR system, it was realised that the measurement of dielectric constant by this method could be greatly simplified by using a Guided-Wave Transmission Line as described by Goubau[54] for sensing the transient response of the froth (Figure (2.6)).

More detailed information about this method can be found in Sections (4.1) and (4.2), while a detailed analysis of Time Domain Spectroscopy and its use in dielectric measurement systems appears in Appendix (D).

2.2 EXPERIMENTS ON FROTH

2.2.1 Conductivity versus Displacement in the Froth

(a) Method

The flotation cell was filled with a quantity of pulp (Rustenburg flotation tails H493), Ethyl Xanthate Collector and Cresylic Acid frother and the air supply and stirrer switched on.

The froth was allowed to rise to the top of the cell and conductivity measurements were taken at 1.5 cm intervals from the surface of the froth to the water/froth interface using the apparatus and procedure described in 2.1.6 and Appendix (C).

(b) Results

The resultant specific conductivities are plotted against displacement in Figure (2.7). The actual readings taken appear in Appendix (E).

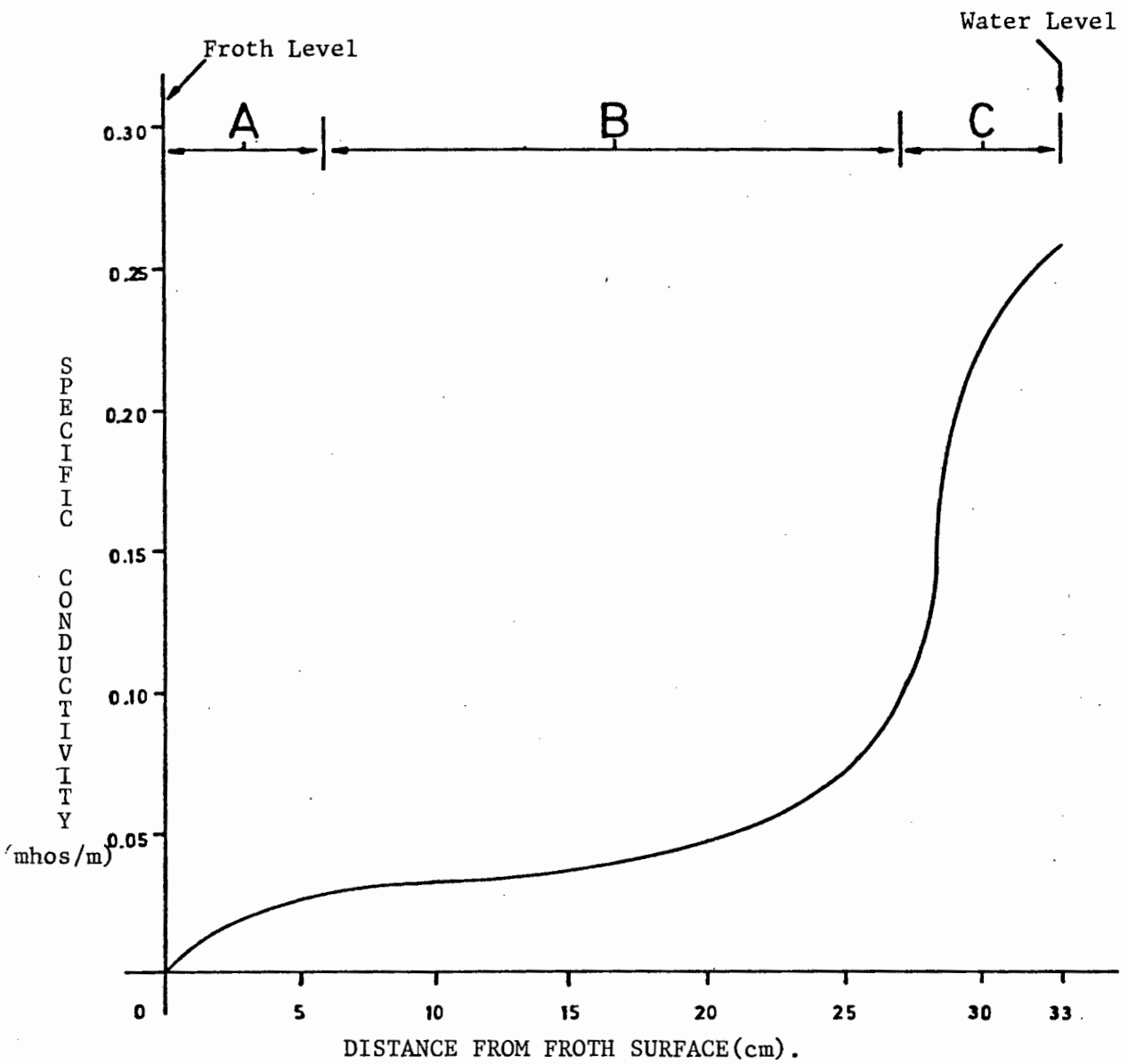

FIGURE 2.7 A PLOT OF CONDUCTIVITY VERSUS POSITION IN THE FROTH.

(c) Discussion

The graph in Figure (2.7) can be divided into 3 distinct regions corresponding to A, B and C.

B stretches from 60 to 270 mm below the surface of the froth and is closely approximated by a straight line. The slope of the line is related to the rate at which the water in the froth is falling back into the pulp mixture.

In this region water content or froth density increases linearly as the water/froth interface is approached.

In the regions corresponding to A (0 to 60 mm) and B (270 to 330 mm) the density does not vary linearly with depth. In the case of A, it is probably as a result of the bubbles becoming too large (i.e. comparable in size to the conductivity probe) for accurate measurement of the bulk conductivity of the froth at that level.

In the case of C, on the other hand, it could be as a result of the small bubbles near the water/froth interface being more strongly 'pushed' from below than the bubbles in region B. This would cause a stronger upwelling of liquid in C, with a corresponding increase in the conductivity in that region. Once the bubbles coalesce and increase in size, higher up in the froth, this liquid falls back into the pulp, restoring the normal froth/liquid balance.

If it is accepted that conductivity is a measure of the froth density, then Figure (2.7) becomes a density profile of the froth. The shape of this profile could have interesting consequences for electromagnetic radiation.

It is well known that if an electromagnetic wave travels from a medium with a certain impedance into a medium with another impedance, then part of

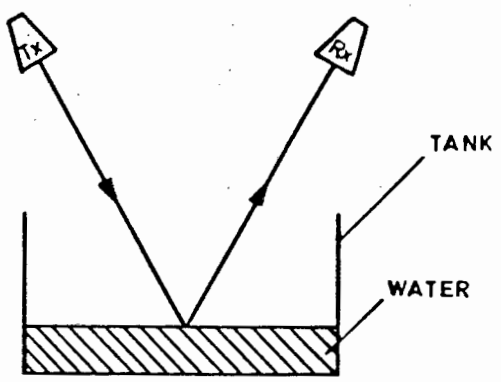

FIGURE 2.8 MICROWAVE REFLECTION MEASUREMENT.

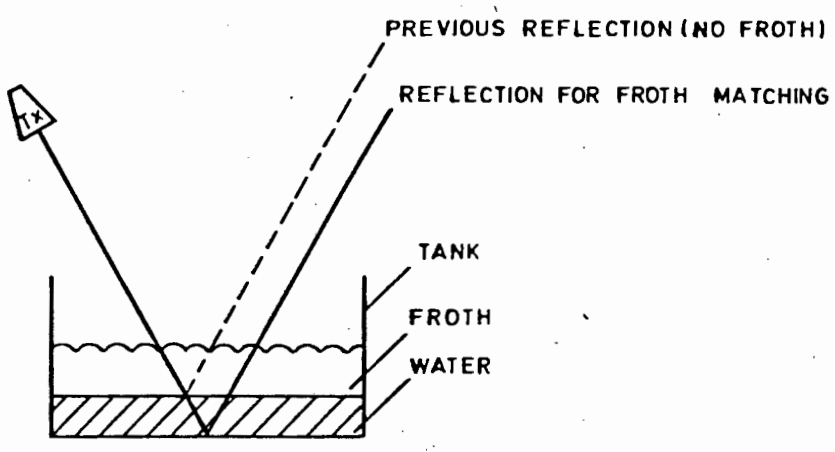

FIGURE 2.9 REFLECTION SHOWING THE EFFECT OF POSSIBLE MATCHING.

the wave's energy will be reflected and part of it will be transmitted. This is the case at an air/water interface.

On the other hand, it is equally well known that if electromagnetic radiation encounters an interface with a gradual transition from one impedance to another, then all the incident radiation will be transmitted.

Such a situation appears to exist in the froth. There is a gradual impedance change from the air to the froth and from the froth to the pulp. The nett result of this could be to make the froth/pulp interface invisible to electromagnetic radiation.

2.2.2 An investigation of Microwave Reflection from a froth-covered Liquid

(a) Method

A large tank half-filled with water and a frothing agent (soap) added. The equipment was set up as shown in Figure (2.8) and the reflected power recorded. The air supply was then switched on until the froth was about 150 mm deep. The reflected power was recorded again.

(b) Result

The return from the tank fell by greater than 70 dB with the froth present.

(c) Discussion

At first this seemed to show that the froth was matching the electromagnetic radiation into the water as postulated in Section 2.2.1. A closer look at the experiment showed, however, that this was an unsatisfactory explanation for the observed phenomenon.

If the microwave energy could be matched into the water, then the reflection from the tank could be matched out into the air. The reflected signal would appear at a slightly different position (Figure (2.9)) attentuated by the

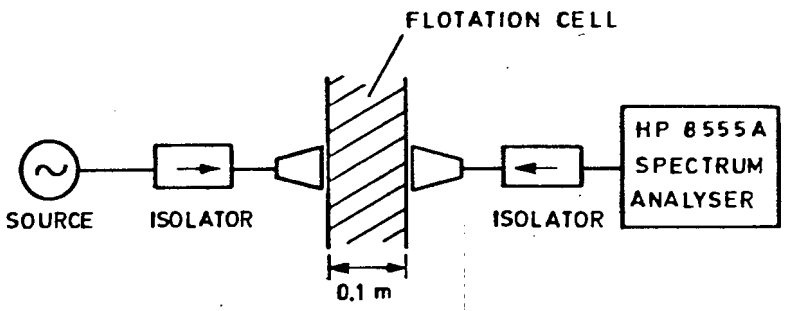

FIGURE 2.10 MEASUREMENT OF ATTENUATION.

propagation loss in the water and froth. A search for this signal was carried out but none was found.

The attenuation α through the water was calculated from

$$\alpha = \omega\sqrt{\left(\sqrt{1+\left(\frac{\sigma}{\omega\varepsilon}\right)^2}-1\right)\left(\frac{\mu\varepsilon}{2}\right)} \quad \text{Np/m see reference (55)}$$

with $\omega = 2\pi \times 10^{10}$ rads/sec

$\mu = 4\pi \times 10^{-7}$ H/m

$\varepsilon = 64(8.85 \times 10^{-12})$F/m

$\sigma = 0.121$ mhos/m

This gives $\alpha = 2.85$ Np/m or 24.7 dB/m. The depth of the water was 150 mm and the wave passed through it twice, so the expected attenuation should be

$$24.7 \times 0.3 = 7.4 \text{ dB}$$

If the attenuation in the water is only 7.4 dB the rest of the attenuation (>60dB) must take place in the froth.

After this experiment it was decided that an investigation of the free-space attenuation of microwave energy in the froth was necessary.

2.2.3 Measurement of the Froth's Free-Space Attenuation

(a) Method

The measurement system described in Section (2.1.7) was used to measure the attenuation of the froth (Figure (2.10)).

The flotation cell was filled with soapy water and the air supply switched on to produce froth. The reduction in transmitted power was recorded. The experiment was then repeated using a flotation frother (Cresylic Acid) instead of soap to produce the foam.

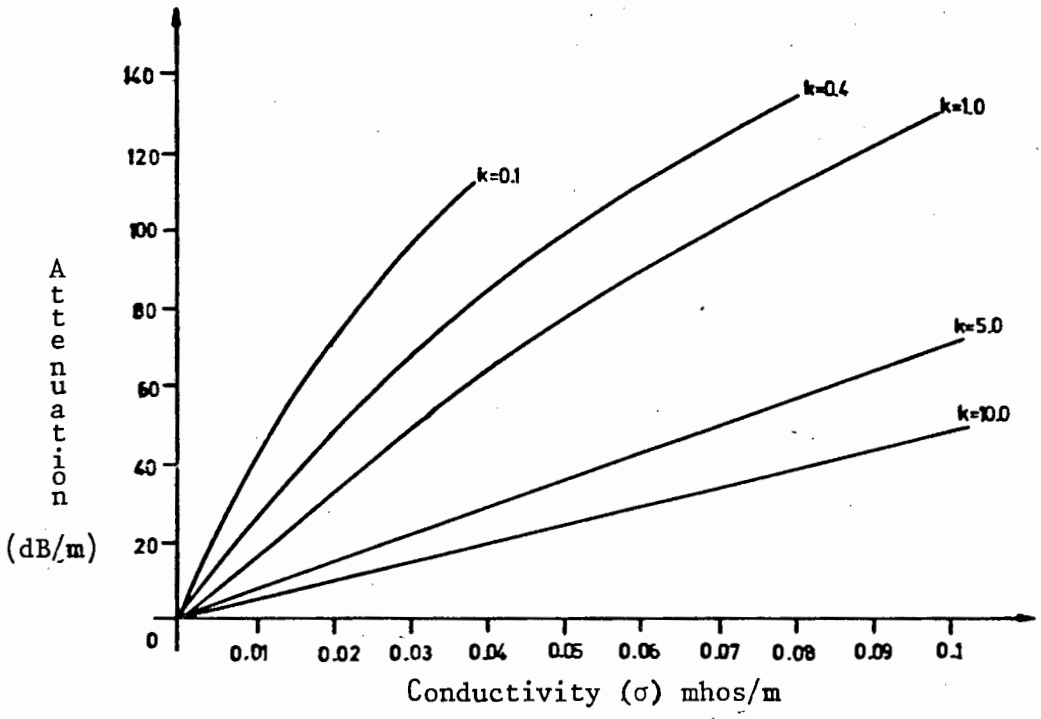

FIGURE 2.11 THEORETICAL ATTENUATION VERSUS CONDUCTIVITY FOR VARIOUS DIELECTRIC CONSTANTS.

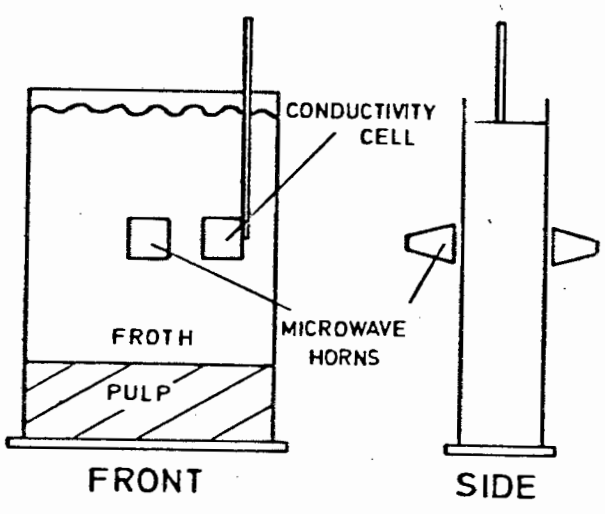

FIGURE 2.12 ATTENUATION VERSUS CONDUCTIVITY MEASUREMENT.

(b) Results

The soap froth attenuated the signal by ± 35 dB while the frother froth attenuated it by ± 45 dB. This is ± 350 dB/m and ± 450 dB/m respectively.

(c) Discussion

The reasons for the different attenuations in the froth is to be found in their physical differences.

The frother froth was wetter in appearance than the soap froth and collapsed far quicker when the cells' air supply was switched off. In fact, the soap froth did not collapse at all. The water drained out of it leaving behind a tenuous framework of bubbles that were dry to the touch. The soap foam appeared more dense with an average bubble size of ± 1.5 mm compared to ± 5 mm for the frother froth.

The conductivity of the soap froth was found to be lower than that of the frother froth. A surprising result considering that the soap froth appeared the denser of the two. The amount of water in the froth therefore has a greater effect on its conductivity than bubble size.

The fact that soap froth was easier and less messy to generate, and exhibited the same electrical characteristics as Cresylic Acid froth, led to its preferential use in later experiments.

2.2.4 Free-Space Attenuation versus Froth Conductivity

The previous experiment showed a relationship between the conductivity of the froth and its attenuation. This is in agreement with theory. To illustrate this, theoretical values of attenuation versus conductivity have been plotted for a range of dielectric constant values (Figure (2.11)). The attenuation equation used in Section 2.2.2 was used for the calculation of these values. As can be seen, attenuation increases linearly with increasing conductivity for $k > 1$.

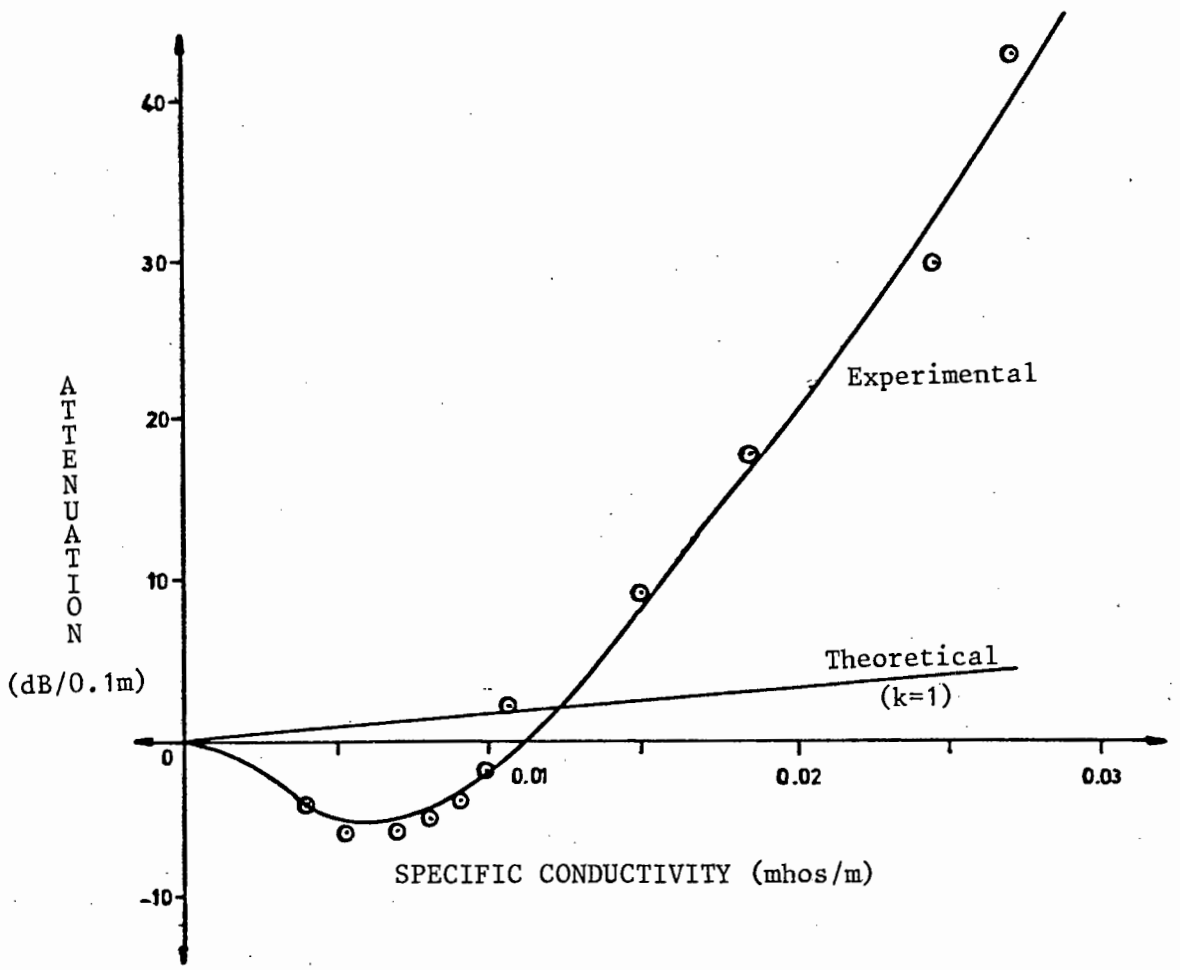

FIGURE 2.13 THEORETICAL AND EXPERIMENTAL ATTENUATION IN THE FROTH AS A FUNCTION OF CONDUCTIVITY.

An experiment was set up to investigate the attenuation versus conductivity properties of the foam.

(a) Method

The apparatus was set up for attenuation measurement as shown in Figure (2.12) and described in Section 2.1.7. A soap froth was chosen because its stability simplified the measurement process. The conductivity probe was placed in the froth at the level of the microwave horns and the air supply switched off. As the water percolated out of the froth, corresponding readings of attenuation and resistance were taken.

(b) Results

The resultant conductivities are plotted against attenuation in Figure (2.13). The actual resistance readings and their conversion to specific conductances appear in Appendix (F).

The power readings obtained on the HP Spectrum Analyser are for transmitted power and these were converted to attenuation.

(c) Discussion

From theoretical considerations, as illustrated in Figure (2.11), it is obvious that for a given conductivity, attenuation increases as dielectric constant decreases. This seems contrary to expectations until it is realised that the power loss normally associated with moving from a medium with one dielectric constant to one with another, is a manifestation of the power lost by reflections off the dielectric interfaces. The important parameter governing power transmission in a medium is the ratio of conductivity (σ) to dielectric constant (k). If (σ/k) decreases the attenuation in the medium decreases, and vice versa.

The fact that the observed and theoretical attenuations in the froth differ so greatly, brought into question the reliability of the conductivity

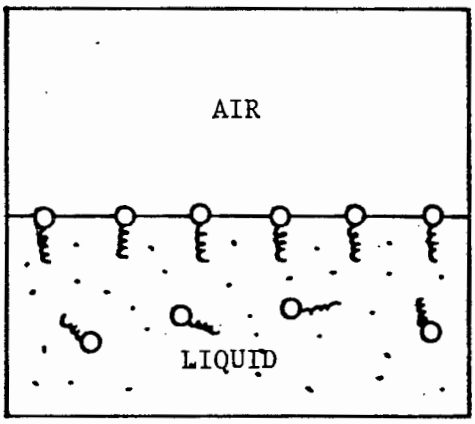

FIGURE 2.14

THE ARRANGEMENT OF MOLECULES AT AN AIR/LIQUID INTERFACE SHOWING THE FORMATION OF A MONOLAYER.

FIGURE 2.15

BUBBLE STRUCTURE IN THE FROTH SHOWING THE MONO-LAYER FILMS AND THE FLUID BETWEEN THEM.

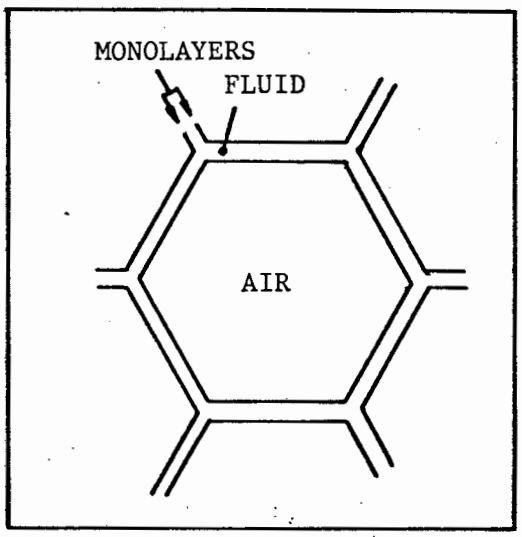

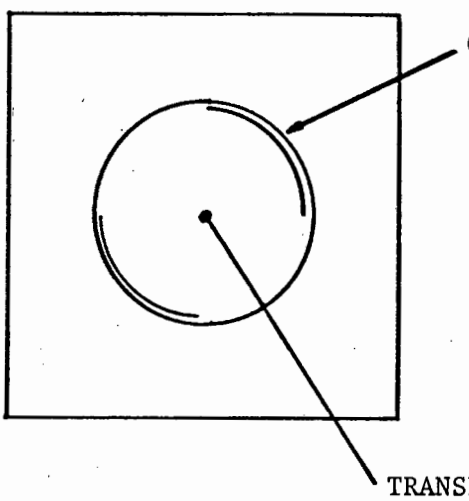

FIGURE 2.16

A SINGLE BUBBLE AS SEEN BY THE MICROWAVE RADIATION.

measurement system used (described in Appendix C). A re-evaluation of the conductivity calibration technique showed that it was providing the correct readings at the measurement frequency of 1 kc/s.

Possible causes of erroneous conductivity readings

A possible reason for the theoretically unexplainable high attenuation in the froth, is that some loss process is manifesting itself at the test frequency of 9.9 GHz, increasing the effective conductivity of the froth at that frequency. The low frequency (1kc/s conductivity) measurement would not reflect this loss process in its conductivity readings.

A look at the available literature[57,58,59] shows that the physical structure of foams and froths is extremely complex and not fully understood. The molecules at a liquid/gas interface allign themselves in such a way as to form what is called a 'monolayer'. Figure (2.14) illustrates this phenomenon. The aerophilic parts of the molecules in the liquid orientate themselves towards the air at the air/liquid interface, forming a stable film or monolayer at this interface.

A number of ionic substances, including long chain fatty acids (i.e. frothers and soaps), can form stable, insoluble monolayer membranes. Sebba[59] proposes the foam model shown in Figure (2.15). The air/liquid monolayer forms a film, or shell, around the air bubbles which allows a continuous film of liquid to exist and flow between them.

This model explains how the water in the soap froth generated in Section 2.2.4 could percolate out and leave a tenuous, dry framework behind without collapsing the bubble structure.

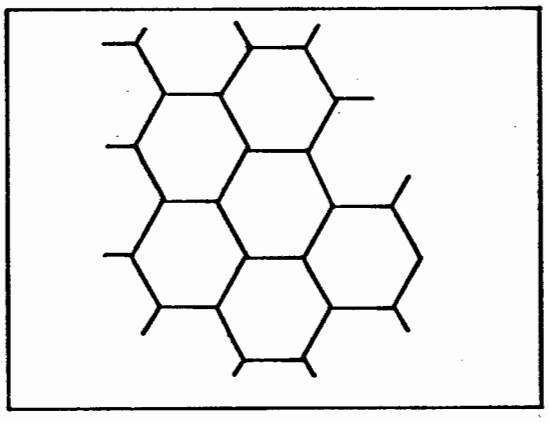

FIGURE 2.17

A SINGLE LAYER OF CONDUCTING BUBBLES FORMING A GRID.

FIGURE 2.18

A SECTION THROUGH THE FROTH WHEN VIEWED FROM ABOVE.

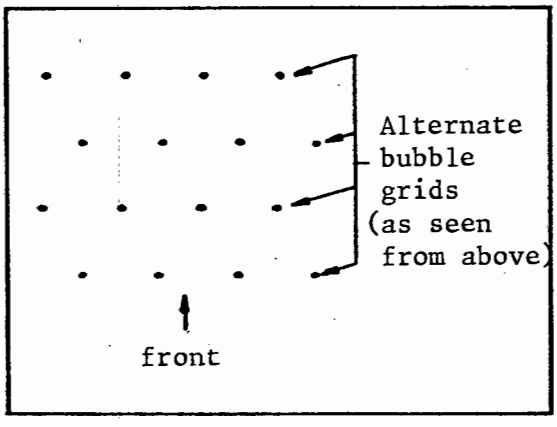

A possible reason for the high propagation loss in the froth can be found in its physical structure. Consider a single bubble as seen from a certain direction (Figure (2.16)). As a result of the thin bubble wall, the centre of the bubble appears transparent while the sides (as viewed from the front) appear as a circle.

A single layer sheet of bubbles would therefore appear as a conducting grid (Figure (2.17)), while a foam would appear as a number of these grids stacked one behind the other (Figure (2.18)). As a result of the bubble size being less than 1/4 wavelength (at 9.9GHz), the radiation would see each grid as a continuous sheet with a bulk conductivity determined by the conductivity of the liquid between the bubbles and the bubble size.

Circulating currents set up in each layer, would then cause the radiation to be progressively attenuated as it passed through the froth. The gradual nature of the transition from one layer to the next would explain the lack of reflections from the froth.

The effect of a dielectric constant of less than one

Figure (2.11) shows that theoretical attenuation in a conducting medium increases steeply for dielectric constants of less than one. This seems a trivial statement as dielectric constants of less than one are not normally encountered. Plasma physics is a special case where they do occur[60].

Plasmas are partly or completely ionised gases, usually encountered in the ionosphere. Due to their physical characteristics (positively and negatively charged ions, free electrons and neutral polar molecules) they exhibit special properties as media for electromagnetic wave propagation. It is felt that the froth, a medium consisting of a mixture of air and ionised liquid might approximate a dense plasma.

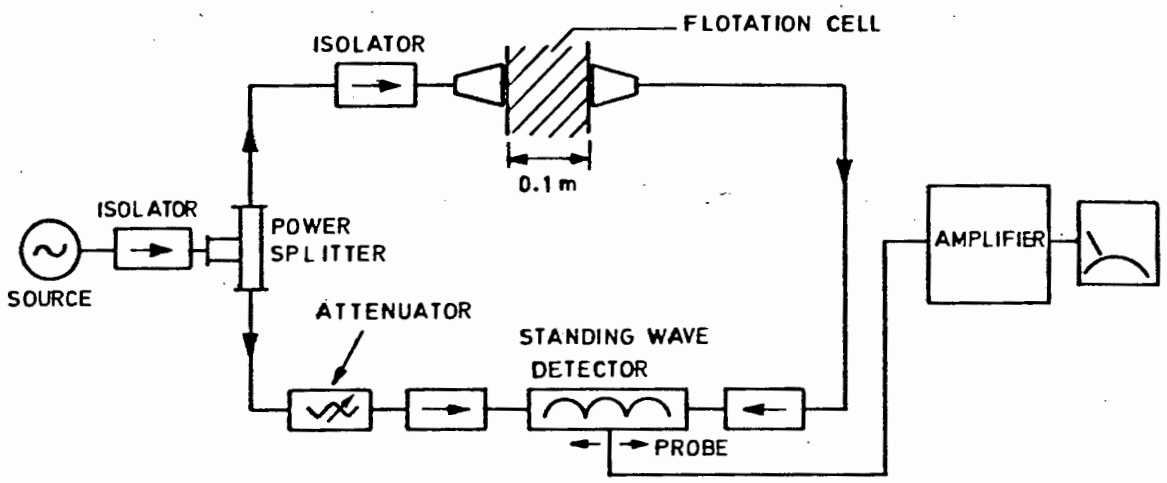

FIGURE 2.19 DIELECTRIC CONSTANT MEASUREMENT

NOTE:

These explanations for the high attenuation experienced in froths have not been investigated in any way and are offered only as possible solutions. Further work still needs to be done to determine the exact nature of the loss mechanism causing the high attenuation of microwave energy in the froth.

Such work is regarded as being beyond the scope of this thesis and the fact of the attenuation's existance will be accepted and used without further comment.

2.2.5 The Measurement of Froth Dielectric Constant

(a) Method.

The schematic diagram of the system used for dielectric constant measurement appears in Figure (2.19). Isolators are used to prevent unwanted reflections from entering the system. Dynamic range improvement is obtained by attenuating the reference wave to a point where it is comparable to the test wave with the cell empty. The output of the microwave source is split equally between the reference and test channels. After passing through the cell, the test signal is fed into one side of a slotted line standing wave detector.

In order to measure dielectric constant the standing wave pattern is plotted with the cell empty. Froth is introduced into the test channel by switching on the tank's air supply. The amount that the standing wave pattern shifts is related to the dielectric constant of the froth (see Appendix G for further information and results).

A useful consequence of this method is that it automatically compensates for the phase shift introduced by the flotation cell.

(b) Result

The high attenuation in the froth made accurate determination of the shift in the standing wave pattern difficult. However, approximate values for the dielectric constant of the froth were obtained. These ranged from 1.1 to 1.3.

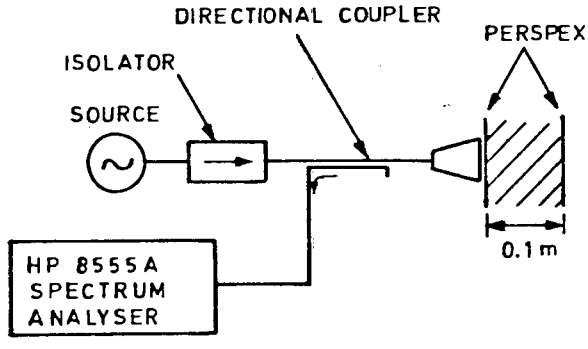

FIGURE 2.20 REFLECTED POWER MEASUREMENT

(c) Discussion

The result of this experiment showed that the froth dielectric constant lies close to one. This is in agreement with the results obtained by Williams who found that the dielectric constant of a froth with 3 mm bubbles lay between 1 and 1.1 (reference 56).

Increased measurement accuracy for a more detailed study of the effect of bubble size and liquid content on the dielectric properties of froth, would merit the use of a more sophisticated phase detection system offering increased dynamic range. The measurement accuracy obtained was sufficient for the purposes of this thesis, so no further work was done to develop such a phase detection system.

This result tends to invalidate the theory that the froth behaves in a manner similar to a plasma. Although it will be accepted that the dielectric constant of the froth is close to one, it is felt that the inaccuracies in the measuring equipment used, allowed errors either side of one to occur. Consequently, the plasma theory should not be scrapped until further, more accurate research shows that it is incorrect.

2.2.6 Measurement of Reflected Power

(a) Method

The apparatus was set up as shown in Figure (2.20). The directional coupler couples only reflected power into the spectrum analyser. This power was measured with the tank empty and then with it full of soap froth.

(b) Results

The reflected power fell by about 4 dB with the foam in the tank.

(c) Discussion

This experiment demonstrates that the apparent attenuation of the micro-wave energy in the froth is not due to the incident wave being reflected

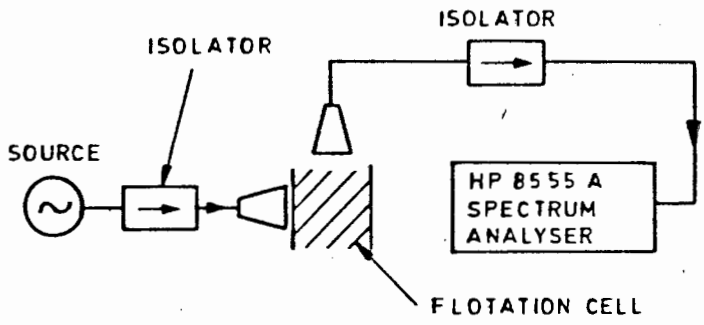

FIGURE 2.21 SCATTERED POWER MEASUREMENT

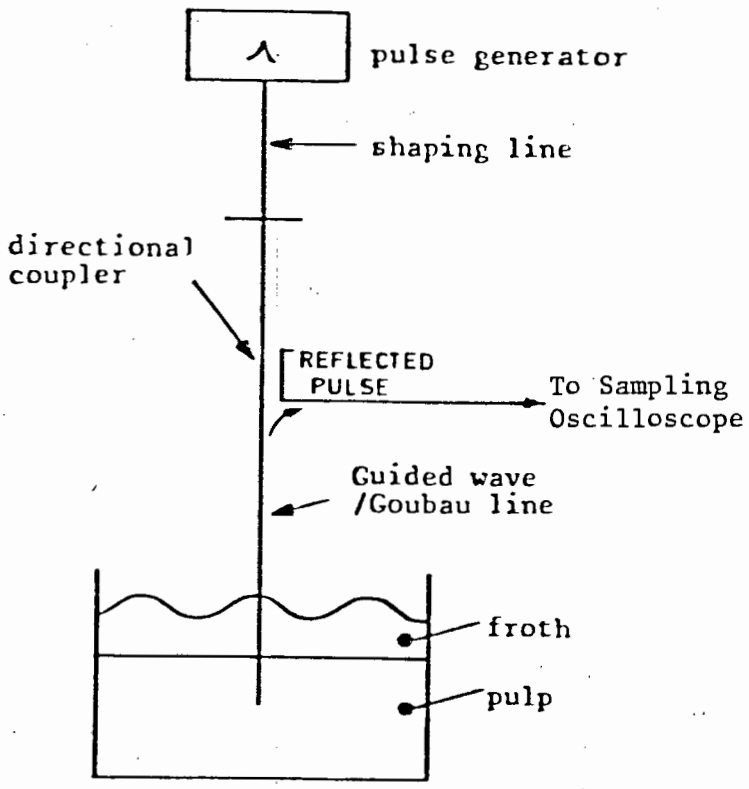

FIGURE 2.22 A SYSTEM FOR PERFORMING TIME DOMAIN REFLECTOMETRY EXPERIMENTS ON FROTH.

from the perspex/froth interfaces. The reason for reduced reflection is that the froth provides a better match into the flotation cell than air.

2.2.7 Measurement of Scattered Power

The possibility that the power is not being dissipated in the froth but is being re-radiated or scattered in all directions led to this investigation.

(a) Method

The apparatus was arranged as shown in Figure (2.21). The power appearing at the mouth of the tank was measured with the tank empty and full of froth.

(b) Results

The radiated power with the flotation cell empty was -23 dBm and it fell to -65 dBm with the froth present.

(c) Discussion

The first power reading appeared to be due to a surface wave travelling up the inside perspex faces of the cell from one horn to the other. The reduction in power observed is due to the attenuation of this wave by the froth.

This experiment demonstrates that the apparent attenuation in the froth is not caused by scattering of the incident radiation.

2.2.8 The effect of Froth on a Pulsed TDR Return

(a) Method

A system for Time Domain Reflectometry measurements was constructed as shown in Figure (2.22). The construction of the individual parts is dealt with in Section 5.0 so a short description of its operation will suffice here.

The pulse generator produces a 1nS pulse with a rise-time of about 500 pS. This pulse passes down the guided-wave or Goubau transmission line and encounters the liquid interface. The sudden impedance change presented at this interface causes the pulse travelling down the line to be reflected back towards the pulse generator. A portion of the reflected pulse's energy (determined by the bandwidth of the coupler) is coupled into the directional coupler and is displayed by the sampling oscilloscope. A large plastic container was used as a flotation cell.

Reflected pulse amplitude was measured with and without a layer of froth (100 mm thick) present.

(b) Results

The pulse amplitude dropped by about 5 per cent ($\simeq$ 0.5 dB) with the foam present. This is an attenuation of about 2.5 dB/m.

(c) Discussion

The TDR pulse return is attenuated far less than its 10 GHz microwave counterpart. This can be attributed to the fact that the major part of the pulses' spectral components are far lower in frequency than 10 GHz and therefore suffer less attenuation.

2.3 Froth Properties

The following facts have been established about the froth experimentally:

(a) It has a conductivity varying from 10^{-1} to 10^{-2} mhos/m depending on where it is measured in the froth, and a dielectric constant close to one.

(b) It attenuates electromagnetic radiation in a frequency dependent manner. The trend is as theory predicts but the amount of attenuation is too high to be explained in terms of the observed froth conductivity and dielectric constant.

(c) The apparent attenuation is not due to the reflection or scattering of the incident radiation.

(d) The process causing the increased attenuation has not been satisfactorily explained or experimentally determined. Such work is regarded as being beyond the scope of this thesis although a tentative explanation, incorporating the monolayer phenomenon and physical structure of the froth, is advanced.

(e) The matching effect of the froth is not gradual enough to match the pulsed TDR signals into the pulp.

3. CONSIDERATION OF THE PROPOSED MICROWAVE LIQUID-LEVEL MEASUREMENT SYSTEMS IN THE LIGHT OF EXPERIMENTAL RESULTS

In Section 1. a number of microwave level measuring systems were described and two of the most promising were proposed for the measurement of liquid height in a flotation cell. Now that something is known about the electrical properties of the flotation froth, it is possible to choose the most suitable system of the two.

3.1 The Multiple Frequency Continuous-Wave System

The system based on the MFCW principle operates at a fundamental frequency of 9.9 GHz in order to provide the required resolution of 10 mm. Unfortunately, as was shown in Section 2.2.3, the attenuation in the froth at this frequency is large. The reflected signal can be expected to experience as much as 80 dB of attenuation, perhaps more, in a 'wet' flotation foam 100 mm thick.

This is not an insurmountable problem, as a well-designed coherent detection system would still be able to extract this reflected signal from the background noise. The price that must be paid, however, is in increased circuit complexity and cost.

3.2 The Time Domain Reflectometry System

The reflected signal in the TDR system also suffers a certain amount of attenuation although to a far lesser degree than that suffered by the signals in the MFCW system.

What makes it more attractive, is that by using a technique involving the comparison of composite transmitted and reflected pulses at an instant in time at different positions on a 'detector line', it is possible to compensate for the effects of attenuation simply and cheaply. A more detailed description of this technique is to be found in Section 5.3.

The proposed TDR system (Section 5.0) uses a guided-wave or Goubau line to direct the pulses into the flotation cell and a combination of directional coupler, delay line and two sampling bridges to effect the composite pulse comparison. An added advantage of this comparison technique is that it also gives information about the direction of liquid-level change in the flotation cell.

A further consideration in choosing the TDR system over the MFCW system, is that of immunity to external disturbances. The MFCW system would be susceptible to spurious reflections from the cell stirrer and people moving nearby. This effect would be enhanced by the fact that the desired signal (i.e. from the froth/liquid interface) would be attenuated to such a degree that it could easily be swamped by the unwanted reflections. The TDR system, on the other hand, is immune to these external disturbances. This is as a direct consequence of the use of the guided-wave transmission line and the pulse comparison technique. The transmission line confines the pulses to the flotation cell, reducing the number of unwanted reflections, while the effect of sampling the composite transmitted and reflected pulse is to gate out any spurious signals.

The ease with which a TDR system can be used for Time Domain Spectroscopy measurements (Appendix D) was a further point in its favour.

After consideration of these points, it was decided that a prototype TDR system, for liquid level measurement in flotation cells, would be built and tested.

4. PRACTICAL CONSIDERATIONS IN THE DESIGN OF A TIME DOMAIN REFLECTOMETRY SYSTEM

4.1 Introduction

It is well known that a linear, time-invariant network can be completely specified by its impulse response[61]. The advent of sampling oscilloscopes, with effective bandwidths of 10 GHz, and baseband pulse generators, with subnanosecond risetime capabilities, made it possible to observe the transient response of distributed networks and materials directly[71].

Use of this technique for wideband system analysis is known as Time Domain Reflectometry (TDR) while its application to material identification is called Time Domain Spectroscopy (TDS).

Early work by Ross[62] verified the correspondence between transient network analysis and experiment, while Davis and Loeb[63] were amongst the first to demonstrate the use of time domain waveforms for obtaining wideband frequency information of two port networks to 1 GHz.

The use of TDR for determining the dielectric constant and relaxation time of various liquids was first reported by Fellner - Feldegg[27] in 1969. Nicolson and Ross[29] presented another method, utilizing reflected and transmitted waves to obtain the complex permittivity of linear materials over a broad range of microwave frequencies in 1970.

More recently, the convenience and accuracy of time to frequency translations has been greatly improved through the use of computer controlled scanning procedures and Fast Fourier Transform techniques[18,64]. Andrews[65] describes an automatic time-domain network analyser, using a minicomputer, with a DC to 18 GHz capability, while the use of a microprocessor to simplify dielectric constant and loss factor measurement is covered by Parisien and Stuchley[66] in their paper on microprocessor-controlled time-domain spectroscopy.

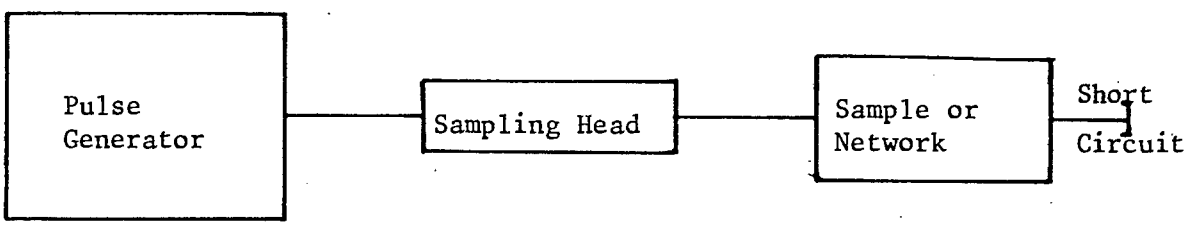

FIGURE 4.1 A TYPICAL TIME DOMAIN REFLECTOMETRY SYSTEM FOR NETWORK OR MATERIAL INVESTIGATION.

At present, further work is being directed towards improving measurement accuracy[67] and processing methods[68], introducing more automation, increasing dynamic range[70] and extending high and low frequency bounds[69].

4.2 A Basic Measurement System

A typical measurement configuration is shown in Figure (4.1). The pulse from the pulse generator (with subnanosecond risetime) propagates down the coaxial line, through the feedthrough sampling head of a sampling oscilloscope, and is incident on the network or sample of material in the test sample holder. The pulse is partially reflected and partially transmitted. The transmitted pulse reflects from the short circuit and returns up the line, passing through the sample on its way to the sampling head. It has been shown[29] that these waveforms yield $S_{11}(\omega)$ and $S_{21}^2(\omega)$, where S_{21} and S_{11} are the scattering coefficients[72] of the network or sample. These scattering coefficients define the frequency domain characteristics of the network or sample.

4.3 Pulses

Since the pulse technologist thinks in the time domain and the microwave engineer in the frequency domain, their cooperation demands a thorough understanding of the inherent relationship between the two domains. A knowledge of pulse terminology and spectral content are necessary to promote this understanding.

Calling a waveform a 'pulse' tells practically nothing about it except that it exists for a short time on the time scale of interest. The need for more precise definitions led to the vocabulary of pulse electronics.

Ideal pulse waveforms have amplitude changes that occur in zero time or at a rate linearly proportional to time. In practice neither are obtainable, although modern pulse generators are providing increasingly better approximations

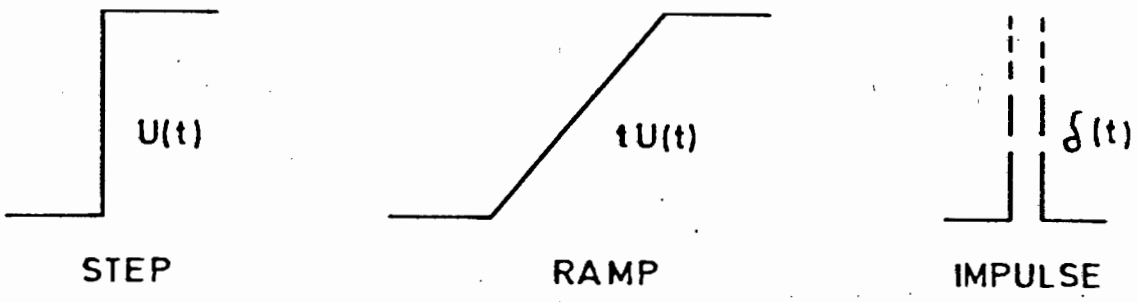

FIGURE 4.2 STANDARD WAVESHAPES

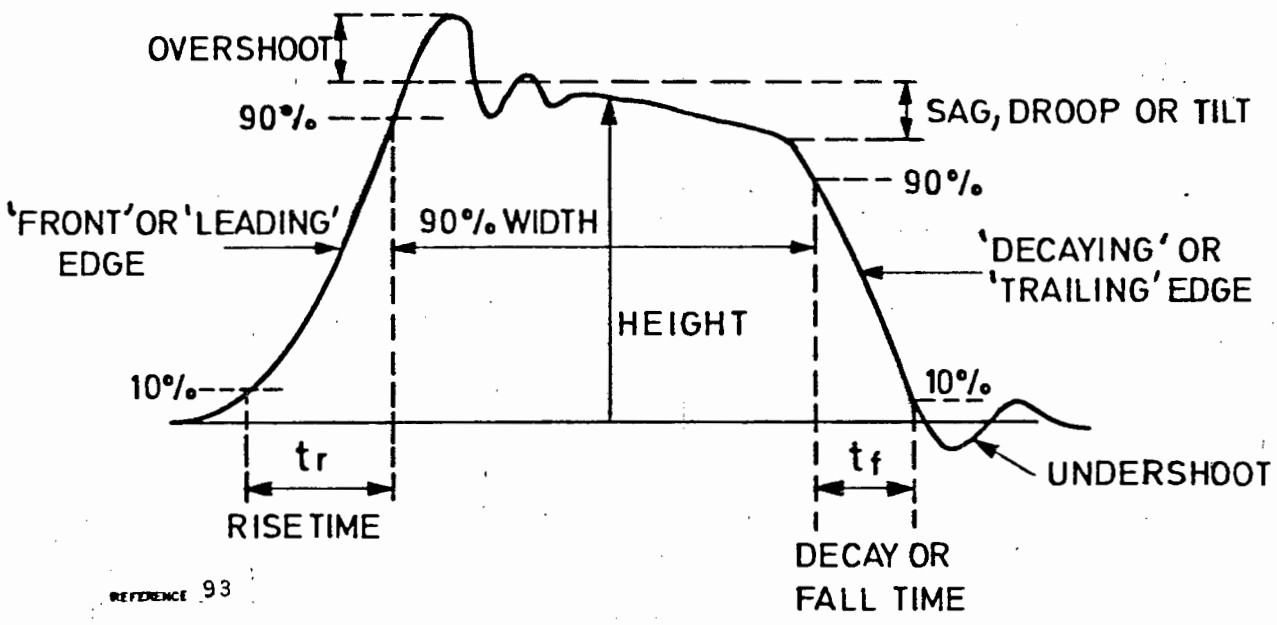

FIGURE 4.3 A DISTORTED PULSE

to the instantaneous amplitude change as device switching speeds increase. For analytical purposes it is convenient to use three 'standard' waveshapes. These are the step, ramp and impulse functions (Figure (4.2)) described mathematically as $U(t)$, $t\,U(t)$ and $\delta(t)$ respectively. Their primary use is for investigating and characterising linear networks in the time domain.

Many names are used to describe the various forms of pulse shapes and they vary from one text to another. In this thesis the IEEE and IEC standards are used as a guide[73,74].

Pulse repetition frequency (prf) is expressed in pulses per second although Hertz are widely accepted. The term 'speed' is used to signify both a high prf and fast switching rate.

Pulse distortion leads to a number of special terms (Figure (4.3)). Rise and fall times are defined by the 10 and 90 per cent amplitude levels to avoid the need to define pulse start and end times. Droop is expressed as a percentage of total height, while overshoot is ignored when defining pulse height. With triangular pulses, as most high-speed pulses are, pulse length is quoted at the base (10 per cent) or at half height (50 per cent), care being taken to specify which it is.

The overall shape of the pulse is often called its profile.

4.4 Pulse Spectra

4.4.1 Rectangular pulses

The pulse shown in Figure (4.4a) may be described by the function

$$f(t) = \begin{cases} 0 & t < -t_p/2 \\ A & -t_p/2 < t < t_p/2 \\ 0 & t > +t_p/2 \end{cases} \qquad \text{(Figure (4.4a))}$$

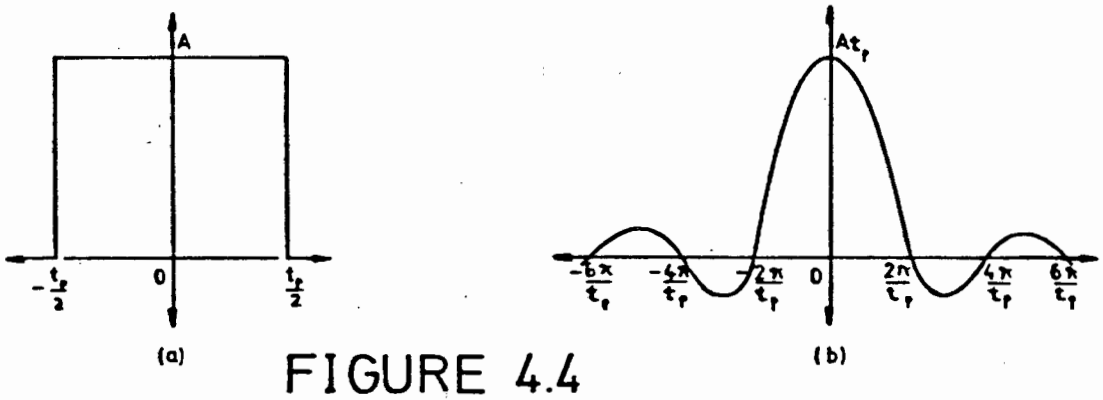

FIGURE 4.4

A SQUARE PULSE AND IT'S FREQUENCY SPECTRUM.

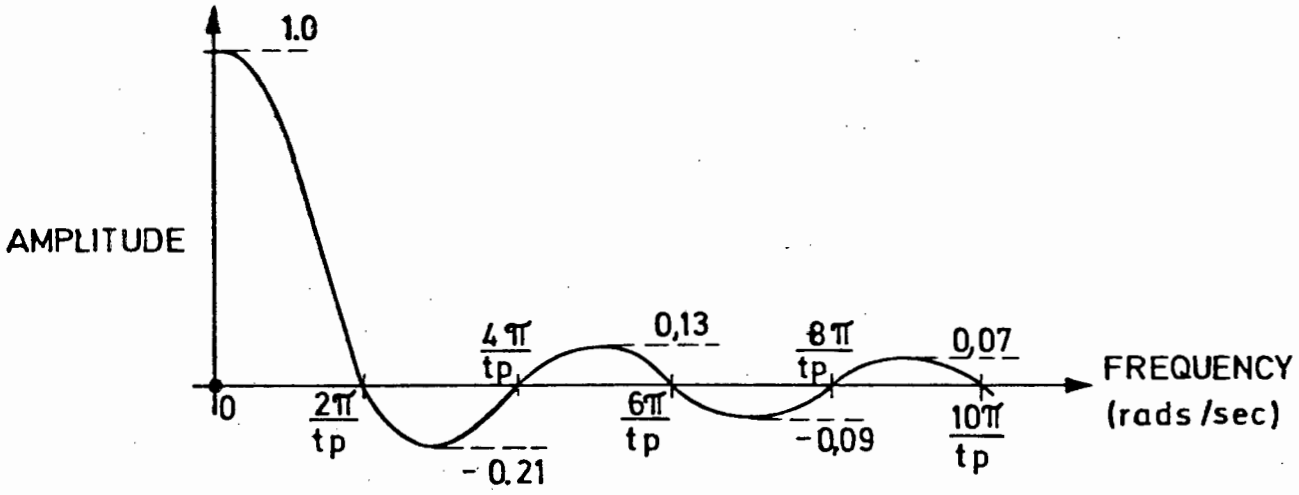

FIGURE 4.5 REDUCTION OF SIDEBAND AMPLITUDE WITH INCREASING FREQUENCY.

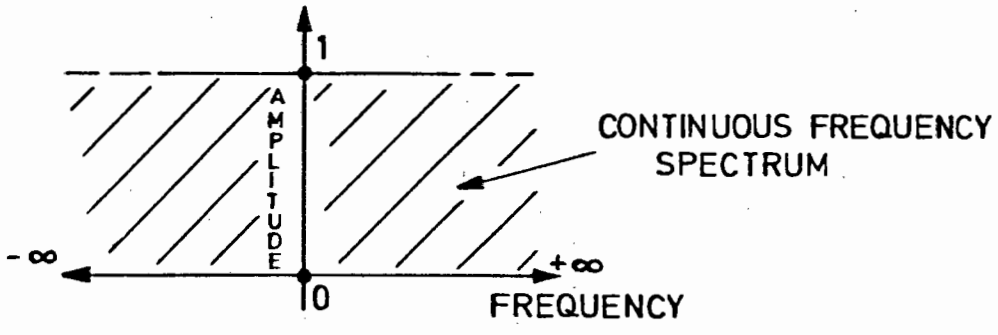

FIGURE 4.6 THE SPECTRUM OF AN IMPULSE

Time-symmetry is achieved by choosing the time origin at the centre of the pulse

The Fourier Transform of the pulse

$$F(\omega) = \int_{t_p/2}^{-t_p/2} Ae^{-j\omega t} = At_p \text{ Sinc } (\omega t_p/2)$$

yields its spectral components. The familiar sinc function is defined by $\text{sinc } x = \frac{\sin x}{x}$ (Figure (4.4b)).

The function has its maximum value of unity at $\omega = 0$, oscillating to positive and negative values, crossing the axis at multiples of $(\frac{2\pi}{t_p})$. For a single pulse the spectrum is continuous, having been obtained by integrating over a continuum of frequency components.

The complete double-sided spectrum contains negative sinusoidal components which do not actually exist. The positive spectrum gives the spread of frequency components, but the true amplitude of any component consists of the sum of both real and imaginary parts.

The spectrum of the single pulse is dominated by the central band which has limits $\pm 2\pi/t_p$. Figure (4.5) shows how the sidebands reduce in size as the spectral frequency increases. As can be seen, very little energy is concentrated in the high frequency region of the spectrum. A network with a bandwidth equal to the reciprocal of the pulse width will not significantly distort the pulse, therefore.

Decreasing t_p spreads the spectrum out to incorporate more high frequency components. If (Axt_p) is kept constant as t_p is decreased to zero, the pulse becomes a better and better approximation of an impulse $\delta(t)$, with a constant amplitude spectrum from $-\infty$ to $+\infty$ (Figure (4.6)).

This is the motivation for using impulses to test networks and systems, they provide simultaneous and equal excitation at all frequencies (ideally).

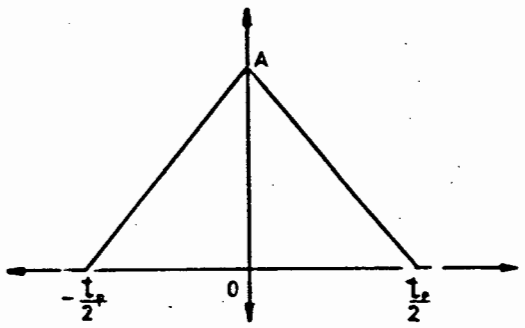

FIGURE 4.7 A TRIANGULAR PULSE

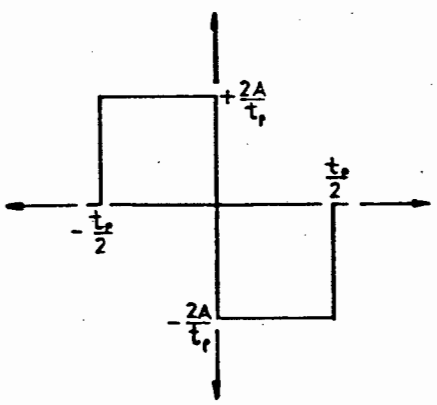

FIGURE 4.8 A DIFFERENTIATED TRIANGULAR PULSE

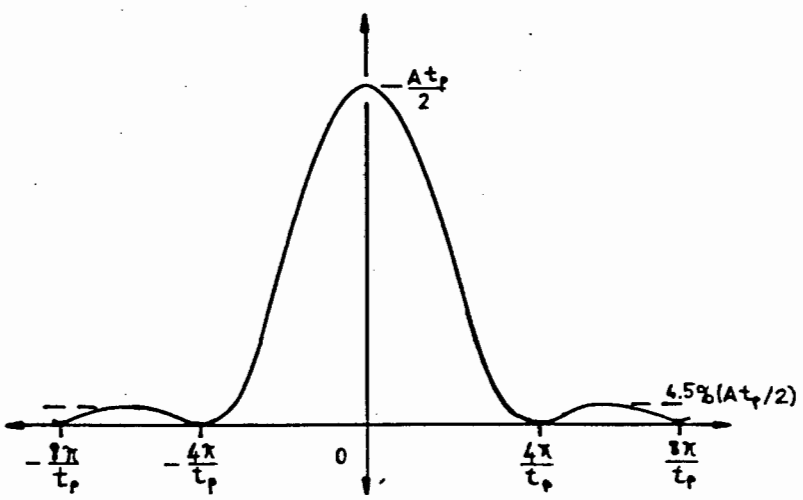

FIGURE 4.9 THE FREQUENCY SPECTRUM OF A TRIANGULAR PULSE.

4.4.2 Triangular pulses

In ultra-high speed systems it is more common to encounter pulses with a triangular shape than a well-defined rectangular shape (Figure (4.7)).

Using the differentiation property of the Fourier Transform

$$F(\omega) = \frac{1}{j\omega} \int_{-\infty}^{\infty} \left| \frac{d}{dt} f(t) \right| e^{-j\omega t} \, dt$$

it is possible to simplify the process of finding the spectral components of the triangular pulse.

Differentiating the pulse shown in (Figure (4.7)) gives that shown in Figure (4.8). Substitution in the Fourier differentiation formula results in

$$F(\omega) = \frac{1}{j\omega} \int_{t_p/2}^{0} \frac{A}{t_p/2} e^{-j\omega t} dt + \frac{1}{j\omega} \int_{0}^{t_p/2} \frac{A}{t_p/2} e^{-j\omega t} \, dt.$$

Standard manipulation gives

$$F(\omega) = \frac{At_p}{2} \left(\text{sinc } \frac{\omega t_p}{4}\right)^2$$

A plot of this frequency spectrum appears in Figure (4.9). The nodes occur at $\omega = \pm 4\pi/t_p, \pm 8\pi/t_p, \ldots$ etc. The maximum of the first sideband occurs at $\pm 6\pi/t_p$ and is 4.5 per cent of the amplitude of the central band. Thus, it can be seen that most of the energy of a triangular pulse is within the frequency range defined by the central band (i.e. between $\pm \frac{4\pi}{t_p}$).

When designing a directional coupler for high speed pulse work, it is therefore necessary to ensure that the bandwidth of the coupler is sufficient to accept the frequencies in this central band.

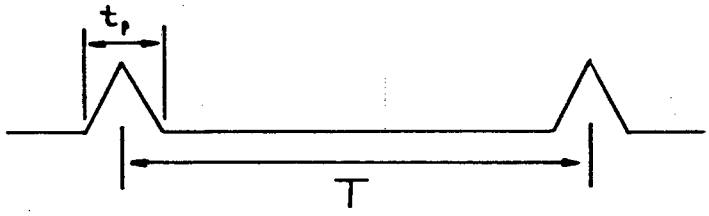

FIGURE 4.10 A PERIODIC PULSE TRAIN.

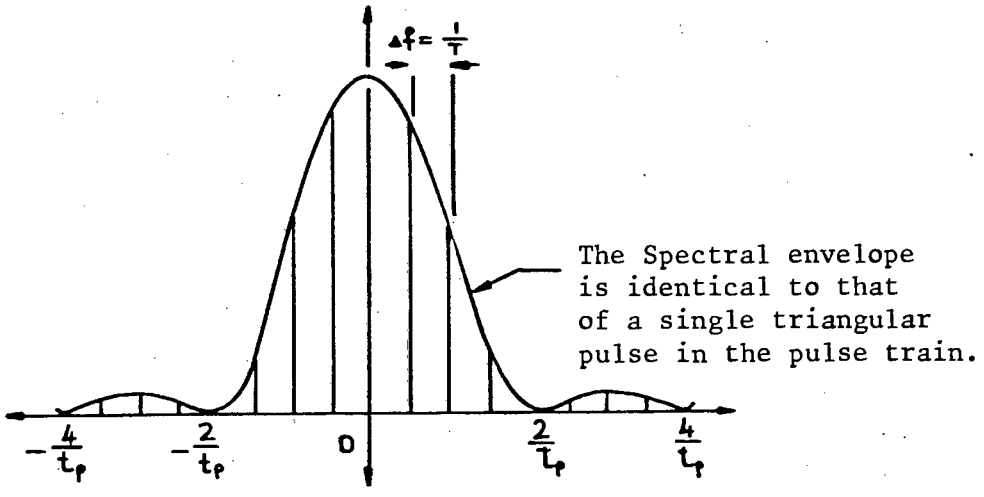

FIGURE 4.11 THE FREQUENCY SPECTRUM OF A PERIODIC TRAIN OF TRIANGULAR PULSES.

4.4.3 Periodic pulses

In practice the case of a single pulse is barely ever encountered, it is more common to use a train of pulses for investigatory work. The spectral content of a train of pulses differs slightly from that of any of the individual pulses in the pulse train.

It can be proven theoretically (Appendix H) that the spectral content of a train of pulses (Figure (4.10)) is as shown in Figure (4.11). Although the envelope of the spectrum is the same as for an individual pulse, it is no longer continuous. The spectral components are separated by a constant frequency, related to the pulse repetition rate.

In order to ensure a reasonably continuous pulse spectrum for test purposes, it is therefore necessary to ensure a high (T/t_p) ratio (i.e. >100).

4.5 THE RELATIONSHIP BETWEEN RISETIME AND FREQUENCY RESPONSE

The rise time capability of an instrument (e.g. oscilloscope) is related to its upper frequency 3-dB point by the expression

$$t_r = k/f_{(3dB)} \quad \text{sec.}$$

where t_r is the risetime in seconds, $f_{(3dB)}$ is the frequency of the upper half power point (c/s). 'k' is a constant between 0.35 and 0.45 cycles, depending on the shape of the instruments' frequency-gain curve. With pulse risetime overshoots of less than 5 per cent, a value of 0.35 for k is reasonably accurate[75].

The observed response time (t_{robs}) of a device under test is a combination of the devices response time (t_{rdev}) and the measurement systems response time (t_{rs}).

The relationship linking these risetimes is

$$t_{robs} = \sqrt{(t_{dev})^2 + (t_{rs})^2}$$

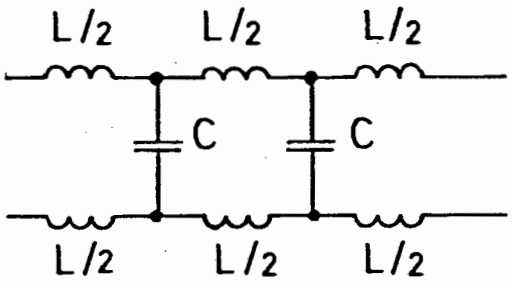

A BALANCED 2-WIRE SYSTEM

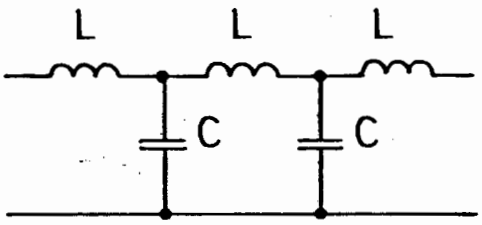

AN UNBALANCED (COAXIAL) SYSTEM

FIGURE 4.12 TRANSMISSION LINE EQUIVALENT CIRCUITS

A good rule of thumb to follow is to have the system response time (t_{rs}) an order of magnitude better than the response (t_{rdev}) of the device under test. This ensures that the percentage error in the observed risetime is less than 0,5 per cent.

4.6 Pulses on Transmission Lines

In order to discuss the performances of pulses on transmission lines it will be necessary to give a brief summary of transmission line theory and parameters

4.6.1 Transmission line analysis

For the purposes of analysis, a transmission line carrying the principal (transverse electromagnetic) wave is usually represented as a distributed constants network having a series impedance $Z = R + j\omega L$ per unit length and a shunt admittance $Y = G + j\omega C$ per unit length. For the special case of perfectly conducting conductors and a lossless dielectric, the series resistance R and shunt conductance G are zero.

The equivalent circuits of a balanced two wire and an unbalanced (coaxial) system appear in Figure (4.12), for this case,

Consideration of the differential equations relating currents and voltages (a full treatment in Appendix I) yields the solutions in equations (4.10) and (4.11).

$$V = V_1 e^{-\gamma z} + V_2 e^{\gamma z} \qquad (4.10)$$

$$I = I_1 e^{-\gamma z} + I_2 e^{\gamma z} \qquad (4.11)$$

where $\gamma^2 = (R + j\omega L)(G + j\omega C)$

The solutions are shown as the sum of two waves, one travelling in the positive Z direction, the other travelling in the negative Z direction.

The voltage to current ratio of the wave travelling in the positive Z direction is $V_1/I_1 = Z_o$

while the ratio for the reflected wave travelling in the opposite direction is $V_2/I_2 = -Z_o$

Z_o is called the characteristic impedance of the line and is related to the primary constants R, L, C and G by

$$Z_o = ((R + j\omega L)/(G + j\omega C))^{\frac{1}{2}}$$

Terminating the line in Z_R at Z = 0 gives

$$Z_R = \frac{V}{I} = \frac{V_1+V_2}{I_1+I_2} = Z_o\frac{(I_1-I_2)}{(I_1+I_2)}$$

on substitution of equations (4.10) and (4.11).

Recombination of these relationships gives the reflection coefficient ρ.

$$\rho = \frac{V_2}{V_1} = \frac{Z_R-Z_o}{Z_R+Z_o} = \frac{-I_2}{I_1}$$

Restating equations (4.10) and (4.11) in hyperbolic form gives

$$V = A_1 \cosh \gamma Z + B_1 \sinh \gamma Z$$

$$I = A_2 \cosh \gamma Z + B_2 \sinh \gamma Z$$

Applying the boundary conditions

$$V = V_R \quad I = I_R \quad \text{at } Z = 0$$

and $$V = V_S \quad I = I_S \quad \text{at } Z = Z_1$$

gives $$V_S = V_R \cosh \gamma Z_1 - Z_0 I_R \sinh \gamma Z$$

$$I_S = I_R \cosh \gamma Z_1 - \frac{V_R}{Z_0} \sinh \gamma Z_1$$

The terminating impedance Z_R is usually made the reference point (i.e. Z = 0). The sending end being to the left of this (i.e. in the -Z direction).

Finally, letting $\ell = -Z_1$ gives

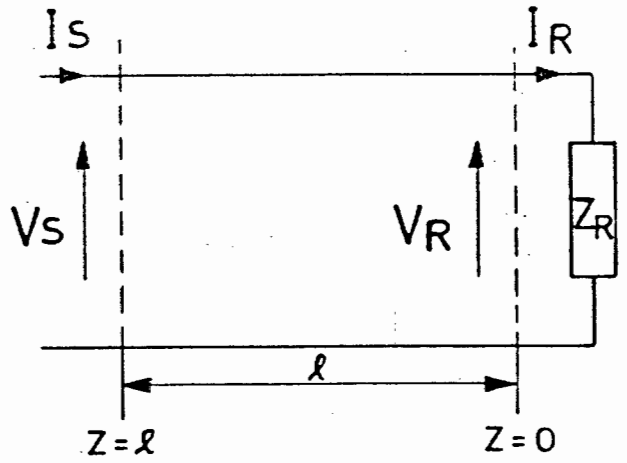

FIGURE 4.13 THE CURRENTS AND VOLTAGES ON A TERMINATED TRANSMISSION LINE.

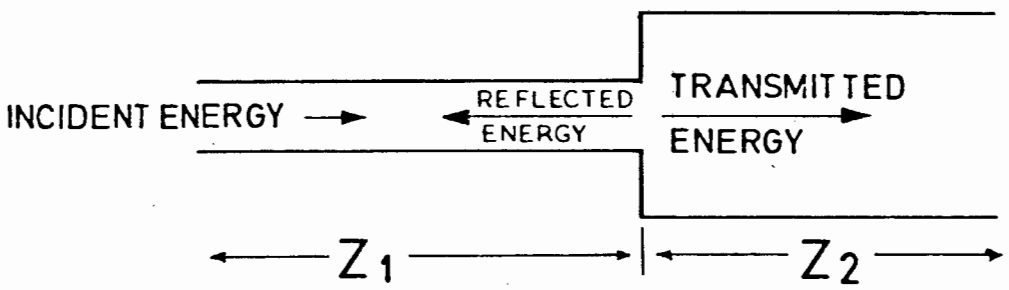

FIGURE 4.14 A STEP IMPEDANCE CHANGE ON A TRANSMISSION LINE.

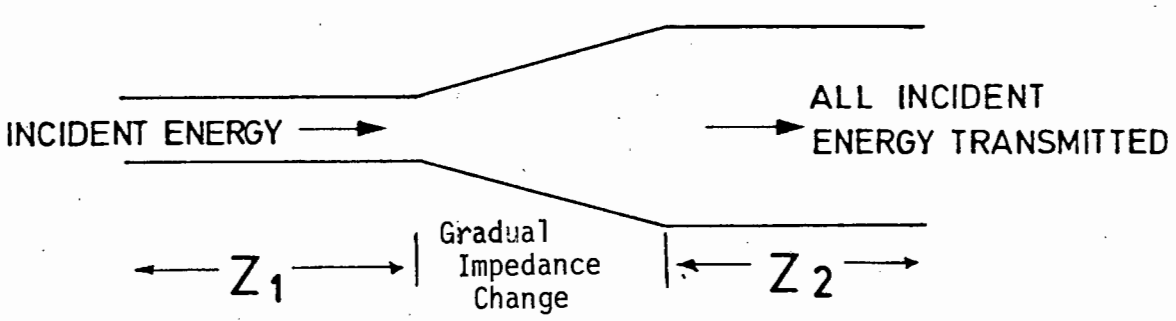

FIGURE 4.15 A TRANSMISSION LINE WITH A GRADUAL IMPEDANCE CHANGE.

$$V_S = V_R \cosh \gamma \ell + Z_0 I_R \sinh \gamma \ell \qquad (4.13)$$

$$I_S = I_R \cosh \gamma \ell + V_R/Z_0 \sinh \gamma \ell \qquad (4.14)$$

where 'ℓ' is measured from the receiving end of the line (Figure (4.13)).

These general transmission line equations relate the voltages and currents at the two ends of the line. Dividing equation (4.13) by equation (4.14) gives the general expression for the impedance of the line (equation 4.15) as seen from $Z = \ell$.

$$Z_{IN} = \frac{V_S}{I_S} = \frac{V_R \cosh \gamma\ell + Z_0 I_R \sinh \gamma\ell}{I_R \cosh \gamma\ell + (V_R/Z_0) \sinh \gamma\ell} \qquad (4.15)$$

With the terminating impedance Z_R equal to the characteristic impedance of the line Z_0, the input impedance of the line becomes Z_0 and the reflected wave reduces to zero. The termination is said to be 'matched'.

All correctly terminated lossless transmission lines present a non-reactive load ($Z_0 = \sqrt{L/C}$) to their signal sources. To energy travelling in the line this load appears as a lossless impedance. Altering the dimensions of the line in any way alters the characteristic impedance of the line, causing a change in the voltage/current values of energy transported by the line.

Any change of impedance that is not gradual causes a discontinuity in the line that causes energy to be reflected back to the source (Figure (4.14)). A gradual impedance change reduces the mismatch, producing a correspondingly smaller signal reflection than the step change in impedance. If the change is gradual enough it is possible to reduce the reflected energy to a negligible amount (Figure (4.15)).

These considerations are extremely important in measurement systems using high frequencies as any discontinuities may introduce extraneous signals that effect measurement accuracy. Care must always be taken, therefore, to ensure that cables and connections are always correctly matched and terminated.

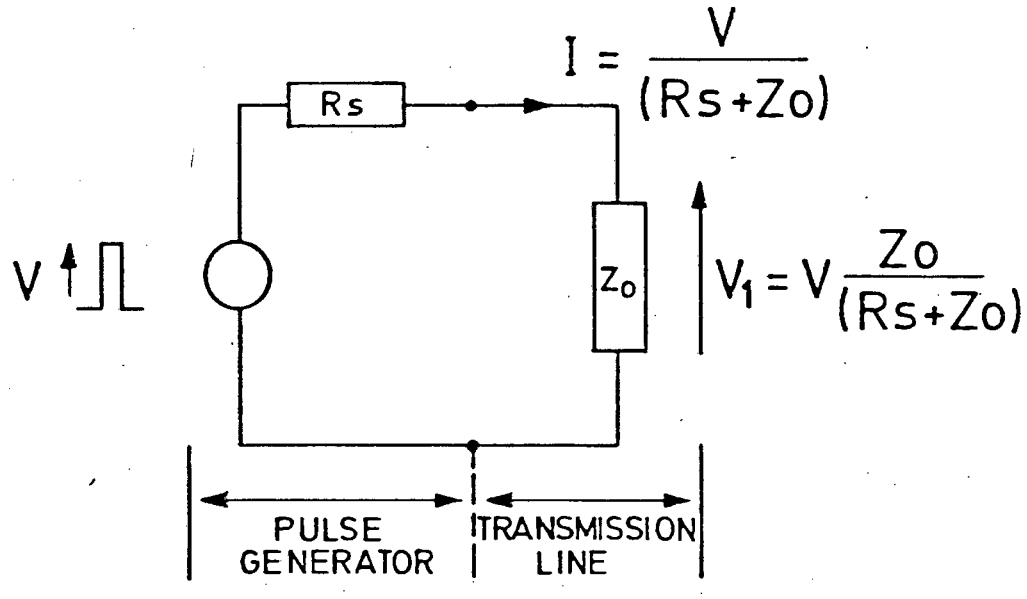

FIGURE 4.16 THE VOLTAGE AND CURRENT RELATIONSHIPS AT THE INPUT TO THE TRANSMISSION LINE.

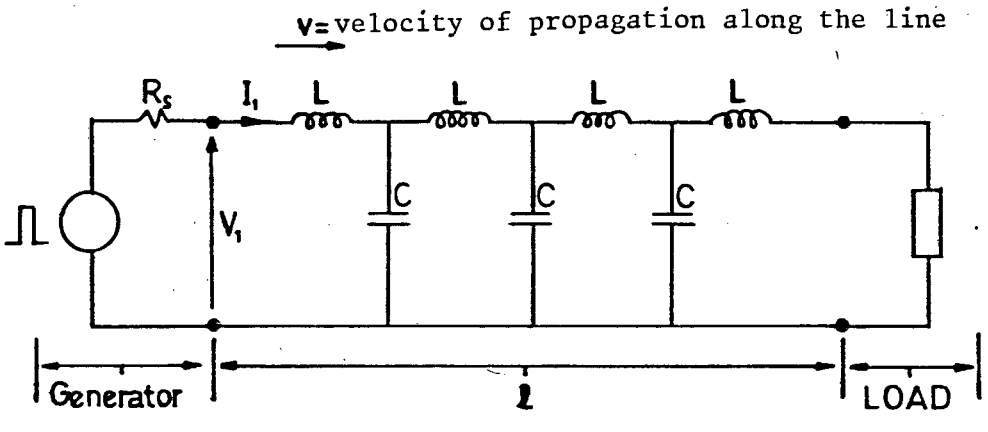

FIGURE 4.17 PULSE PROPAGATION ALONG A LINE.

TERMINATION	ρ	SEEN FROM SOURCE END	$1+\rho$	SEEN FROM LOAD END
MATCHED $Z_R = Z_o$	0	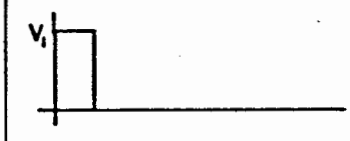	1	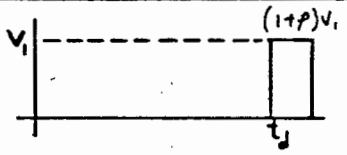
SHORT CIRCUIT $Z_R = 0$	-1	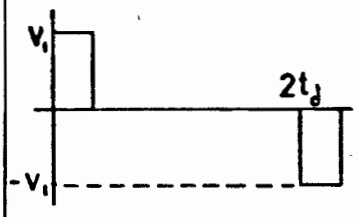	0	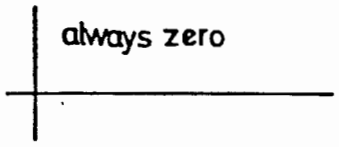
OPEN CIRCUIT $Z_R = \infty$	+1	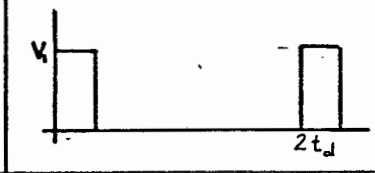	2	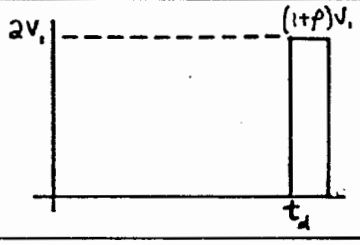
$R_L < Z_o$	-ve	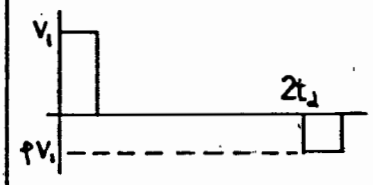	+ve	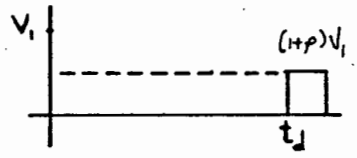
$R_L > Z_o$	+ve	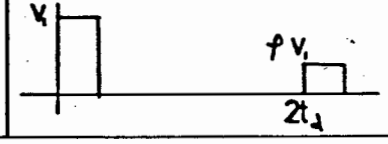	+ve	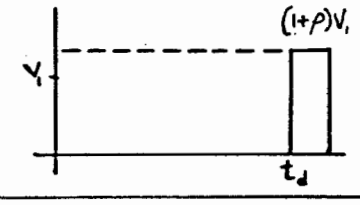

FIGURE 4.18

THE SIGNAL SEEN AT THE INPUT AND OUTPUT OF THE LINE FOR VARIOUS RESISTIVE TERMINATIONS.

4.6.2 The effect of various unmatched resistive terminations on the reflection of pulses from the end of a transmission line

When a pulse signal is first applied to the input end of a line, the line current and voltage established depend only on the relative values of the source impedance and the characteristic impedance of the line. The form or value of the impedance at the output end is immaterial, since it is still seperated by the total delay of the line from the input end.

The amplitude of a voltage pulse launched into the line is given by

$$V_1 = V\ (Z_0/(R_S + Z_0))$$

where V is the internal generator pulse amplitude and R_S is its internal resistance (Figure (4.16)). The corresponding current that flows is given by

$$I_1 = V/(R_S + Z_0).$$

The pulse travels down the line progressively charging and discharging the distributed capacitance to V_1 and supplying line current I_1, to the distributed inductance (Fig. (4.17)). After a time $t_d = (\ell/v)$ the pulse arrives at the load. If the termination is equal to Z_0, the problem is trivial as the $Z_0 = (V_1/I_1)$ ratio is satisfied and the pulse appears across the load for the duration of its pulse length.

With $R_L \neq Z_0$, however, the (V_1/I_1)ratio is no longer satisfied and reflections are set up in such a way as to make the ratio of nett voltage and nett current at the load end equal to R_L. The amplitude of the pulse seen at the receiving end is given by $(1 + \rho)V_1$ while the amplitude of the reflected pulse sent back to the receiving end is given by (ρV_1) (Figure (4.18)). V_1 is the incident pulse amplitude and ρ is the reflection coefficient as defined in (4.6.1).

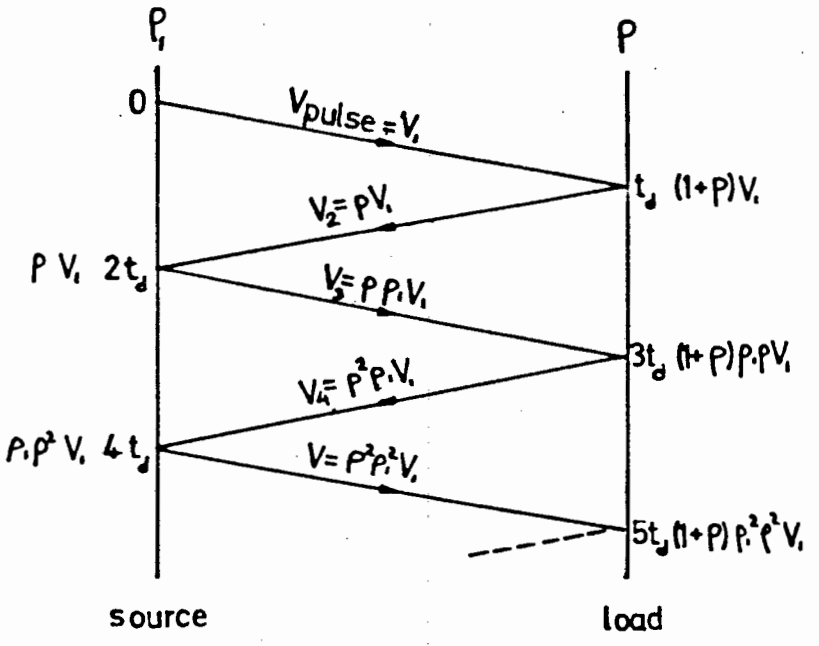

FIGURE 4.19 THE LATTICE DIAGRAM

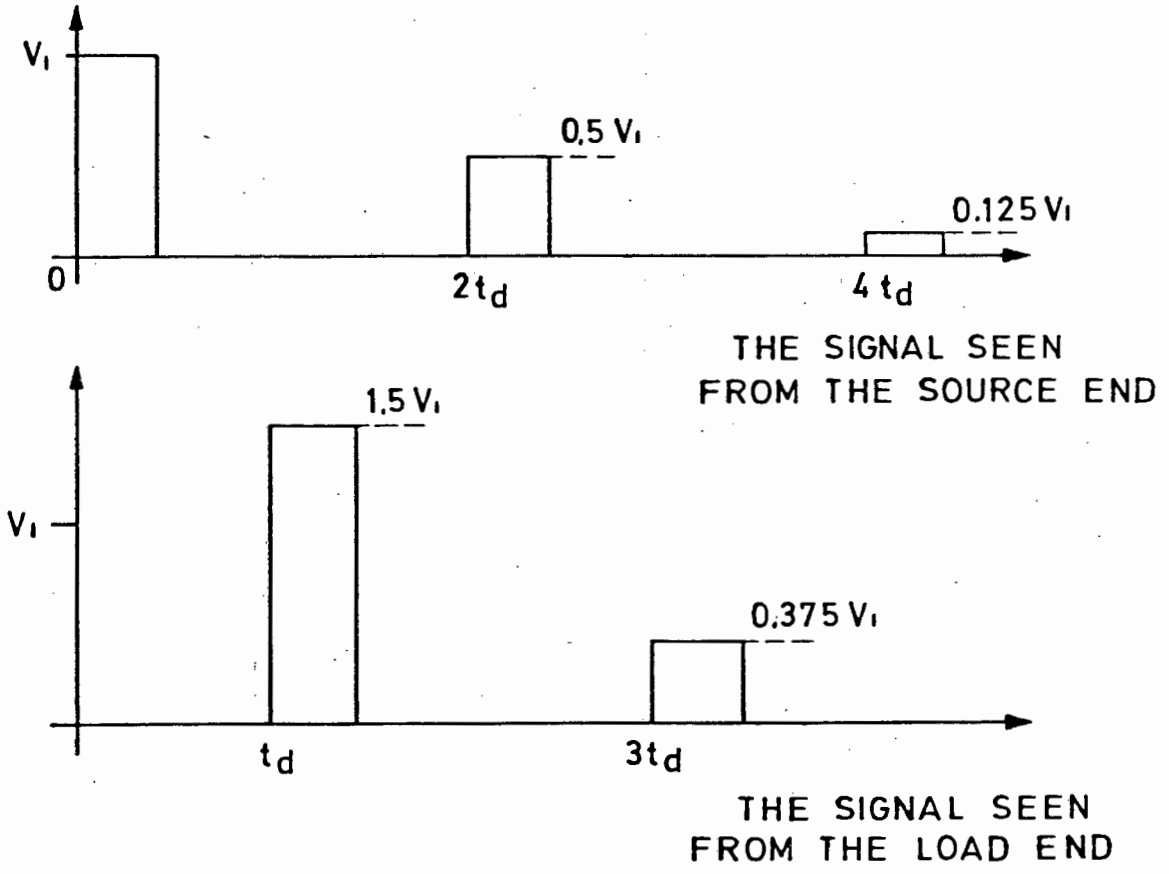

FIGURE 4.20 REFLECTED PULSES ON A TRANSMISSION LINE SHOWN FOR ρ=0.5 AT BOTH ENDS.

If the source is not matched to the line the reflected pulse produces a further reflection ($\rho_1 \rho V_1$) at the source end, where ρ_1 is the reflection coefficient at that end. This general case with the reflections continuing at both ends can be best illustrated using a reflection chart called a lattice diagram (Figure (4.19)). A graphical representation containing the same information as the lattice diagram can be found in Figure (4.20)).

4.6.3 The effect of inductive and capacitive components in the termination

In practice there are usually additional reactive components such as series inductance and shunt capacitance in the termination. An analysis of the effect of these components on the reflected pulse is given in Appendix (J).

The effect of the reactive components is to give a complex reflection coefficient which in turn introduces exponential terms into the reflected pulses. Fig.(4.21) illustrates this for a number of termination combinations. The dotted lines show the equilibrium values that would be reached if the incident pulse lengths were long enough.

The effect of shunt capacitance as shown in the last case has been to introduce a risetime, with time constant of

$$\tau = R_L Z_0 C/(R_L + Z_0) \qquad \text{(Appendix J)}$$

In order to illustrate the importance of this result, assume that a square pulse with negligible rise and fall times is travelling along a 75Ω line to an oscilloscope. The oscilloscope has an input impedance of 10MΩ in parallel with 20 pF (Fig.(4.22)). Substituting these values in the above equation shows that the resulting pulse displayed on the scope will have a risetime of 3,3 nS. Using 50Ω coaxial cable and terminating it correctly reduces this risetime to 1,2 nS.

This demonstrates how much care must be taken in designing a high speed

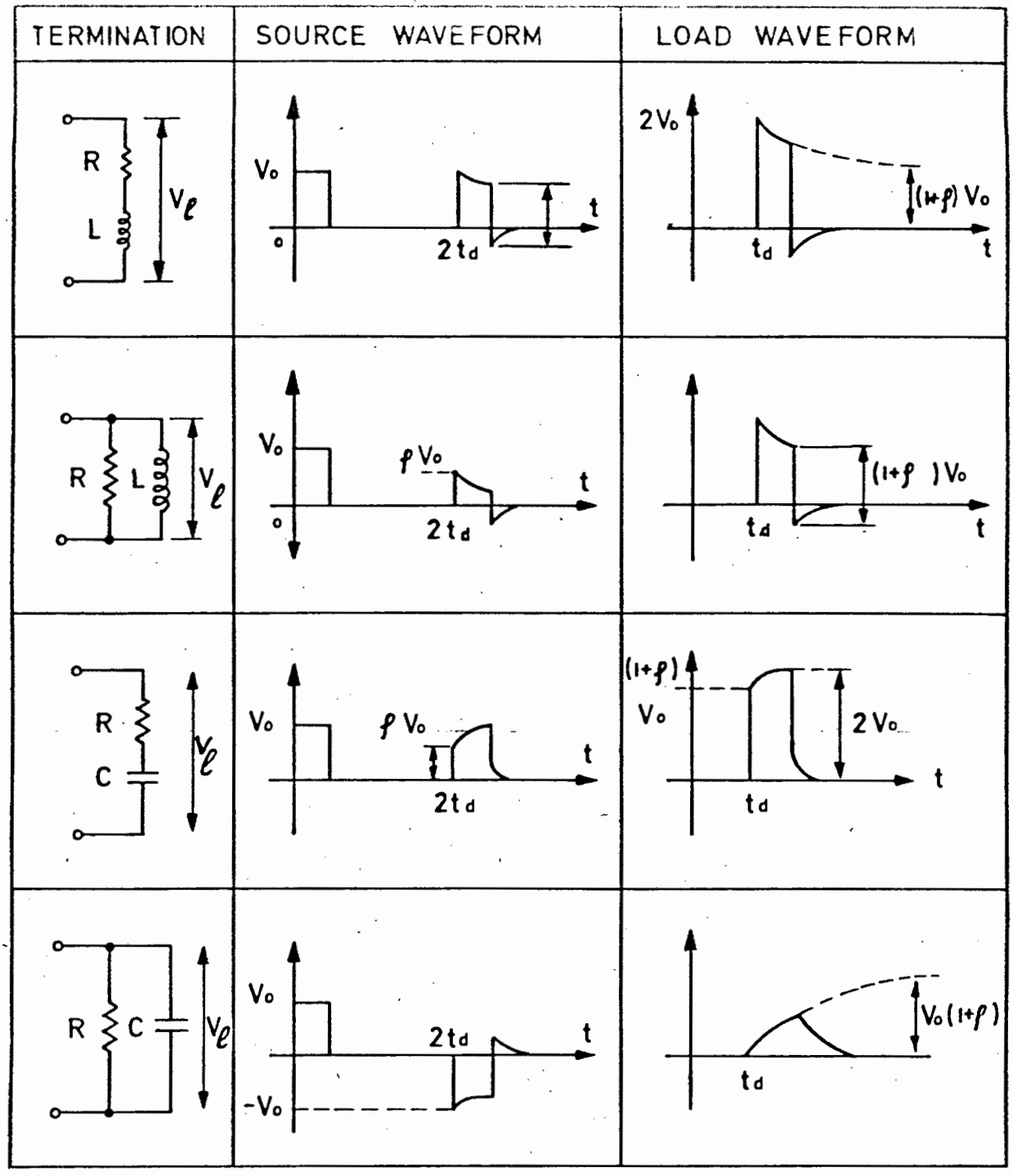

REFERENCE 75

FIGURE 4.21 REFLECTED PULSES OBTAINED WITH VARIOUS REACTIVE TERMINATIONS.

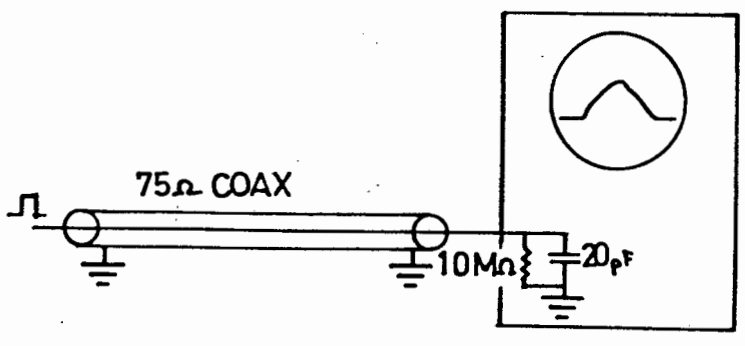

FIGURE 4.22 THE EFFECT OF SHUNT CAPACITANCE ON RISETIME.

pulse measurement system.

4.6.4 Practical coaxial transmission lines

Practical coaxial transmission lines suffer from a number of imperfections[75,76,77,78].

(a) Low frequency or DC series resistance losses.

(b) High frequency skin effect series resistance losses.

(c) Ultra-high frequency (UHF) dielectric losses.

(d) UHF leakage loss through the holes of the cable braid.

(e) Mode conversion losses (due to UHF signals changing from TEM to TE_{11} mode in the coax and not being returned at the receiving end).

(f) Rare shunt conductance losses.

(g) Inductance of individual wires in the coaxial braiding.

The effect of (d) and (g) can be reduced to a large extent by using cables with a combination aluminium tape/copper braid outside conductor. This shielding also helps to combat the cross talk problems that are encountered in fast pulse work.

Not very much can be done about (b) and (c) and these frequency related losses are responsible for causing pulse distortion on transmission lines.

Conductance loss (f) is small and reasonably constant over a large frequency range, and therefore contributes little to pulse distortion.

4.6.5 Pulse distortion on coaxial transmission lines

For the purposes of analysis it has been assumed that a pulse or step function will propagate along a line without changing shape in any way (i.e. the line was assumed to be ideal). Unfortunately this is not so and a pulse travelling on a real line will change shape as a result of attenuation and dispersion. Dispersion simply indicates a condition where the phase velocity

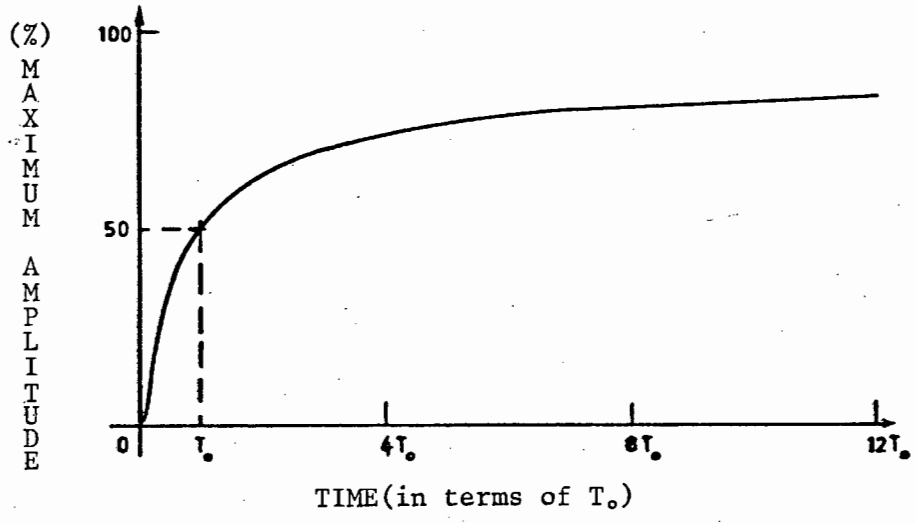

FIGURE 4.23 THE STEP RESPONSE OF A SKIN EFFECT LIMITED COAXIAL CABLE.

of a signal depends on its frequency, regardless of what effects are responsible for this dependence.

A single pulse is composed of a continuous spectrum, the various components of which add at the input to give the applied pulse waveform. If all the spectral components of the pulse propagate down the line at the same velocity with no attenuation, then they will add at any given point on the line to produce an identical waveform to that at the input.

Distortion comes about when attenuation and/or velocity of propagation differs for various spectral components.

The effects of loss and dispersion on the pulse response of a transmission line can best be shown by the step response. Nahman and Wigington[77] investigated the transient response of coaxial cables in 1957, and showed that simple skin effect is the dominant distortion mechanism. Their analysis showed a unit step function input pulse, after traversing a length 'ℓ' of cable has a shape given by:

$$V = 1 - \text{erf}\ (\ell\alpha_o/2\sqrt{\Pi f_o t})$$

where α_o is the attenuation (in Nepers/m) at some particular frequency f_o (Hertz and t is the time (sec), excluding the normal delay of the line (Figure (4.23)). As can be seen from the figure the leading edge of the step rises slowly to the 50 per cent mark and then very slowly to the final value equal to the input pulse amplitude.

Kirsten[78] normalised the abscissa and defined T_o as the time for the wavefront to attain 50 per cent amplitude. T_o can be calculated from

$$T_o = 4{,}55 \times 10^{-12}(A^2\ell^2) \text{ seconds},$$

where A = attenuation of the cable at 1000 MHz in dB/m.

ℓ = length of cable in metres.

TABLE 4.1	
PERCENTAGE AMPLITUDE	RISETIME ($\%T_o$)
10	0.17
20	0.28
50	1.00
70	3.10
90	29.00
95	110.00

PERCENTAGE AMPLITUDE
VERSUS
RISETIME

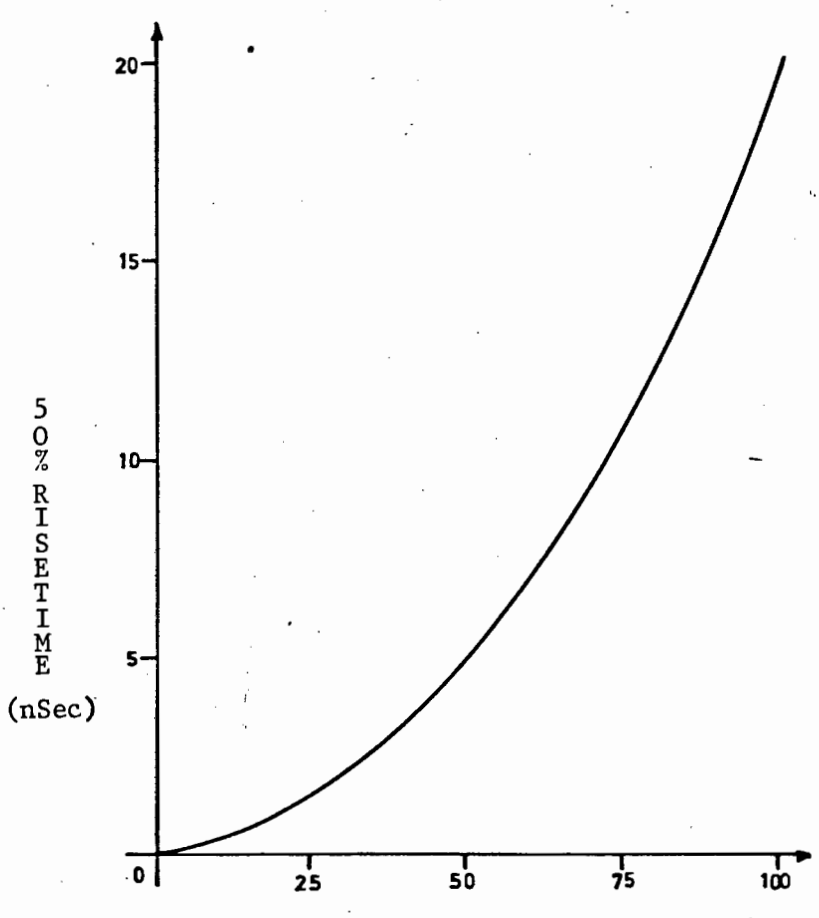

FIGURE 4.24 STEP FUNCTION RESPONSE IN RG58U COAXIAL CABLE WITH ATTENUATION OF 0.65dB per METER.

In cases where the attenuation is known only at a frequency other than 1000 MHz

$$T_o = (4{,}55 \times 10^{-3}\ \alpha_f{}^2 \ell^2)/f$$

where α_f = attenuation of cable at frequency f in dB/m

f = frequency (Hertz)

Table (4.1) details the time taken (in terms of T_o) for the pulse to reach various amplitudes. Notice that the 10 per cent to 90 per cent response time of such a skin-effect limited cables is 28,83 T_o.

A plot of T_o versus cable length appears in Fig. (4.24). As can be seen, the $T = \sqrt{\Sigma t_r^2}$ law (section 4.5) does not apply in the case of a cable. In order to find the T_o value for a cable composed of composite lengths it is necessary to calculate T_o from the equations given, using the total length of the composite cable for ℓ.

4.7 Resolution versus rise-time

Time resolution, as opposed to amplitude resolution (which is related to system noise), is primarily limited by system rise-time. It refers to the ability of a TDR system to distinguish between two point discontinuities that are located close together and may be defined as:

The minimum time spacing of two equal point discontinuities which gives rise to a 50 per cent valley between the two displayed reflections.[33]

In equation form $d = (\frac{v\ t_{rs}}{4})$

where d = resolution

v = velocity of pulse propagation in the system

t_{rs} = system rise-time (or pulse rise-time, if system rise-time is at least 10 times that of the pulse)

In section 4.6.5 it is described how high frequency transmission line losses affect system rise-time. A consequence of these losses is that it may be possible to resolve two closely spaced discontinuities 2 metres down a coaxial line while the same two discontinuities may appear smeared together at 10 metres.

Care must be taken not to degrade system rise-time by careless use of bad connectors and long runs of coaxial cable.

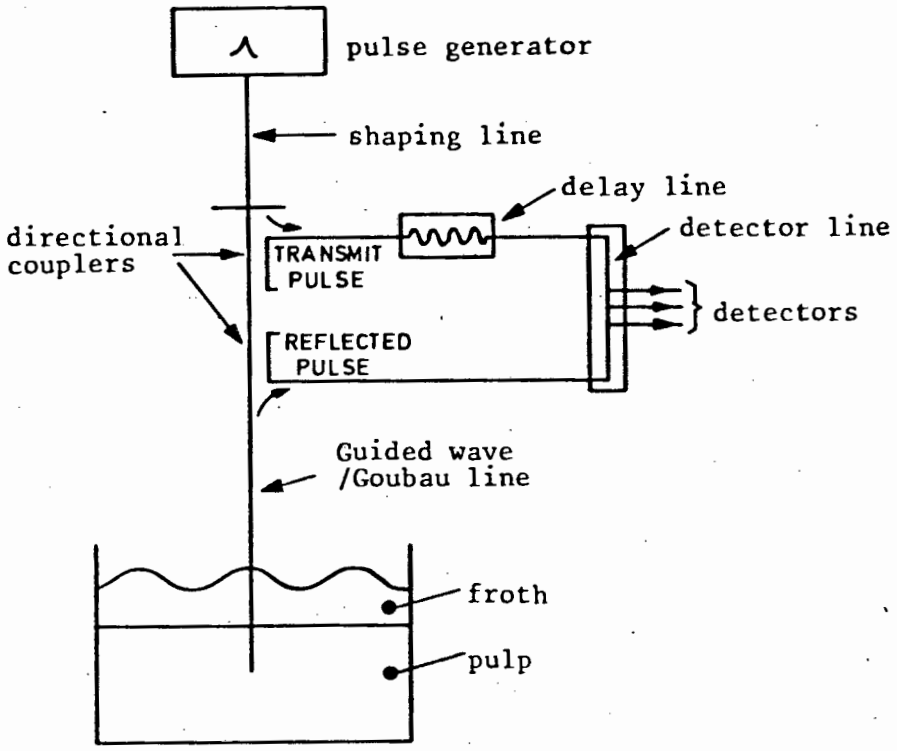

FIGURE 5.1 THE TDR LEVEL MEASUREMENT SYSTEM

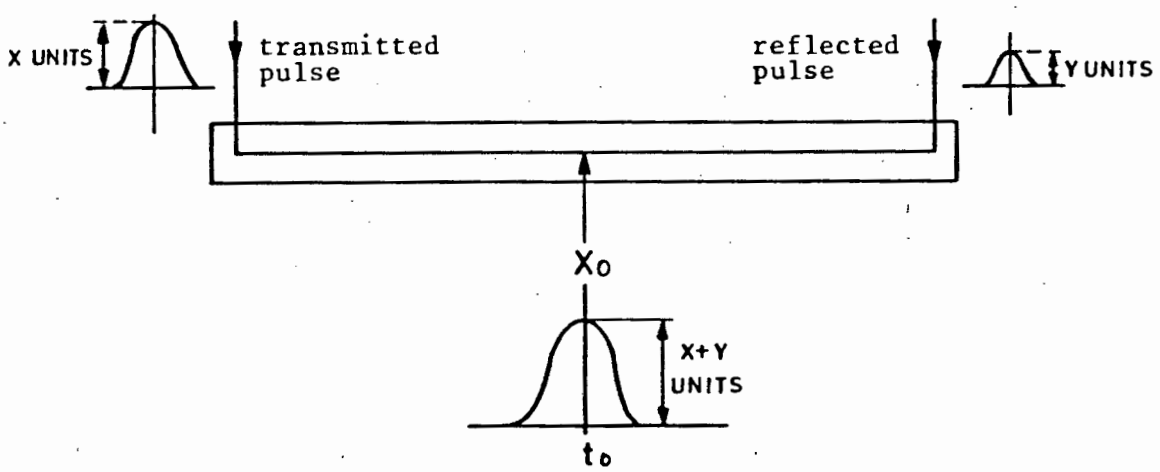

FIGURE 5.2 THE DETECTOR LINE WITH THE COMPOSITE REFLECTED AND TRANSMITTED PULSE PEAKING AT TIME t_o.

5. A TIME DOMAIN REFLECTOMETRY SYSTEM FOR LIQUID LEVEL MEASUREMENT AND CONTROL IN MINERAL FLOTATION CELLS

In previous chapters, a number of microwave measurement systems were discussed and two were proposed for liquid level measurement in flotation cells. After the experimental determination of the flotation froths' properties it was decided that a system incorporating TDR techniques should be developed.

5.1 The Envisaged Liquid Level Measurement System

A short description of a similar system has already been given in Section 2.2.8. A more comprehensive discussion of the instrument will be given here.

A block diagram of the basic TDR system, providing information about liquid level, is shown in Figure (5.1).

The generated pulse passes through the pulse shaping line (Section (5.9)) into the guided-wave transmission line (Section (5.10)). At the air/liquid interface it encounters a sudden impedance change and is reflected back towards the pulse generator.

The directional couplers selectively couple the transmitted and reflected pulses, and feed them into the signal processing section of the instrument. A length of delay line delays the transmitted pulse sufficiently to allow it to arrive in a length of 'detector' line (Figure (5.2)) at the same time as the reflected pulse. The detector line is merely a length of coaxial cable with a number of detection points on it.

5.2 The Operation of the Detector Line

The coupled reflected and transmitted pulses enter the detector line from opposite ends. The 'slide' past one another and add algebraicly, giving a maximum voltage where both pulse peaks coincide. Call this point x_o and the time of coincidence, t_o.

Figures (5.3) through (5.7) detail the space distribution of the transmitted, reflected and composite (i.e. combined transmitted and reflected) pulses on the detector line at various times.

Figure (5.3) shows the position at time $t = t_o - \Delta t_1$. The pulses have just entered the detector line and are moving towards position x_o. The voltage at x_o is zero.

Figure (5.4) shows the pulses at time $t = t_o - \Delta t_2$. Both transmitted and reflected pulses have reached x_o, although their peaks have yet to. The voltage at x_o is the sum of the reflected and transmitted pulse voltages seen there (i.e. $V_{out} = V_t + V_r$).

At time $t = t_o$, the pulse peaks coincide at x_o (Figure (5.5)) to give an output voltage equal to the sum of the individual pulse peaks at x_o.

After time t_o(i.e. $t = t_o + \Delta t_2$), the pulses have not completely moved away from position x_o, although their peaks have passed it (Figure (5.6)). Voltage output at x_o is once again the sum of the component pulse voltages at that point (i.e. $V_{out} = V_t + V_r$). Note that, because of time and pulse symmetry, the output voltage for this case is the same as for Figure (5.4).

Figure (5.7) shows the situation at time $t = t_o + \Delta t_1$. Both transmitted and reflected pulses have passed x_o and are leaving the detector line. Output voltage at x_o is once again equal to zero.

If no attenuation took place in the froth it would be possible to build a very simple level detection system by placing a number of detectors, set to trigger on the composite pulse peak, at positions along the detector line. Variations in liquid level would cause the reflected pulse arrival time to vary, causing the composite pulse to peak under a different detector depending on the liquid level at the time.

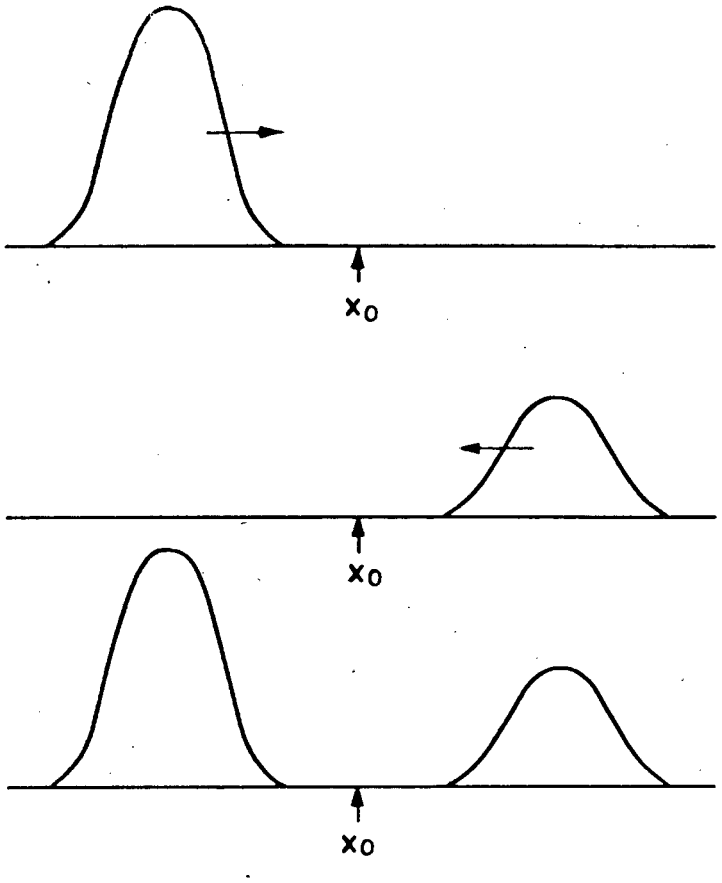

transmitted pulse at $t = t_o - \Delta t_1$

reflected pulse at $t = t_o - \Delta t_1$

composite pulse at $t = t_o - \Delta t_1$

FIGURE 5.3 SPACE DISTRIBUTION OF PULSES ON THE DETECTOR LINE AT $t = t_o - \Delta t_1$

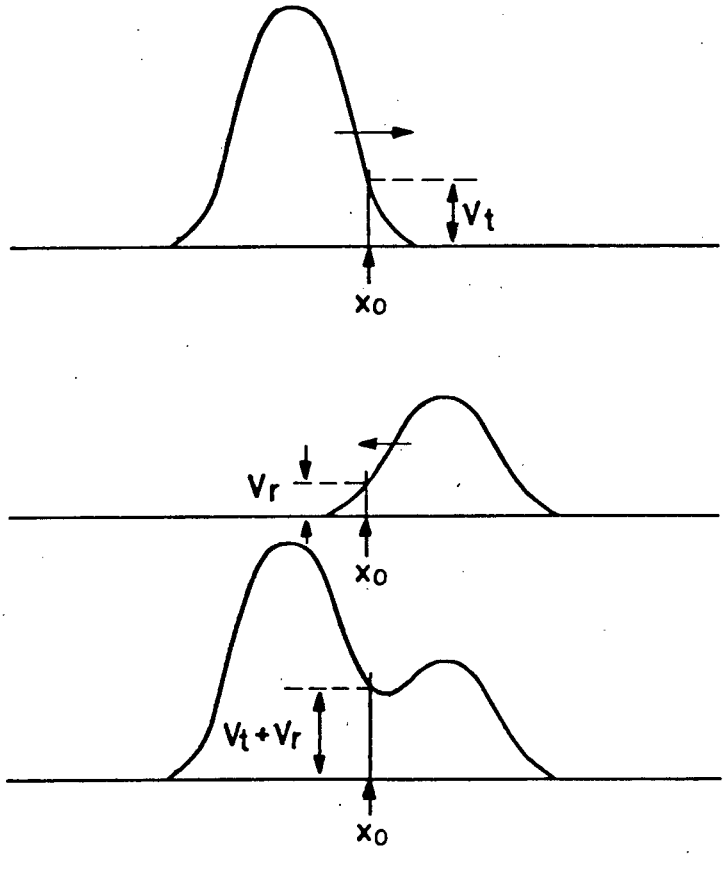

transmitted pulse at $t = t_o - \Delta t_2$

reflected pulse at $t = t_o - \Delta t_2$

composite pulse at $t = t_o - \Delta t_2$

FIGURE 5.4 SPACE DISTRIBUTION OF PULSES ON THE DETECTOR LINE AT $t = t_o - \Delta t_2$

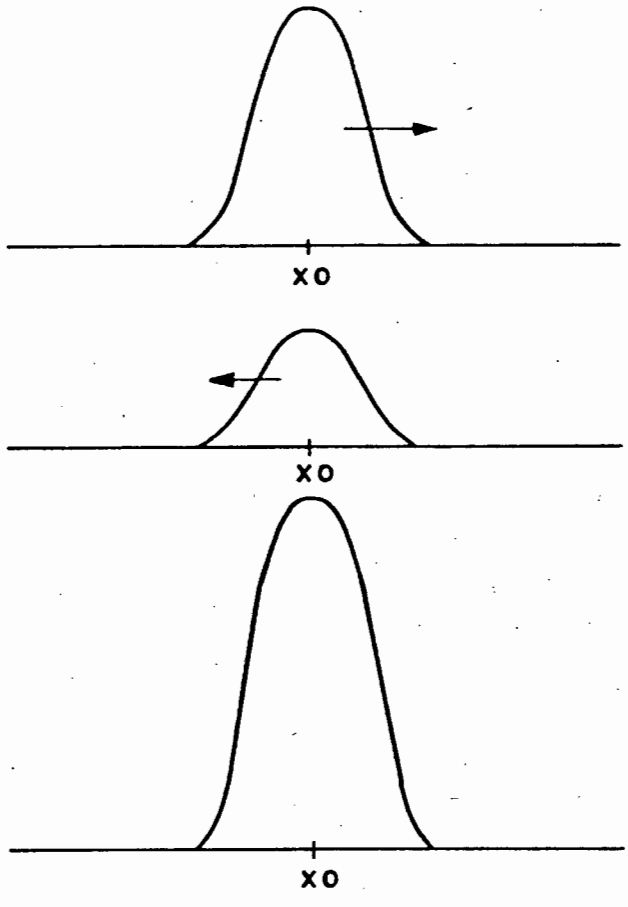

transmitted pulse at $t = t_o$

reflected pulse at $t = t_o$

composite pulse at $t = t_o$

FIGURE 5.5 SPACE DISTRIBUTION OF PULSES ON THE DETECTOR LINE AT $t = t_o$

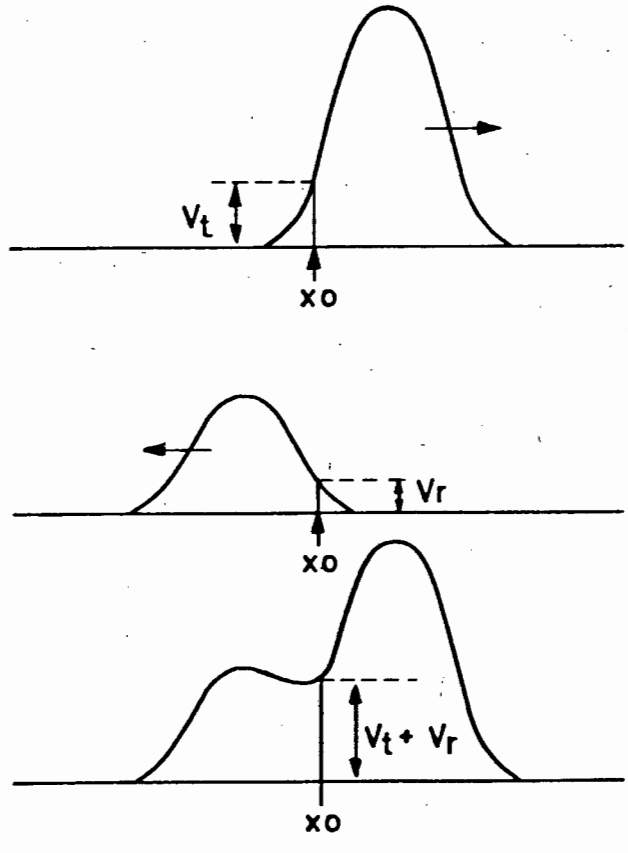

transmitted pulse at $t = t_o+\Delta t_2$

reflected pulse at $t = t_o+\Delta t_2$

composite pulse at $t = t_o+\Delta t_2$

FIGURE 5.6 SPACE DISTRIBUTION OF PULSES ON THE DETECTOR LINE AT $t = t_o+\Delta t_2$

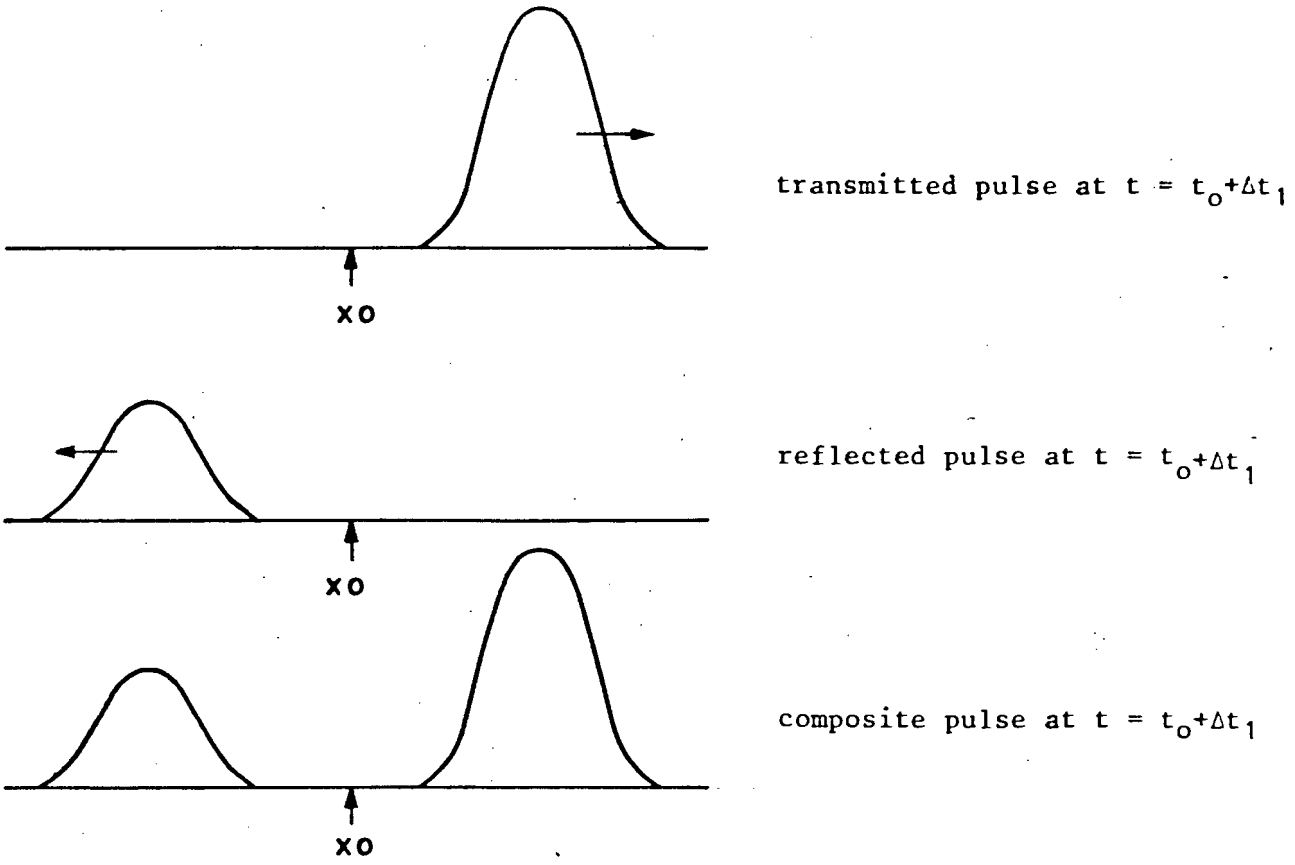

FIGURE 5.7 SPACE DISTRIBUTION OF PULSES ON THE DETECTOR LINE AT t = $t_o+\Delta t_1$

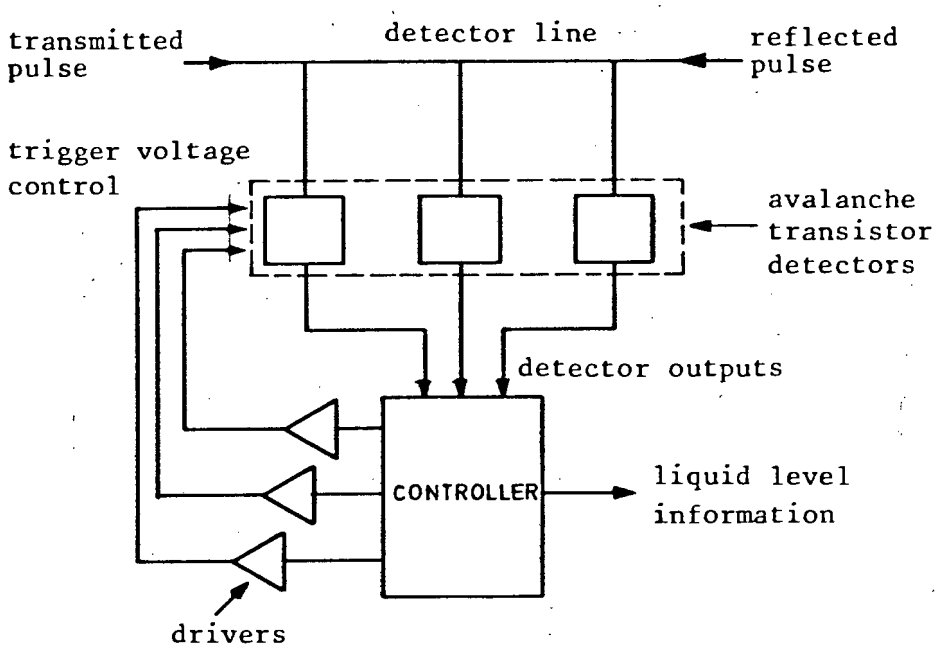

FIGURE 5.8 A PEAK DETECTION SYSTEM UTILIZING AUTOMATIC LEVEL CONTROL.

Unfortunately,variations in composite peak height unrelated to pulse arrival time, are caused by attenuation in the froth. This complicates the simple measurement system proposed above by imposing the need for some means of automatic level control (ALC) to compensate for such peak variations. A detection system utilising ALC was considered (Figure (5.8)). Only three detectors are shown for the purposes of illustration. The controller ensures that no more than one detector triggers at any time by adjusting the detector's trigger voltage level.

Construction is complicated by the fact that no two detectors (tunnel diode aided avalanche transistors) require the same bias current for a given trigger voltage. This means that individual control of each detector is necessary. A further problem is that the detectors cannot differentiate implicitly between pulses of the same amplitude arriving at different times. Time gating of unwanted signals from the sides of the flotation cell and people moving nearby would have to be performed by the controller, no easy task at nanosecond pulse intervals.

A simpler, more effective means of froth attenuation compensation was sought.

5.3 Sampling and the Detector Line

The essence of the attenuation compensation technique to be described is that it compares the composite transmitted and reflected pulse voltages at two points on the detector line to give an output related only to reflected pulse arrival time.

Figure (5.9) shows the space-distribution of reflected and transmitted pulses simultaneously peaking at position x_0 and time t_0. Consider now what is seen, at time t_0, at positions x_{-1} and x_1, equal distances either side of x_0. The voltage output at x_{-1} is $V_{out} = (V+v)$ and because of pulse and time symmetry, the output at x_1 is the same.

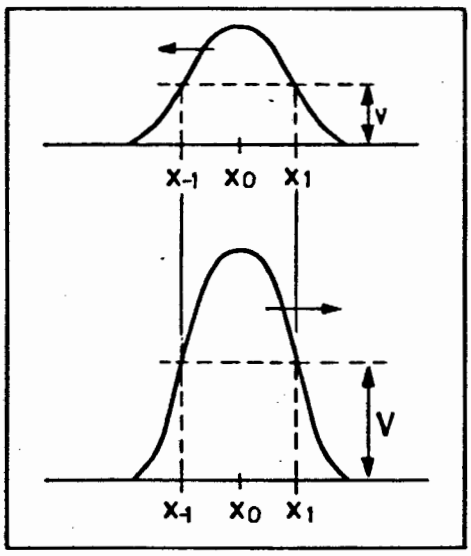

FIGURE 5.9

THE COMPONENT PULSES PEAKING SIMULTANEOUSLY AT x_o AND t_o. DETECTOR OUTPUTS ARE BOTH (V+v).

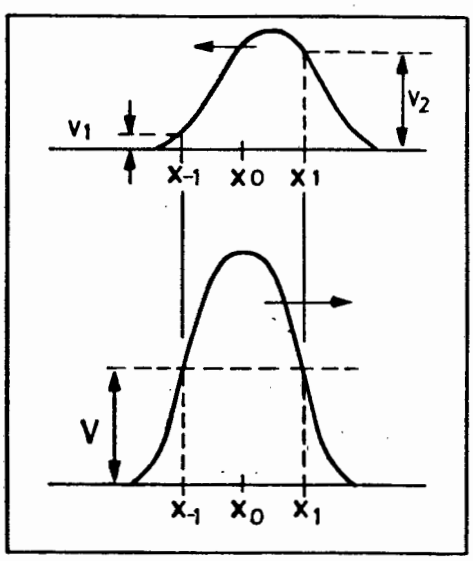

FIGURE 5.10

THE COMPONENT PULSES WITH THE REFLECTED PULSE DELAYED AND NO LONGER PEAKING AT x_o AND t_o OWING TO v_2 BEING GREATER THAN v_1, VOLTAGE OUTPUT AT x_1 IS GREATER THAN THAT AT x_{-1}.

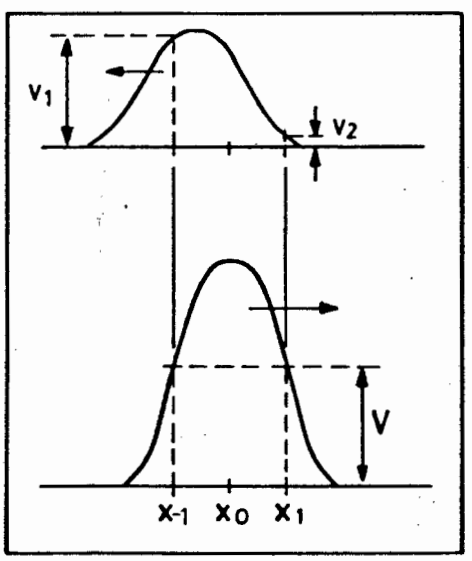

FIGURE 5.11

THE COMPONENT PULSES WITH THE REFLECTED PULSE ARRIVING EARLIER AND NO LONGER PEAKING AT x_o AND t_o OWING TO v_1 BEING GREATER THAN v_2, VOLTAGE OUTPUT AT x_{-1} IS GREATER THAN THAT AT x_1.

Assume now that the reflected pulse is delayed slightly in time (Figure (5.10)) and no longer peaks at x_0, at time t_0. As a consequence, the voltage seen at x_1 at time t_0 will be larger than that seen at x_{-1}, at the same time.

A similar situation exists when the reflected pulse arrives slightly earlier in time (Figure (5.11)). The voltage as seen at x_{-1} at time t_0 will be larger than that seen at x_1, at the same time.

The output of the sampling detectors will only be equal for a reflection from a certain point on the Goubau line which delays the reflected pulse the right amount, allowing it to peak at position x_0 and time t_0.

By sampling the composite pulse voltages at x_1 and x_{-1}, equal distances either side of the equilibrium position x_0 on the detector line, it is possible to detect changes in reflected pulse arrival time caused by variations of liquid level in a flotation cell. Comparing the voltages obtained gives the direction of liquid level change.

Variations in reflected pulse amplitude caused by the flotation froth do not affect the measurement at all. This is owing to the fact that voltages obtained at the sampling points are both attenuated by the same amount and comparing them gives the same answer, with or without the froth present.

This signal processing method allows only changes in reflected pulse arrival time to be detected and ignores attenuation effects completely. By looking at a particular time 'window' it automatically gates out any spurious signals that might be present due to the flotation cell or people moving nearby.

5.4 Timing Control

Accurate timing control is necessary to ensure that the detectors, at points x_{-1}, and x_1, sample simultaneously and at time t_0.

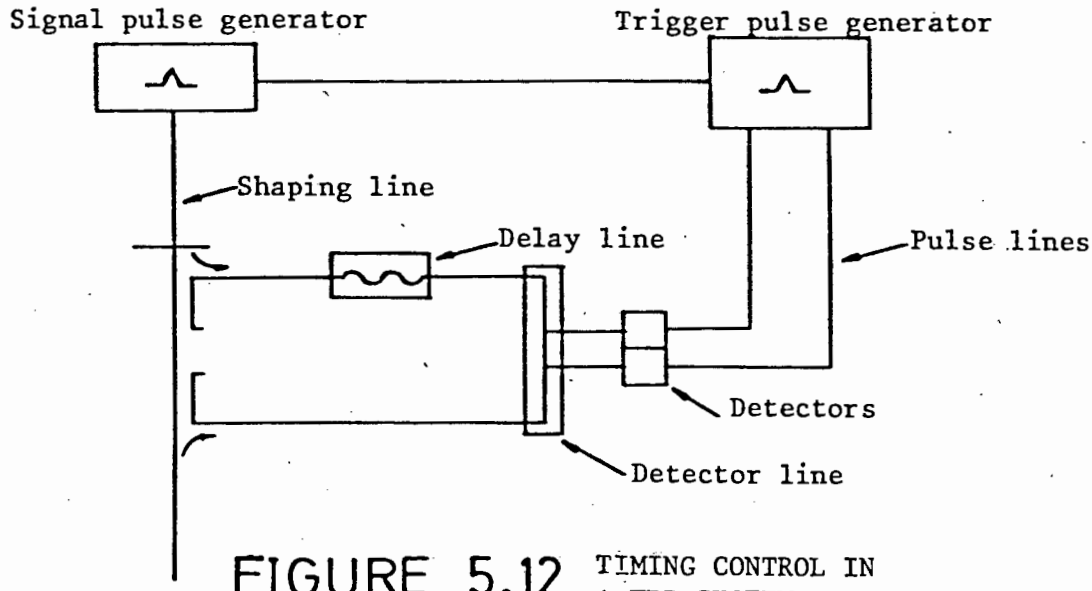

FIGURE 5.12 TIMING CONTROL IN A TDR SYSTEM

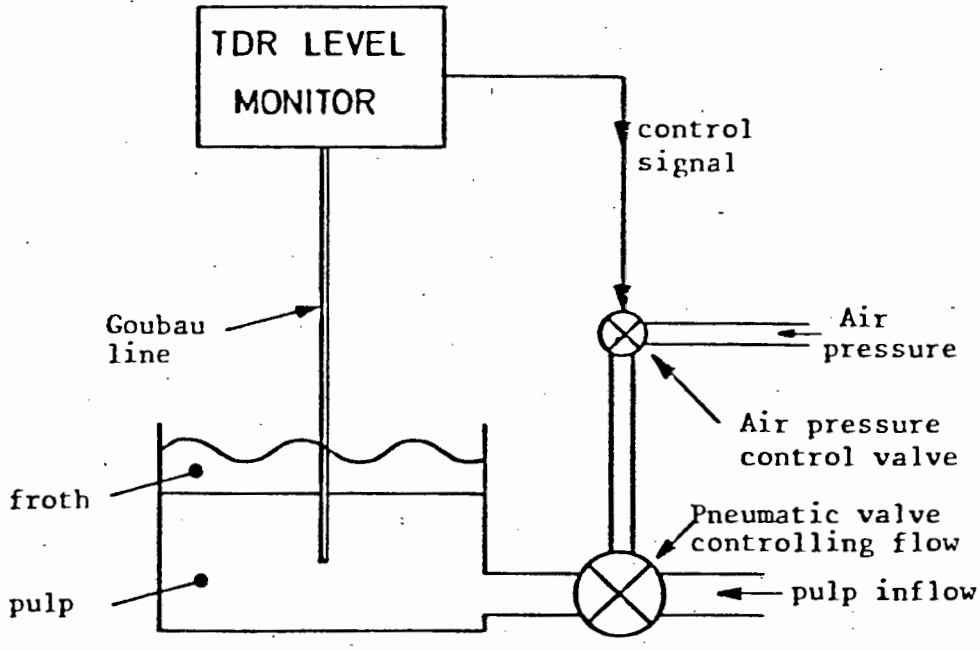

FIGURE 5.13 LIQUID LEVEL CONTROL IN A FLOTATION CELL

A pulse generator producing fast trigger pulses provides this control (Figure (5.12)). Separate lines are used to supply the trigger pulse to each sampling detector in order to prevent them from interfering with one another and triggering spuriously.

The length of the pulse lines determines the correct sampling time for the detectors.

Further information about the trigger pulse generator can be found in section (5.8).

5.5 Application in an Industrial Environment

The envisaged application of this system is for liquid level control in mineral flotation cells. In the flotation process (Appendix A) it is necessary to keep the liquid level constant to ensure efficient extraction.

Using a TDR system with a fixed delay line and the detection system described in Section 5.3 it is possible to monitor and automatically keep the liquid level in a cell at a preset value. Figure (5.13) shows the TDR system in such an application. The instrument monitors the liquid level and feeds back a control signal to the pneumatically operated valve controlling the flow of pulp into the cell.

A fall in liquid level will result in the valve being opened further to allow a faster flow of pulp into the cell. Once the preset liquid level is again reached, the TDR system will automatically adjust the pulp flow to hold it there.

A similar procedure will adjust for a rise in liquid level.

The desired liquid level is set by adjusting the height of the instrument above the tank so that the output from the detectors on the detector line are equal

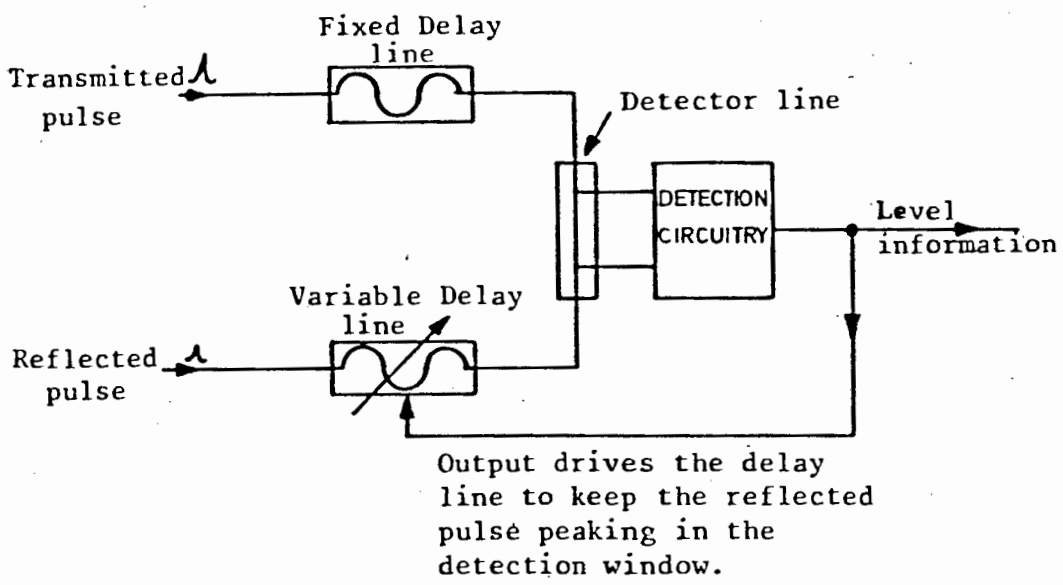

FIGURE 5.14 CONTINUOUS LEVEL MONITORING

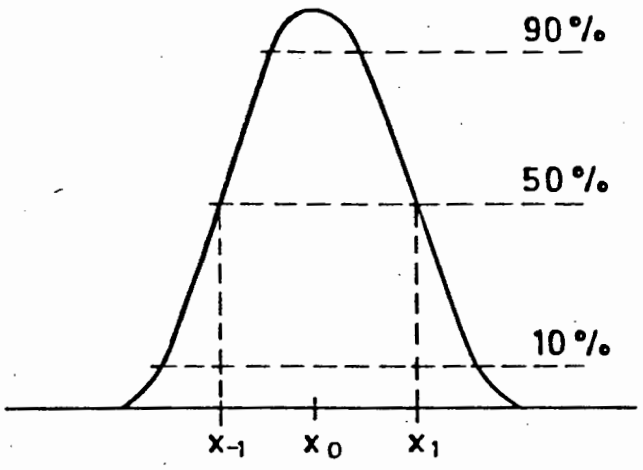

FIGURE 5.15 DEMONSTRATES THAT THE STEEPEST CHANGE IN AMPLITUDE OCCURS AT THE 50% PULSE AMPLITUDE LEVEL

(i.e. so that the reflected pulse 'peaks' at position x_o and time t_o) for that liquid level.

Adjusting the height of the TDR instrument above the flotation cell ensures that the reflected pulse occurs in the sampled composite pulse 'window' for a certain liquid level. Incorporating a variable delay line to automatically do this (Figure (5.14)) allows the instrument to continuously monitor liquid level. The amount of delay necessary to place the reflected pulse in the sampled window being a measure of liquid level in the flotation cell.

Wideband variable delay lines pose a unique design problem and are dealt with in Section (5.14).

5.6 Selecting the Sampling Points on the Detector Line

Care must be taken when positioning the sampling points as they have a direct bearing on resolution.

Looking at Figure (5.15) shows that the steepest change in pulse amplitude occurs at the 50 per cent amplitude point on the leading and trailing edges of the reflected pulse. Remember also that the output from the detectors is the sum of two voltages, a constant term due to the transmitted pulse and a variable term dependent on the position of the reflected pulse on the detector line at the time of sampling. Therefore, in order to maximize the voltage change in the output of the detectors for a given variation in liquid level, it is necessary to ensure that they are a distance on the detector line, equivalent to the 50 per cent pulse length, apart (i.e. roughly half the 10 per cent pulse length).

If it is assumed that the reference pulse is in the equilibrium position (peaking at x_o and time t_o), then any change in liquid level will give the maximum possible voltage change at both detectors, for a given reflected pulse.

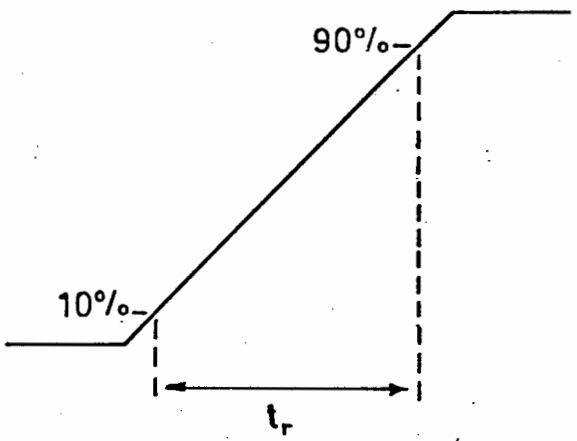

FIGURE 5.16 APPROXIMATION OF A PULSES'LEADING EDGE

5.7 Resolution of a Sampled Detector Line System

The relationship between pulse risetime and system resolution (Section (4.7)) dictates that the pulse risetime should be in the region of 200 pS for a resolution of 10 mm. Further consideration of the measurement problem shows that this need not necessarily be so, however. The resolution criteria stated in Section 4.7 are those necessary for the resolution of two closely spaced discontinuities on a line. The flotation cell liquid level is only one discontinuity and as such furnishes only one return. The time of this return determines the position of the liquid interface at any given instant.

As previously stated, the detector output voltages are the sum of two voltages. A constant voltage due to the transmitted pulse, and a variable voltage dependent on the return time of the reflected pulse.

The smallest detectable variation in voltage due to a variation in liquid height in the flotation cell, for a given pulse risetime, determines the system's resolution.

The smallest detectable variation in voltage is equal to the noise voltage (V_N) in the system.

Assuming a linear ramp function for the leading edge of the pulse (Figure (5.16)) it is possible to formulate an expression for the system resolution. A variation in voltage (ΔV) due to a given variation of liquid level is related to the pulse risetime by

$$\Delta V = \frac{V}{t_r} \left(\frac{2d}{c}\right) \qquad -(5.1)$$

where V = pulse voltage excursion between 10 and 90 per cent pulse amplitudes (volts)

t_r = pulse risetime as defined by the 10 and 90 per cent pulse amplitudes (seconds)

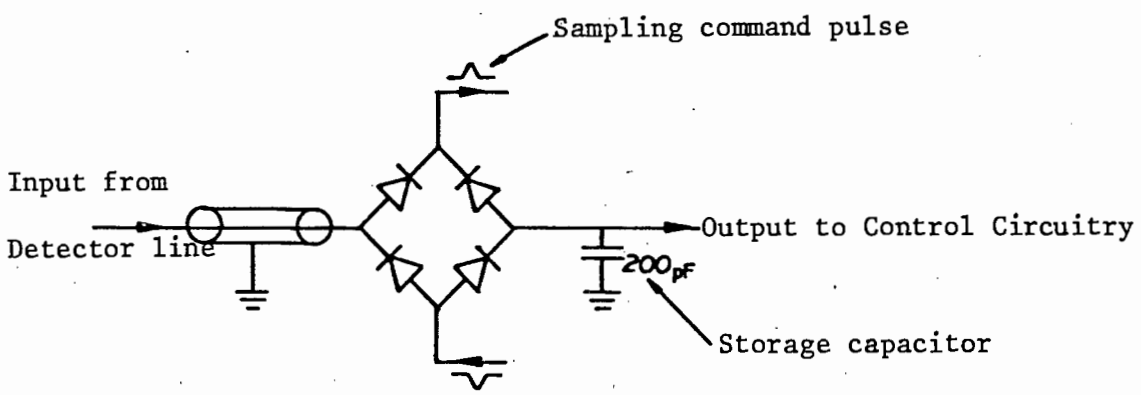

FIGURE 5.17 DIODE SAMPLING BRIDGE

d = variation in liquid level (metres) negative for up
positive for down

c = free space velocity of electromagnetic wave propagation (on the Goubau Line)

The (2d/c) factor gives the time delay (negative for a rise, and positive for a fall) associated with a variation in liquid level. The effective delay is twice that introduced by a one-way level change, owing to the fact that the incident and reflected pulses both experience the same delay.

Manipulation of Equation (5.1) gives

$$d = (\Delta V\ t_r c/2V)$$

and letting the variation in detector output voltage (ΔV) equal the system noise voltage (V_N) gives the system resolution (δ):

$$\delta = (V_N\ t_r c/2V) \qquad -(5.2)$$

Using equation (5.2) it is possible to decide what pulse risetime is necessary to provide a given resolution, for a given system noise voltage.

It should be mentioned that the resolution determined here is for a single detector system. An improvement in system resolution is obtained when the outputs from two separate detectors, positioned as specified in Section 5.6, are compared to give an output proportional to a variation in liquid level. This is discussed later in Section (5.13).

Previous experimentation showed that a coupled reflected pulse amplitude of about 1V could be expected in the detector line. Sampling efficiency of a diode sampling bridge (Figure (5.17)) can be expected to be in the region of 10 per cent (Ref.79). This gives a 10 to 90 per cent voltage variation of (1(0.1)(0.8)) = 80 mV. Assuming a noise voltage V_N of 5 mV (which seemed reasonable) and substituting these figures along with δ = 0.01m in equation (5.2), gave a pulse risetime slightly in excess of 1 nS.

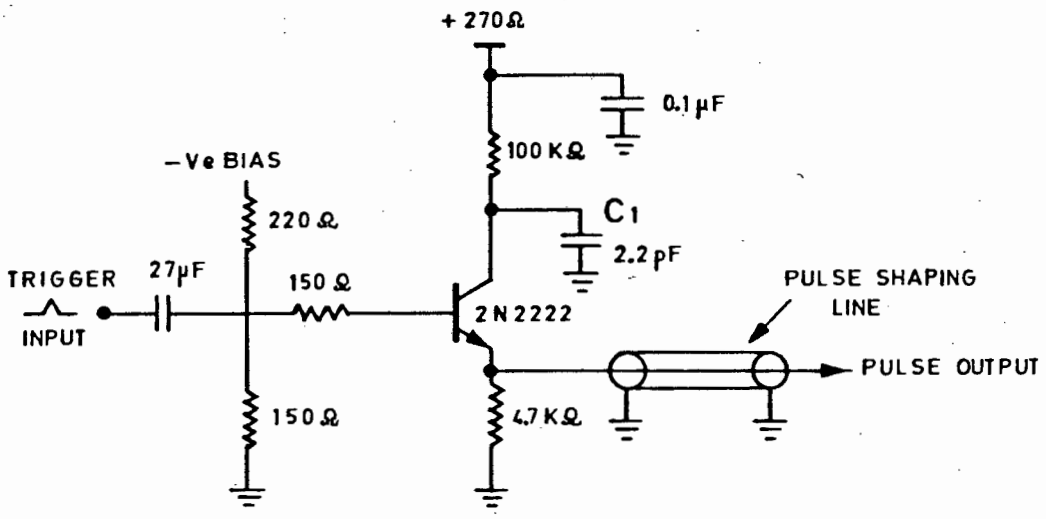

FIGURE 5.18 THE SIGNAL PULSE GENERATOR

Therefore, in order to ensure a system resolution of 10 mm with the above parameters, it is necessary to provide a pulse with a risetime of 1nS or better.

5.8 Pulse Generation

Investigation showed that avalanche transistor pulse generation was the method best suited to TDR work with a Goubau line. It provided the necessary pulse risetime (<1nS) at a reasonable voltage (≈20V).

The use of tunnel and step recovery diodes for this purpose was rejected because of their local unavailability and low voltage output. Mercury switches were rejected because of their low pulse repetition frequency (200 Hz maximum).

The necessary theoretical background for an understanding of avalanche switching is given in (80) along with a number of practical circuits. Further ideas were obtained from Vandre (98), D'yakonov (81 through 85) and Larin *et al* (86).

Figure (5.18) shows the final circuit as used for the pulse generator. A common, easily obtainable 2N2222 switching transistor is used in the avalanche mode to switch the accumulated charge in a 2.2 pF capacitor into the pulse shaping line to produce fast pulses.

Briefly, the voltage on the storage capacitor C_1 rises to a value determined by the collector-emitter leakage current of the transistor (about 100V). By controlling the injection of ionizing carriers into the collector with a negative base bias voltage, it is possible to prevent the transistor from avalanching spontaneously.

The arrival of a positive pulse at the trigger input momentarily removes the negative bias voltage from the transistor base, allowing avalanching to commence. Once avalanching has begun, it continues until all the charge stored in the storage capacitor has been discharged into the shaping line. At this point

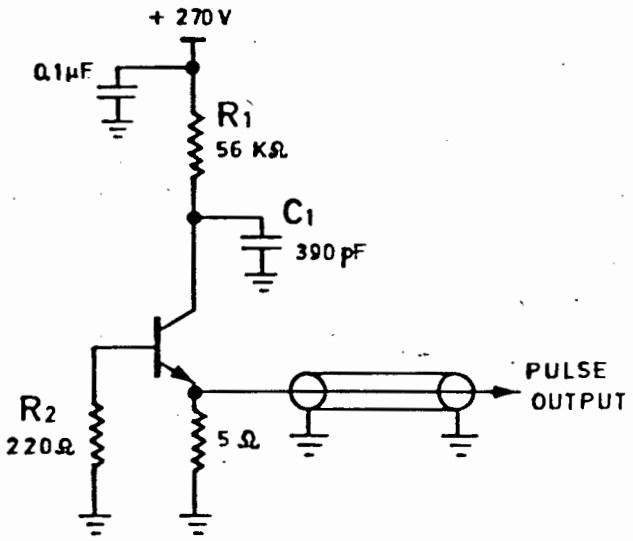

FIGURE 5.19 THE TRIGGER PULSE GENERATOR

the transistor turns off, allowing the storage capacitor to recharge in time for the next trigger cycle.

The fact that the transistors used in this circuit (2N2222's) are not primarily designed for avalanche mode work, manifested itself as a variation in the results obtained for a number of different transistors.

Risetimes ranged from 400 pS to 600pS while output pulse amplitudes varied from 10V to 25V. A large number were therefore screened and the best ones, with fastest risetimes (500pS and better) and highest pulse amplitudes (20V and better), selected.

This basic avalanche transistor pulse generator circuit was also used, with minor modifications, for the construction of a trigger pulse generator and sampling pulse generator. The sampling pulse generator is described in section (5.12) as part of the sampling detector. A circuit diagram of the trigger pulse generator appears in Figure (5.19).

The major difference between this circuit and that of the pulse generator (Figure (5.18)) is that there is no negative bias voltage to inhibit spontaneous avalanching of the transistor. The combination of R_1C_1 and R_2 provide a pulse repetition frequency in the region of 50 kHz. R_2 determines the collector voltage at which the transistor will avalanche, while R_1 and C_1 determine how long the collector voltage takes to rise to this value once C_1 has been discharged.

The pulse produced is of an amplitude (30V) far greater, and a duration (5nS) far longer than is necessary for triggering purposes. High pass filters on the trigger inputs of the pulse generator and sampling detectors reduce the pulse length and amplitude to more reasonable dimensions (about 1nS and 5V).

5.9 The Necessity for a Pulse Shaping Line

The speed with which the avalanche transistor discharges the pulse generator's storage capacitor into the pulse shaping line determines the rise-time and profile of the pulse produced.

Suppose that a short line (about a quarter as long as a pulse normally produced by the generator) is attached at the generator output and is left open circuit at its furthest end.

Triggering the generator starts the discharge of the capacitor into the line in the normal way. After a time the reflection of the pulses' leading edge, from the end of the open circuited transmission line, reaches the pulse generator. This causes the voltage at the input to the transmission to rise causing the flow of current from the storage capacitor to slow down. The nett effect of this is to increase the pulse duration and slow down its rise- and fall-times. In severe cases this effect causes the avalanche transistor to switch off even before the storage capacitor is fully discharged.

This phenomenon is clearly demonstrated by experiment. In order to produce fast pulses with 'clean' leading and trailing edges it is necessary to provide a length of line, sufficiently long enough to allow complete discharge of the storage capacitor, between the pulse generator and the Goubau line.

Theoretically one would expect a length equivalent to half the pulse length on the line to be sufficient, but because of pulse undershoot it is better to ensure that the line is one pulse length long, or longer.

5.10 The Guided Wave or Goubau Line

Two possible systems, using free-space and guided transmission line methods, were investigated for directing TDR pulses into the flotation cell.

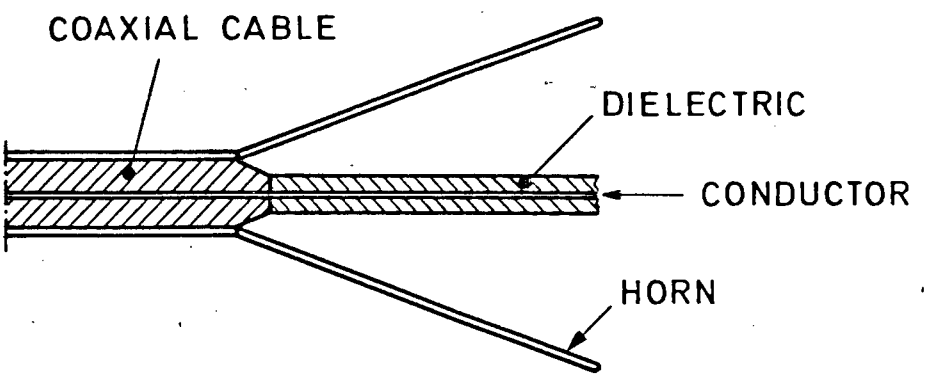

FIGURE 5.20 A MATCHING HORN FOR LAUNCHING SOMMERFELD'S WAVE ONTO A GOUBAU LINE.

The use of a wideband, dielectrically loaded horn antenna for pulse work is described by Daniels[24] in his paper dealing with subsurface radar returns. The design of such an antenna is an involved process and the resulting horn extremely bulky (0.5 m x 0.5 m aperture) and easily damaged. Consideration of this and the fact that a guided line system would be less susceptible to unwanted reflections, led to its' choice in favour of the free-space system.

Various types of transmission lines have been used for the remote sensing of liquid interfaces and properties. These include Lecher wires[43], coaxial lines[35] and Goubau lines[32].

The least familiar of the three mentioned above is the Goubau or Guided-Wave Line. Its' most striking feature is that it consists of only a single conductor.

A paper by Sommerfeld in 1899[87] laid the theoretical foundation for the understanding of this type of line, while work done by Goubau in the 1950's[53,54] showed that practical lines of this nature were feasible.

Theory shows that the only wave mode capable of being guided by a single conductor is the radially symmetrical transverse magnetic mode (with cylindrical field components). The main difficulty associated with using the Goubau line is finding an efficient method of launching this mode onto the line. Sommerfeld's surface wave, as it is called, normally requires large launching devices ('matching' horns) at either end of a line for efficient transmission over long distances.

Goubau overcomes this problem by coating the conductor with a dielectric layer. This concentrates more of the wave's field near the surface of the conductor, allowing smaller launching horns to be used (Figure (5.20).

Consideration of the measurement environment showed that any two wire system would become clogged with flotation particles and would require regular cleaning and maintenance.

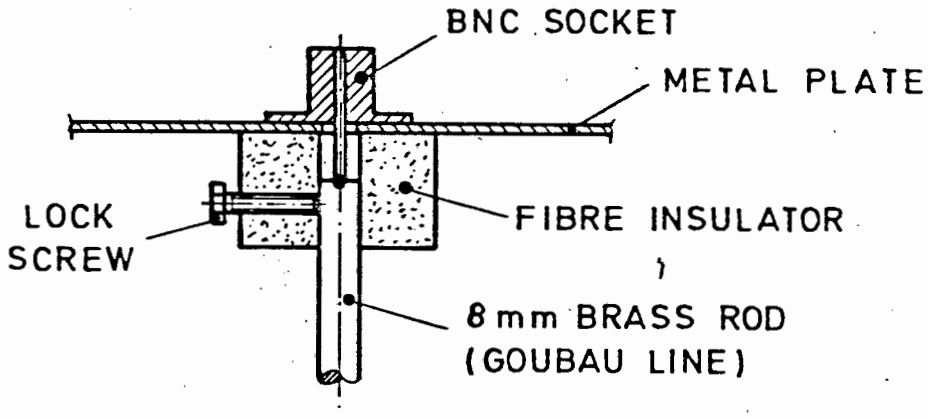

FIGURE 5.21 A PRACTICAL COUPLING SYSTEM

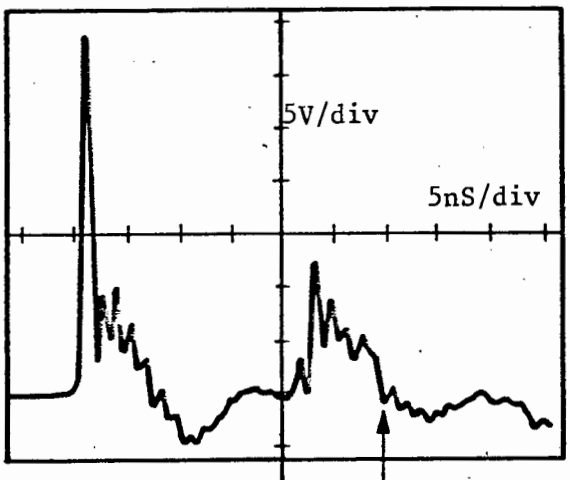

FIGURE 5.22

SIGNALS SEEN AT THE PULSE GENERATOR OUTPUT IN THE SYSTEM SHOWN IN FIGURE 5.1. THE FIRST IS THE TRANSMITTED PULSE AND THE SECOND IS THE REFLECTED PULSE FROM THE END OF THE SHAPING LINE.THE REFLECTION FROM THE WATER IN THE TANK IS ARROWED.

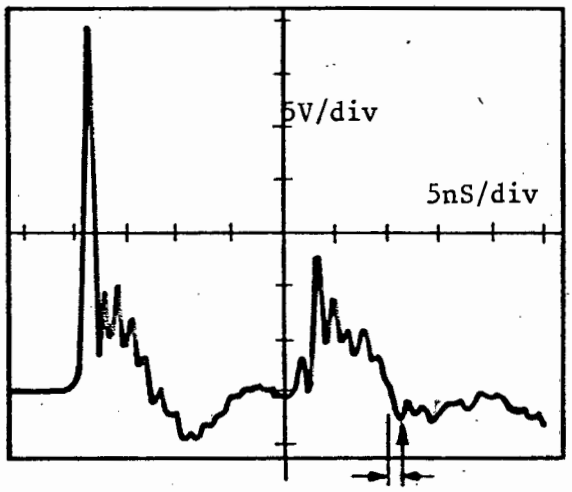

FIGURE 5.23

THE SAME SYSTEM AS THAT DESCRIBED IN FIGURE 5.22 BUT WITH A DIFFERENT WATER LEVEL IN THE TANK.THE NEW REFLECTED PULSE POSITION IS ARROWED AND THE CHANGE IN POSITION (1nS) IS INDICATED.

Therefore, a TDR system using a Goubau line to direct pulses into the flotation cell was built and tested. It was found that sufficient energy, for measurement purposes, was coupled onto the line (an 8 mm brass rod) using the crude system shown in Figure (5.21).

Future intended improvements to the system include the coating of the rod with Teflon to inhibit particle deposition. This should also have the added advantage of allowing more energy to be coupled to the line. Further improved coupling can be provided by a matching horn, if necessary.

Experiments artificially coating the line with a layer of mineral particles, showed that it is immune to interference from this source. This is to be expected as the pulse energy travels, not in the line, but in the space surrounding it.

5.11 Directional Couplers

The Problem of how to separate the transmitted and reflected pulses from one another and the multiple reflections in the system was encountered early on in the development of the TDR system. The magnitude of the signal processing problem can be appreciated when Figures (5.22) and (5.23) are examined.

These sketches of actual photographs illustrate the signals seen at the output of the pulse generator in a system such as that shown in Figure (5.1). The first pulse is that generated by the pulse generator while the second is that reflected from the end of the pulse shaping line where it joins the Goubau Line. The reflection from the water interface on the Goubau Line can be seen (arrowed) in each Figure. The difference in arrival time of these two reflected pulses (1nS) is an indication of a 750 mm liquid level variation in the flotation cell.

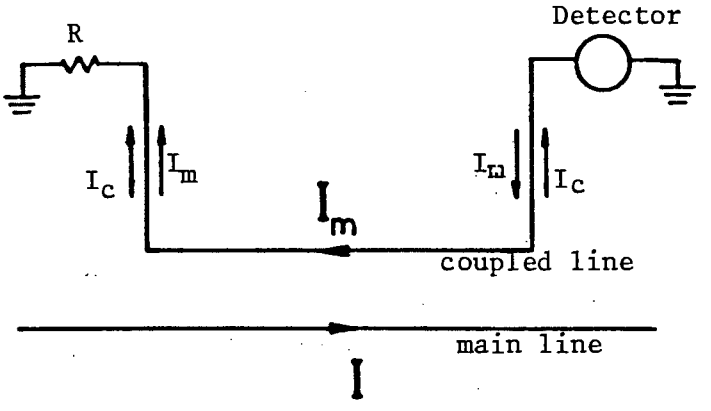

FIGURE 5.24 INDUCED CURRENTS IN THE DIRECTIONAL COUPLER

It was decided that directional couplers should be used for separating the transmitted and reflected pulses and that they should be located on the Goubau Line to minimise the number of unwanted reflections coupled into the signal processing circuitry. Placing the couplers somewhere on the shaping line would give a reflected pulse output that included the unwanted reflection from the end of the shaping line.

Detailed theoretical and practical information on the design of directional couplers can be found in[91] and [92]. A short, simplified summary of the principles involved will be given here as an aid to understanding their operation.

If a line whose length is short compared to frequency is introduced into the field of, and parallel to, another line which is carrying a signal then a second signal directly proportional to the signal in the main line will be coupled into the secondary line.

A current I_m is inductively coupled into this line and flows in the opposite direction to that in the main line (Figure (5.24)). In addition, capacitive coupling between the loop and the main conductor causes a current I_c to flow in each leg of the loop. In the resistive arm I_c and I_m are additive while in the other arm they are in opposition. By adjusting the capacitance C and mutual inductance M it is possible to make I_c and I_m cancel in the detector arm.

The detector will now 'see' no signals flowing in the direction of that in the main line but will 'see' signals flowing in the opposite direction.

Adjusting R also improves the cancellation of I_m and I_c in the detector arm. Ideally, it is necessary to have $R = \sqrt{L/C}$ for wideband use, where L and C are the distributed inductance and capacitance of the coupled lines, respectively.

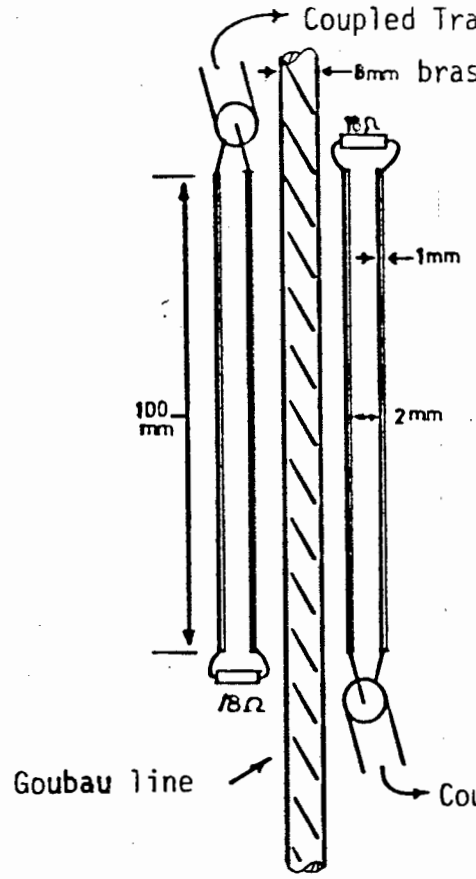

FIGURE 5.25

SHOWS THE DIMENSIONS AND CONSTRUCTION OF THE DIRECTIONAL COUPLERS.

To the Flotation Cell

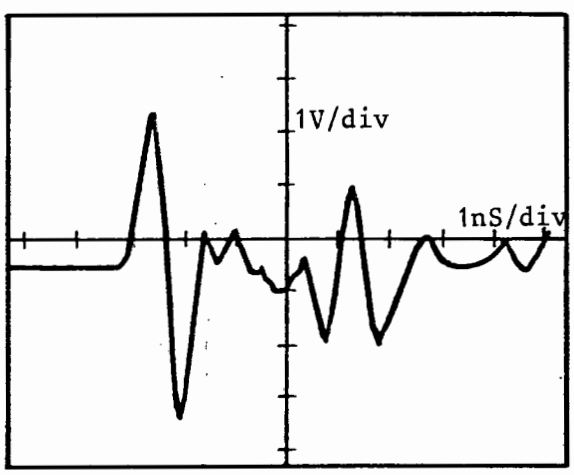

FIGURE 5.26

THE COUPLED TRANSMITTED AND REFLECTED PULSES SEEN ON THE DETECTOR LINE.

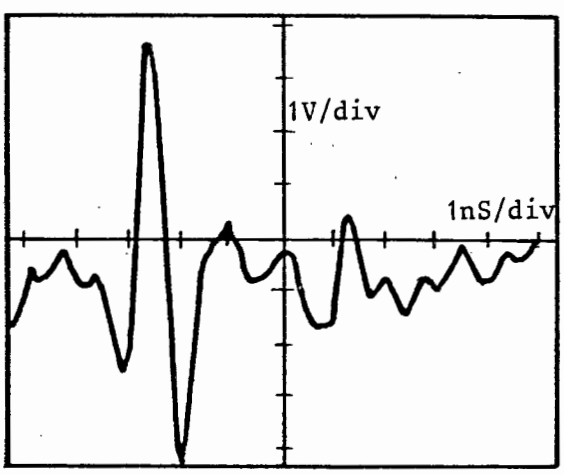

FIGURE 5.27

THE COUPLED PULSES PEAKING TOGETHER AND FORMING A COMPOSITE PULSE.

A coupler has a bandwidth determined primarily by R,L and C, while its midband coupling frequency F_o is determined by the length of coupled section (L). This midband frequency can be found from

$$F_o = (v/_{4L}) \text{ where } L = \text{length of coupled section} \qquad (5.3)$$
$$v = \text{velocity of wave propagation in the line}$$

A centre frequency (F_o) of 0,75 GHz was chosen for the coupler after consideration of the generated pulses' frequency spectrum (Section 4.4.2). Most of a triangular pulses' energy is contained in the central band between the frequencies defined by $\pm (\frac{4\pi}{t_p})$, where t_p is the pulse length.

The position of the first amplitude node in the frequency spectrum of a perfect 1nS triangular pulse is, therefore, theoretically 2GHz. In practice, however, perfectly triangular pulses do not occur. Pulse peaks tend to be rounded rather than pointed. The effect of this is to reduce the amount of spectral energy present at higher frequencies.

With this in mind, the centre frequency of the coupler was chosen to be 0.75GHz rather than 1GHz.This gives a theoretical coupled length of 100mm (in air) for the coupler on substitution in equation (5.3). Cancellation of I_m and I_c in the detector arm of the coupler was found, experimentally, to be optimized for a resistance of R = 18Ω (with the coupler dimensions as shown in Figure (5.25)).

The directional coupler was tested by sending a pulse signal through it first in one direction, and then in the other and comparing the two coupled signals obtained. It was found that a signal travelling through the coupler in the reverse direction was reduced by 26 dB over the same signal travelling through the coupler in the desired direction.

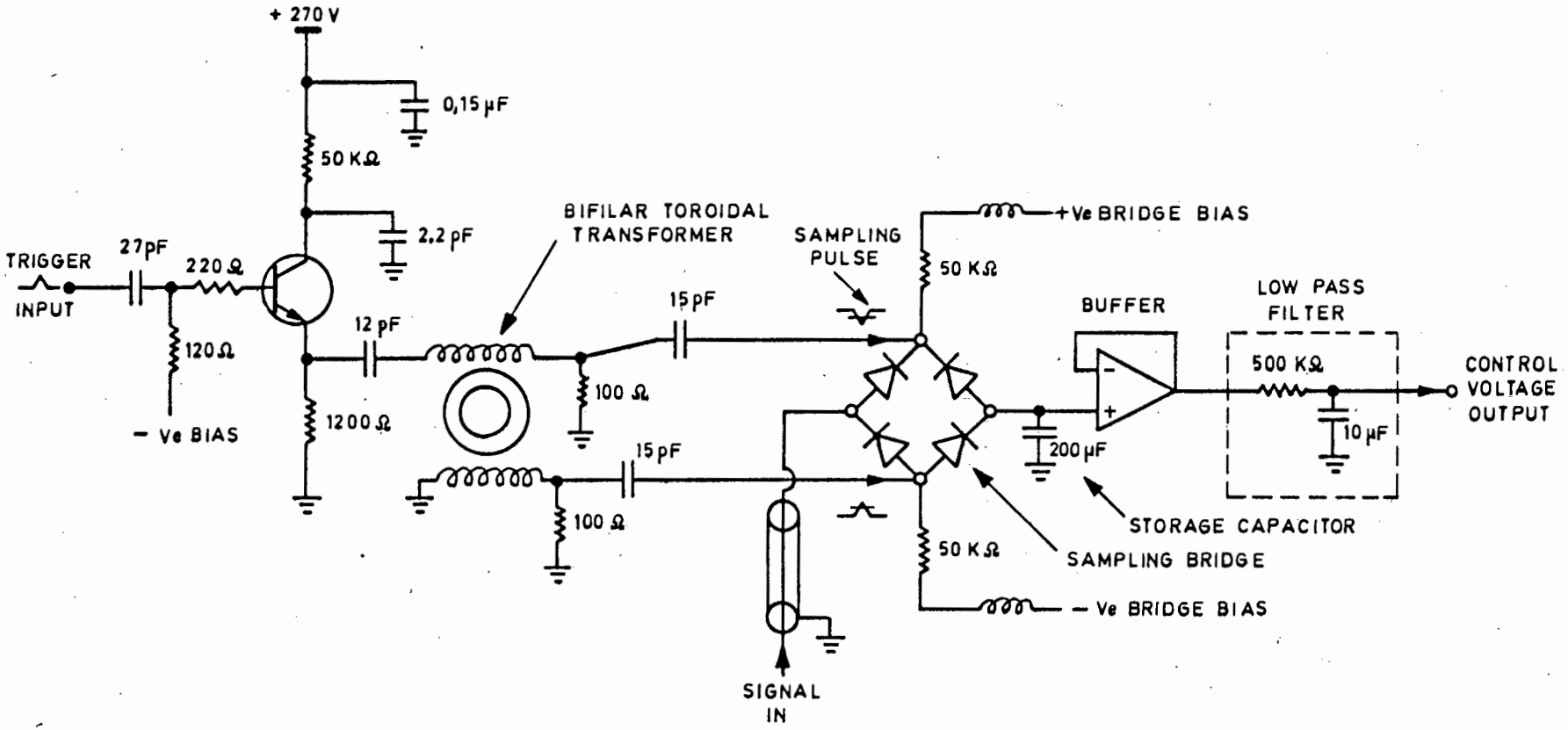

FIGURE:5.28 THE SAMPLING DETECTOR

Figures (5.26) and (5.27) (sketches of photographs) show the coupled transmitted and reflected pulses in the detector-line. In Figure (5.26) the pulses are not peaking together at the same point on the line and so appear as two individual pulses separated in time. Figure (5.27) shows the reflected pulse peaking simultaneously with the transmitted pulse and forming a composite pulse at that point in time. Moving the reflected pulse to the left has also brought an unwanted reflection (to the right of the composite pulse in Figure (5.27)) into the picture from the right. This should not be confused with the reflected pulse in a similar position in the previous Figure.

The success of the directional couplers in separating the transmitted and reflected pulses on the Goubau Line greatly simplifies the signal processing required for the TDR level measurement system.

5.12 The Sampling Detector

The feasibility of the whole TDR level measuring instrument described so far hinges around the ability to sample the composite pulse at a given position on the detector line, precisely at a given time. Consequently as lot of work went into the development of a reliable sampling unit. A circuit diagram of this unit appears in Figure (5.28).

The heart of the detector, which operates on a sample and hold principle, is a diode sampling bridge using Schottky or Hot Carrier diodes. These diodes are specially designed to have low package inductance and capacitance and a small amount of stored charge, making them ideal for high-speed applications.

The operation of the sampler is as follows. A sampling command pulse is supplied to the sampling bridge by the avalanche transistor circuit, which triggers on a pulse from the trigger pulse generator (Figure (5.12)). This ensures that the composite pulse is sampled at the correct time. The negative bias control on the base of the transistor allows fine adjustment of this sampling time over a range of approximately 500 pS.

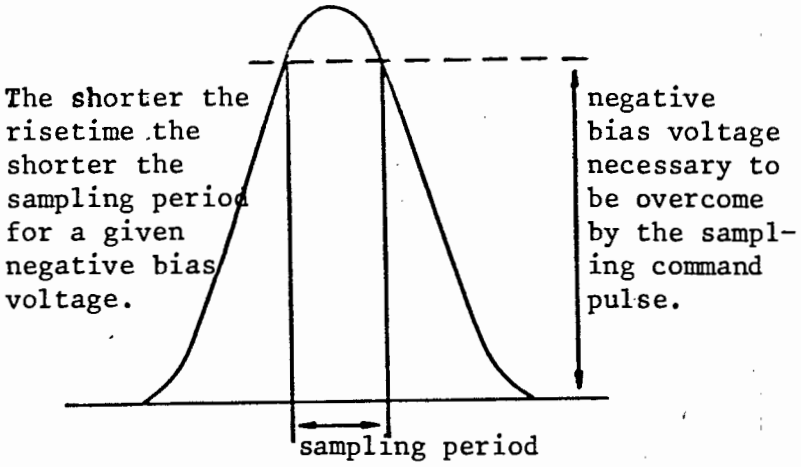

FIGURE 5.29

SHOWS THE SAMPLING COMMAND PULSE WITH THE NEGATIVE BIAS VOLTAGE SUPERIMPOSED ON IT.

FIGURE 5.30

THE EFFECT OF A FINITE SAMPLING PERIOD. (SAMPLING THE COMPOSITE PULSE IN THIS WAY GIVES THE SAME OUTPUT AS IF THE PULSE HAD BEEN SAMPLED AT THE 50% AMPLITUDE POINTS).

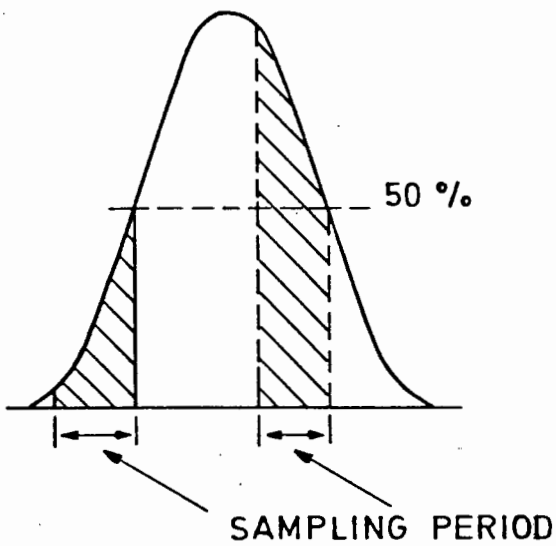

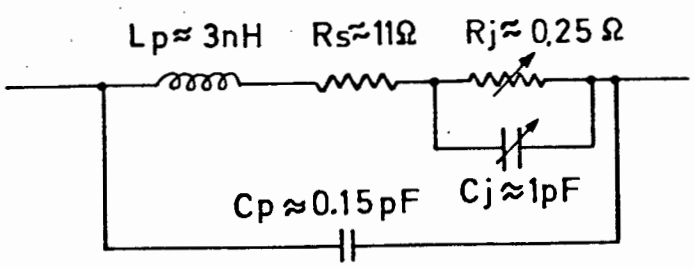

FIGURE 5.31

THE EQUIVALENT CIRCUIT OF A HOT CARRIER DIODE WITH TYPICAL PARAMETER VALUES INSERTED.

L_p and C_p =Package Inductance and Capacitance

R_j and C_j =Junction Resistance and Capacitance

R_s =Series Resistance

The length of the sampling period is determined by the rise-time of the sampling command pulse and the magnitude of the negative bias on the bridge (Figure (5.29)). For this reason a transistor with the fastest available rise-time (400 pS) was chosen to produce sampling command pulses in the detector. The resultant effective sampling period is about 300 pS. By ensuring that the sampling interval is so placed as to include the 50 per cent amplitude points on the reflected pulse, in the equilibrium position, (Figure (5.30), it is possible to achieve the resolution for the system as stated in Section 5.7.

The bifilar toroidal winding is used in the manner of a balun transformer to convert the ground referred, unbalanced sampling pulse from the avalanche transistor into a balanced signal. This is done in order to prevent the sampling pulse from appearing at the output of the sampling bridge as a common mode signal, and interfering with the sampled signal.

The design of broadband toroidal pulse transformers is well documented and extensive use was made of papers by Ruthroff[88], Winningstad[89] and Matick[90] during construction of this section of the sampling unit.

During the sampling period, the sampling command pulse overcomes the reverse bias on the bridge, driving it into conduction and allowing current to flow from the bridge sampling input into the storage capacitor. The current that flows is dependent upon the input voltage and the series impedance of the source and the diodes. Investigation of a typical diodes' impedance (Figure (5.31)) shows that there are series resistance as well as leakage (capacitive) losses. Series resistance losses introduce a finite voltage drop across the diode while series capacitances reduce the effective current flow by allowing reverse currents to leak out of the storage capacitor during the non-sampling period.

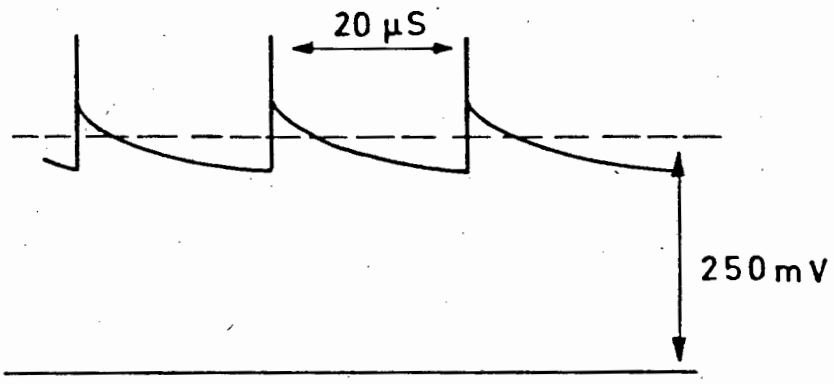

FIGURE 5.32 THE SIGNAL SEEN ON THE STORAGE CAPACITOR FOR AN INPUT SIGNAL OF 2.4 VOLTS.

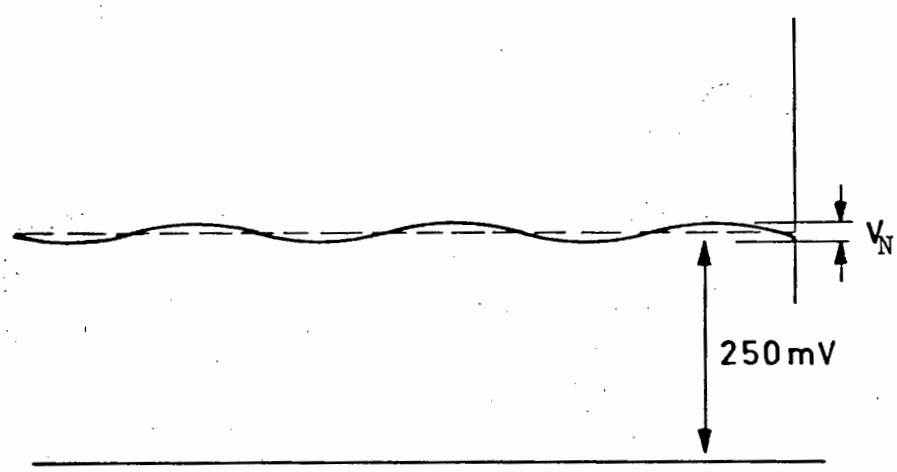

FIGURE 5.33 THE OUTPUT OF THE SAMPLING DETECTOR AFTER BUFFERING AND LOW PASS FILTERING.

A further important effect responsible for the reduced efficiency of the sampler is that the samples of the input signal are 'spikes', with a large range of spectral frequency components. The storage capacitor (in combination with the source and diode impedances) is part of a low pass filter that 'sees' only a small fraction of the sampled pulses' total energy.

Sampling efficiency[96] is defined as:

$$\eta = \text{(storage capacitor voltage)/(input voltage)}$$

Using a DC source as an input signal to the sampling bridge gave a sampling efficiency of about 10 per cent. This is in agreement with what is to be found in the literature[79].

The raw sampled voltage on the storage capacitor (Figure (5.32)) needs to be processed before it can be useful as a control voltage. A buffer stage followed by a low pass filter performs this processing very simply. The resultant signal (Figure (5.33)) is a DC level with a small sinusoidal ripple voltage, at the sampling frequency, superimposed on it. A 2 mV ripple was observed for an RC time constant of 5.

A further result of low pass filtering is to average the random noise in the system to zero. This leaves the small voltage variation due to the sampling process as the only 'noise' voltage present. Substituting this for the noise voltage (V_N) and using a value of 70 mV for the reflected pulse 10 to 90 per cent amplitude change, gives a theoretical resolution (Section 5.7) of 2 mm, for the system as it stands (i.e. with t_r = 500 pS).

A future development will be the incorporation of Step Recovery Diodes into the sampler design to provide shorter sampling pulses. These improved sampling units will then be used to 'draw' accurate reflected pulse profiles for Time Domain Spectroscopy work.

5.13 The Resolution of a Two-Detector Comparison System

Until now system resolution has only been defined for a single detector system. It will be shown that comparing the signals from two detectors, as suggested in Section 5.3, favourably affects the system resolution.

Assume that the detector output signals are $A(t) = A_1+A_2 \sin \omega t$ and $B(t) = B_1+B_2 \sin (\omega t+\theta)$ (where A, and B are the DC components and $A_2 \sin \omega t$ and $B_2 \sin (\omega t + \theta)$ are the time varying components of the sampled signals, ω being the sampling frequency). Normally, with the reflected pulse in the equilibrium position, $A_1 = B_1$. A variation in pulse arrival time causes one value to increase and the other to decrease a similar amount. Comparing these signals (by subtraction) then gives an output voltage

$$V_{comp} = A(t) - B(t) = (A_1-B_1) + (A_2 \sin \omega t - B_2 \sin (\omega t + \theta))$$

As a consequence of the simultaneous sampling of A(t) and B(t), it can be seen that the two time varying components must be in phase (i.e. $\theta = 0$). This leads directly to

$$V_{comp} = (A_1 - B_1) + (A_2 - B_2) \sin \omega t$$

The magnitudes of A_2 and B_2 should ideally be equally, but slight differences in component values and parameters are likely to make them differ.

The change in output detector voltage, for a given change in reflected pulse arrival time, in a dual detector system is twice that obtained in a similar single detector system. An added bonus is that the resultant noise voltage in due dual system is, for the worst case, equal to that in a single detector system. At best it is equal to zero.

Taking the worst case as being representative, gives dual system resolution as twice that of a single detector system,

$$\delta_{dual} = \left(\frac{V_N}{4V} t_r c\right)$$

where V_N = the largest 'noise' voltage of the two signals

V = 10% to 90% voltage excursion of the reflected pulse (as for a single detector)

t_r = pulse risetime

c = 3×10^8 m/S (velocity of propagation on Goubau line)

This resolution is the worst possible case. Note also that reducing the 'noise' voltage on one detector to zero is more likely to degrade the system resolution than improve it. It is of more benefit to ensure that both 'noise' voltages are of equal amplitude. This eases the restraint on system response time imposed by the low pass filter on the output of the detector.

This consideration is not important in the present application but may be in a system designed to measure surface profile, say. Here increased resolution and response time would both be important.

5.14 Variable Delays

The incorporation of a wideband variable delay line into the TDR instrument to allow continuous monitoring of the flotation cell liquid level is dealt with in Section (5.5).

Variable delay can be introduced by mechanical or electrical means and both are discussed here.

Mechanically Variable Delay

The easiest way of ensuring that the reflected pulse stays within the required sampling window is to drive the whole TDR instrument up or down, tracking any fluctuations in flotation cell liquid level. This method was successfully used to test the resolution of the prototype system and is described in the next chapter.

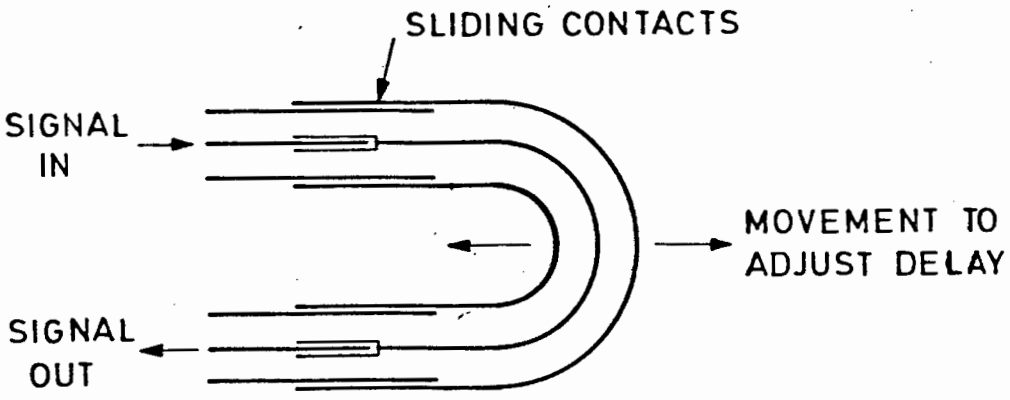

FIGURE 5.34 A TROMBONE LINE

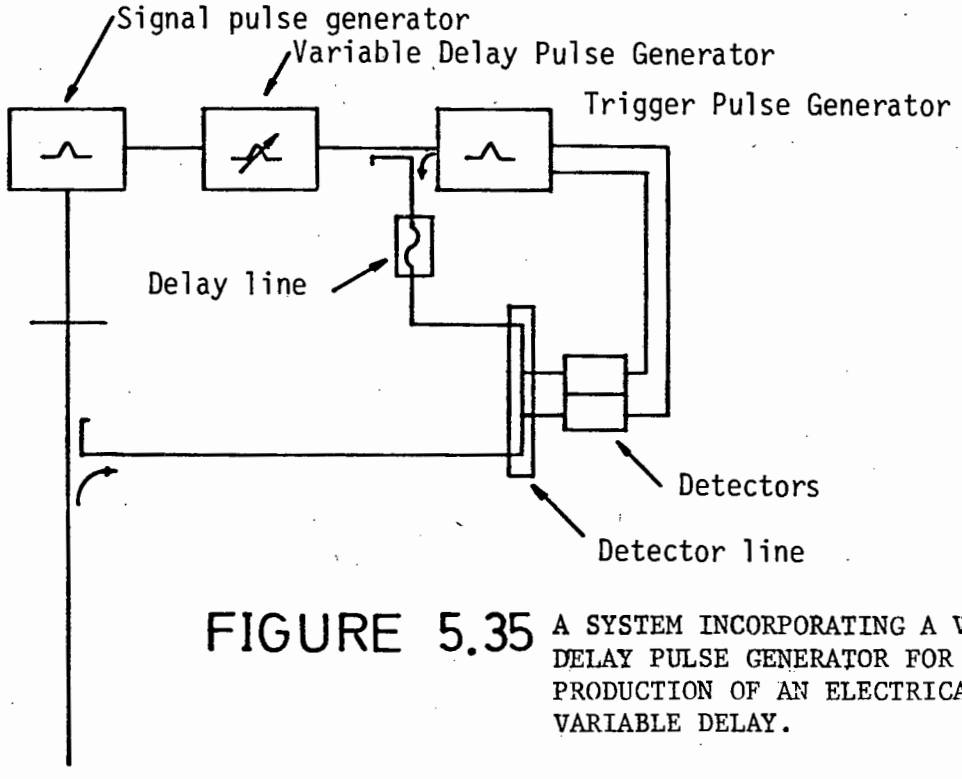

FIGURE 5.35 A SYSTEM INCORPORATING A VARIABLE DELAY PULSE GENERATOR FOR THE PRODUCTION OF AN ELECTRICALLY VARIABLE DELAY.

It was felt, however, that this method would not be suitable for use in the hostile, industrial environment of a mineral processing plant.

A second more acceptable way of providing mechanically variable delay for the reflected pulse, is to construct a line similar to the familiar coaxial trombone line (Figure (5.34)). Sliding the trombone in and out varies the effective length of the line and therefore the delay experienced by any pulses passing along it. Housing this device and its' driving circuitry in a suitable enclosure would protect it from the environment and allow the instrument to monitor the liquid level continuously while being securely fixed in one position above the flotation cell. Unfortunately, the trombone line is a precision component requiring very exact machining and would increase the cost of the final instrument considerably.

The most promising mechanical method of introducing a variable delay into the system, involves driving the reflected pulse directional coupler to an equilibrium position on the Goubau Line. With the coupler in this position the reflected pulse 'peaks' in the sampling window at t_o. Any variation of the liquid level in the cell would cause the reflected pulse coupler to be driven to a new position on the Goubau Line, in such a way as to ensure that the reflected pulse continued 'peaking' in the sampling window at t_o. Directional coupler position would then be a measure of liquid level.

Electrically Variable Delays

In order for there to be no moving parts in the TDR continuous level monitoring instrument, it will be necessary to have some method of introducing an electrically variable delay into the reflected pulse return path.

One way of doing this involves redesigning the whole system as it stands (see Figure (5.35)).

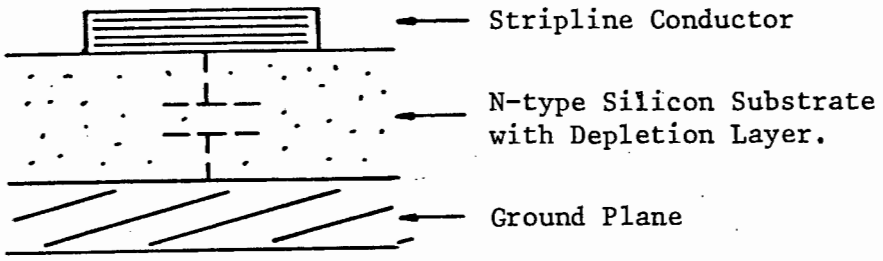

FIGURE 5.36 THE CONSTRUCTION OF THE SCHOTTKY BARRIER MICROSTRIP LINE.

In the new system the trigger pulse generator drives a variable delay pulse generator as well as supplying a pulse to the detector line. The variable delay pulse generator in turn supplies a trigger pulse to the signal pulse generator. By varying the time of the trigger command pulse from the variable delay pulse generator it is possible to ensure that the reflected pulse peaks in the detection window for various liquid level heights in the flotation cell. Construction of a variable delay pulse generator would involve using the charge storage properties of Step Recovery Diodes as mentioned by Coekin in[93].

This system looks promising but is dependent on external supply sources for the Step Recovery Diodes. Nonetheless further development is to continue along these lines.

Two other methods of introducing electrically variable delay into a system were investigated. They both vary propagation time through a section of line by electrically varying the properties of the medium of which the line is constructed.

Jäger and Rabus[94] construct microstrip lines on a substrate of N-type Silicon about 0,2 mm thick. A Schottky Barrier complete with depletion layer is formed between the stripline and the groundplane underneath (Figure (5.36)). Varying the DC bias on the line causes the width of the depletion layer to vary, in the manner of a varactor diode. It is therefore possible to vary the distributed capacitance, and hence the phase delay, of the line with a control voltage.

Adam *et al*[95] use magnetostatic-wave (MSW) devices at Gigahertz frequencies to perform functions normally associated with surface acoustic-wave (SAW) devices at lower frequencies. The MSW devices operate over a 1 to 20 GHz frequency range with bandwidths of 0,5 to 1 GHz which makes them suitable for the application in mind.

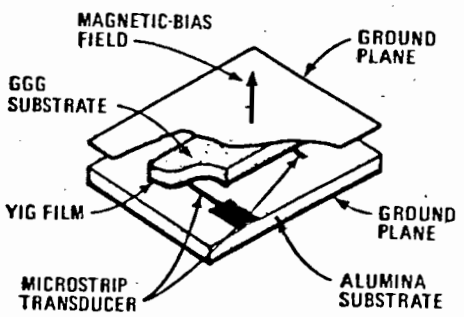

REFERENCE 95

FIGURE 5.37

THE CONSTRUCTION OF A MAGNETOSTATIC-WAVE DEVICE.

Briefly, the basic MSW device is a constant delay line, which delays a signal applied at its input port a fixed amount of time before it arrives at the output port. By applying a steady magnetic field normal to an yttrium-iron-garnet film, and positioning two ground planes, one above and one below the film, at appropriate distances from it, it is possible to produce this constant delay over a useful frequency range. Figure (5.37) illustrates the construction of this device.

Propagation time through the MSW device is varied by varying the strength of the magnetic biasing field.

Use of the Schottky microstrip lines and the magnetostatic-wave devices in the TDR instrument is dependent on the ability of local institutions, or industry, to supply the necessary technology. The possibility of this is small, so future development of the instrument will concentrate on using the mechanically-driven directional coupler and variable delay pulse generator (Figure (5.35)) approaches to supply the necessary control of reflected pulse arrival time.

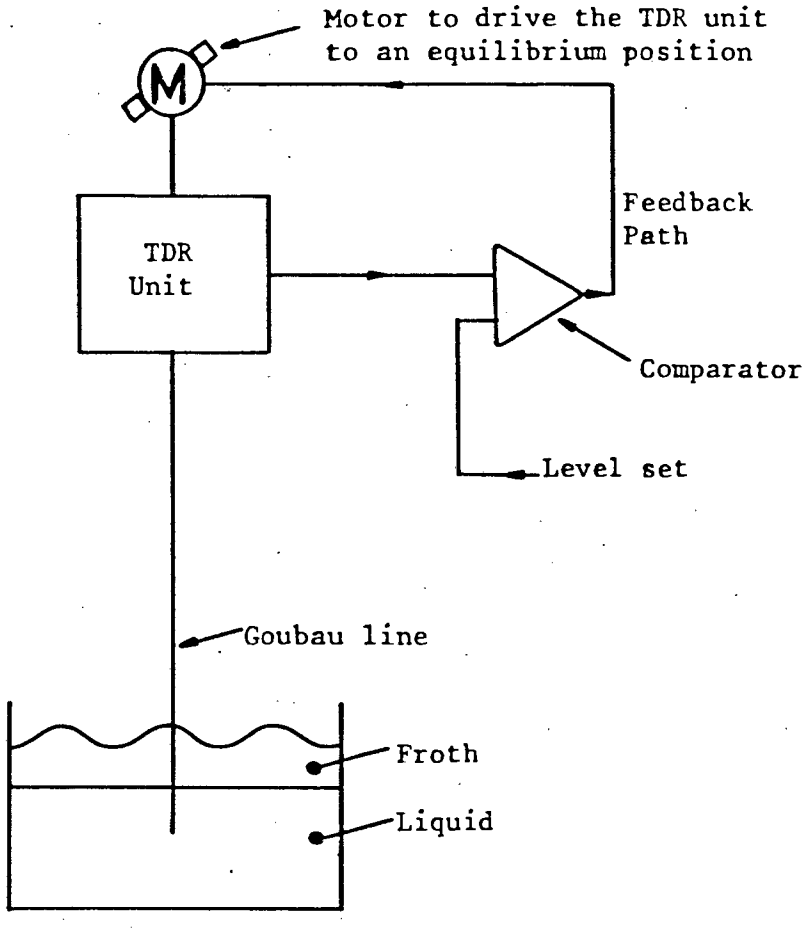

FIGURE 6.1 A MOTORISED LIQUID LEVEL MONITORING SYSTEM.

6. TESTING OF THE PROTOTYPE TIME DOMAIN LIQUID-LEVEL MEASURING INSTRUMENT AND DISCUSSION OF POSSIBLE IMPROVEMENTS

After the completion of a basic prototype instrument, tests were carried out, using a single detector system, to determine whether the theoretical resolution of the TDR system was obtainable or not.

The whole TDR unit was attached to a motorised carriage which was driven up or down in such a way as to ensure that the output of the sampling detector was always a preset value (Figure (6.1)) (i.e. that the reflected pulse return time was always constant). The preset value was adjusted so that the return pulse was always sampled at its 50 per cent amplitude point.

6.1 Determination of the TDR System's Resolution with a Single Detector

(a) Method

The apparatus was set up as shown in Figure (6.1) and the equilibrium point chosen. The position of the motorised carriage was carefully recorded against a calibrated rule fixed alongside it. A beaker of water was then removed from the tank causing the motor to drive the TDR unit down towards the liquid until the equilibrium position was once again reached (i.e. until a point was reached such that the reflected pulse return time was the same as previously).

Once this equilibrium position was reached, the beaker of water was emptied back into the tank, causing the motor to lift the TDR unit back to its previous position.

The scale reading on the calibrated rule was then recorded once more and compared with the first reading. The difference between the two was taken as the system resolution.

This procedure was repeated a number of times with varying amounts of liquid.

(b) Results

The difference between the first and second values recorded was always within $\pm$ 1 mm.

(c) Discussion

Theoretically, the expected resolution is 2 mm (Section 5.12).

A reason for the improved resolution of 1 mm was sought and it was realised that the 'noise' voltage quoted in Section 5.12 is peak-to-peak. This means that the value quoted for the theoretical resolution is representative of the difference between the largest and smallest values obtainable.

This is in excellent agreement with the practical results obtained (i.e. $\pm$ 1 mm is equivalent to a range of 2 mm).

This experiment showed that the theoretical resolution for the system could be obtained in practice.

6.2 The Effect of a Turbulent Surface on the Resolution of the System

It was necessary to find out what the effect of turbulent conditions on system resolution was, as the resolution determined in the previous experiment was only valid for a still surface.

(a) Method

The apparatus was set up as for the previous experiment. A sintered glass dish was placed in the tank and an air supply connected.

(b) Result

The TDR unit was lifted about 5 millimetres to a new equilibrium position and stayed there. At first it was thought that this demonstrated that the average surface level of the liquid was raised by surface

disturbances. Then it was realised that introducing air into the liquid effectively raised the liquid level and masked any turbulent effects.

The experiment was repeated with a motorised stirrer to churn up the surface.

With this arrangement, the TDR unit was raised only a millimetre once the stirrer was switched on and then stayed at that position. Varying the speed of the motor did not seem to affect the position of the unit at all.

(c) Discussion

This demonstrates that the time constant of the TDR instrument is slow enough (RC=5) to smooth out any variations in liquid height caused by the stirrer. The average liquid height stays more or less constant, even with fairly severe surface disturbances.

6.3 The Effect of a Layer of Froth

Although it was known that a layer of froth would attenuate the reflected pulse to a certain extent, and that the single detector system would not compensate for this, it was decided to see what error a layer of foam would introduce into a single detector system.

(a) Method

The apparatus was assembled as in Figure (6.1) and soap powder added to the water in the tank. The sintered glass dish was placed in the tank and the air supply switch on. Once a layer of froth about 100 mm thick had built up, the air supply was switched off to stop the air bubbles in the water interfering with the measurement. The equilibrium position of the unit with the froth present was recorded and compared to that of the unit with no froth present.

(b) Results

The TDR unit's equilibrium position with the froth present was 6 mm lower than with the froth absent. As the froth collapsed the unit returned to its original position.

(c) Discussion

This is as expected since the reflected pulse is attenuated by the froth and the sampling detector must sample at a point above the 50 per cent amplitude level on the reflected pulse, in order to see the same voltage as that seen previously at the 50 per cent amplitude level.

The way this is achieved is to lower the TDR unit, causing the reflected pulse to arrive sooner at the sampling detector. This ensures that the pulse is sampled at a point later than the 50 per cent amplitude level.

Although the attenuation in the froth affects the level measurement in a single detector system, it is encouraging to see that the difference between measurement with and without froth is still within the desired resolution limit of 10 mm.

Use of a two detector system will compensate for the attenuation in the froth and, through its comparison technique, improve on the resolution obtained with the single detector system.

6.4 Resolution

Two primary reasons can be found for the high system resolution. The first is that the sampling time of the sampling detectors is tied to the triggering of the signal pulse generator by a trigger pulse. This means that any variation in detector output can only be due to variations in liquid level on Goubau line causing the reflected pulse return time to vary.

One disadvantage of using a variable delay pulse generator to trigger the signal pulse generator is that the detectors and the signal pulse generator

are no longer linked together, time-wise, by a single trigger pulse. It is hoped that any error introduced by this will be reduced to a negligible amount by using a careful variable delay generator design.

Another reason for the high system resolution is that the final control voltage is averaged over many pulse samples (50 000 per second). The effect of this is to smooth out any noise, including that due to surface turbulence, giving a well-defined control voltage for processing purposes.

6.5 Summary of Test Results

The tests on a single detector system verified:

(a) that the system can achieve its theoretical resolution;

(b) that the response time of the system is slow enough to damp out surface disturbances caused by the flotation cell stirrer and give an average reading related to the surface level of the liquid in the tank.

6.6 Discussion of Possible Improvements to the TDR Level Measurement System

As the aim of this thesis was to prove the feasibility of a microwave method of liquid level measurement applicable to flotation cells, no attempt was made to optimise the prototype design beyond the point necessary for the proof of the measurement principle involved.

Although the performance of the prototype TDR system was satisfactory, a number of improvements are to be investigated.

A dielectric Teflon coating is to be applied to the Goubau line for the dual purpose of inhibiting particle deposition and improving the coupling of the relevant propagation mode to the line. It is thought that a small launching horn will also reduce the effects of radiation from the line, an important consideration for Time Domain Spectroscopy work.

Both methods of varying the reflected pulse return time, utilizing mechanical and electrical delay control, are to be developed. That using the driven directional coupler system is to be developed first, as the Step Recovery Diodes necessary for the construction of the variable delay trigger generator in the second, are not locally available. The eventual aim is to produce a TDR system with no moving parts. By using the driven directional coupler method it will be possible to construct a complete working instrument for evaluation on a flotation plant with a minimum of delay. Later, after the successful construction of the variable delay trigger generator it is hoped that it will be possible to convert the instrument to the electrically variable delay system.

In order to provide an accurate picture of the reflected pulses' profile for TDS work it will be necessary to reduce the width of the sampling bridges' sampling period. This requires the use of Step Recovery Diodes for the provision of a very short sampling command pulse. Once again, this improvement is dependent on the supply of Step Recovery Diodes from outside the country.

This means that the cruder sampling system, using the avalanche transistor for sampling command pulse generation will be used for simple level measurement while a special unit will later be developed for TDS work.

The present directional coupler and signal pulse generator designs perform sufficiently well as to need no redesigning.

By utilizing hybrid packaging[99] and microwave stripline techniques[100] it is hoped to greatly reduce the final size of the instrument. This method of construction should also reduce the cost of a unit when producing large quantities.

CONCLUSION

After consideration of the available microwave level measuring systems and in the light of experimental results, it was decided that Time Domain Reflectometry (TDR) is the most appropriate technique for the measurement of liquid level in flotation cells. With this system it is possible to overcome the problem of attenuation in the froth.

A prototype instrument, based on TDR principles and using a single conductor guided-wave transmission line to direct the TDR pulses into the flotation cell, has been developed and tested.

Results of the tests show that the instrument easily satisfies the system resolution criterion of 10mm proposed at the outset of its' design. Furthermore, as a result of the response time chosen, it exhibits a high immunity to surface disturbances of short duration, giving an output related to the average liquid level in the flotation cell. Owing to the relatively slow mechanical level control apparatus in the cell, it was possible to choose the response time in such a way as to provide this smoothing action and still control the liquid level effectively.

The use of a Goubau or guided-wave line (Section 5.10) simplifies the design by replacing the wideband horn antennas that would otherwise be necessary for baseband pulse transmission and reception. A dielectric Teflon coating is to be applied to it for the dual purpose of inhibiting particle deposition and improving the coupling of the relevant propagation mode to the line. An added advantage of the Goubau line is that it restricts the field of the pulses to the flotation cell reducing unwanted reflections to a minimum.

The use of locally available components throughout greatly reduces the production cost of the basic level measuring instrument. The use of hybrid packaging and microwave stripline techniques should further reduce the final size and cost of the instrument, while improving its' reliability.

These factors combine to provide an instrument that is cheap, robust and easy to maintain on line at a mineral processing plant.

This system is not seen as an end in itself, as its' analytical properties lend themselves to the characterisation of flotation froth. Development of a more sophisticated sampling detector, for recording reflected pulse profiles accurately, is proceeding, and it is likely that the resulting Time Domain Spectroscopy instrument will become a powerful tool in the mineral processing field.

This thesis has shown, in principle, that it is possible to accurately detect liquid level changes, under a layer of attenuating froth, using Time Domain Reflectometry techniques and a novel signal processing system.

REFERENCES

1. GOODMAN, J.W. An Introduction to the Principles and Applications of Holography. *Proc. IEEE*, vol. 59, no. 9, Sept. 1971, pp. 1292-1304.

2. MUELLER, R.K. Acoustic Holography. *Proc. IEEE*, vol. 59, no. 9, Sept. 1971, pp. 1319-1335.

3. LEITH, E.N. Quasi-Holographic Techniques in the Microwave Region. *Proc. IEEE*, vol. 59, no. 9. Sept. 1971, pp. 1305-1318.

4. TOMIYASU, K. Tutorial Review of Synthetic Aperture Radar (SAR) with Applications to Imaging of the Ocean Surface. *Proc. IEEE*, vol. 66, no. 5, May 1978, pp. 563-583.

5. BROOKES, S.R. Synthetic Aperture Radar - An Introduction to space-borne systems. *The Marconi Review Second Quarter*, 1979, pp. 88-103.

6. ELLIS, A.B.E. Processing of synthetic aperture rader from a satellite. *GEC Jnl of Science*, vol. 45, no. 3 pp. 123-128.

7. SKOLNIK. Radar Handbook Chapter 23. Synthetic Aperture Radar, McGraw-Hill, 1970.

8. DE VELIS/REYNOLDS. Theory and Applications of Holography. Addison-Wesley. 1967.

9. G. TRICOLES/NABIL H. FARHAT. Microwave Holography. Applications and Techniques. *Proc. IEEE*, vol. 65, no. 1. Jan. 1977, pp. 108-121.

10. ANDERSON, A.P. Microwave Holography. *Proc. IEEE*, vol. 124, no. 11R, Nov. 1977, *IEE Reviews*, pp. 946-962.

11. DESCHAMPS, G.A. Some Remarks on Radar-Frequency Holography. *Proc. IEEE letters*, April. 1967, pp. 570-571.

12. OGURA/IIZUKA. Hologram Matrix and its Application to a novel radar. *Proc. IEEE letters*, July 1973, pp. 1040-1041.

13. IIZUKA/OGURA/YEN/NGUYEN/WEEDMARK. Performances of a Hologram Matrix Radar. *Proc. IEEE letters*, December 1974, pp. 1718-1719.

14. OGURA/FUKUOKA. Imaging of a Two-Dimensional Target by means of Hologram Matrix. *Proc. IEEE letters*, March 1976, pp. 364-366.

15. NILSEN/SWINGLER. Quasi-Real Time Inertialess Microwave Holography. *Proc. IEEE letters*, vol. 65, no. 3, Mar. 1977, pp. 491-492.

16. IIZUKA/OGURA/YEN/NGUYEN/WEEDMARK. A Hologram Matrix Radar. *Proc. IEEE*, vol. 64, no. 10, Oct. 1976, pp. 1493-1504.

17. COOLEY/LEWIS/WELCH. Historical Notes on the Fast Fourier Transform. *Proc. IEEE*, vol. 55, no. 10, Oct. 1967, pp. 1675-1677.

18. COCHRAN / COOLEY / FAVIN / HELMS / KAENEL/ LANG/ MALING / NELSON / RADER/ WELCH. What is the Fast Fourier Transform? *Proc. IEEE*, vol. 55, no. 10, Oct. 1967, pp. 1664-1674.

19. ROTH, P. Digital Fourier Analysis. *Hewlett Packard Jnl*, June 1976, pp. 2-9.

20. HUANG, T.S. Digital Holography. *Proc. IEEE*, vol. 59, no. 9, Sept. 1971, pp. 1335-1346.

21. IIZUKA, K. Subtractive HISS Radar. *Proc. IEEE letters*, July 1977, pp. 1081-1083.

22. ROSS, G.F. Barbi - A new precollision sensor for airbag activation in automobiles. *European Microwave Proceedings, 4th Conference, Sept. 10 to 13th 1974, Montreux, Switzerland.*

23. ROSS, G.F. Barbi - A new radar concept for precollision sensing. *International Conference on Occupant Protection, 3rd July, 1974.*

24. DANIELS, D.G. The use of Radar in Geophysical Prospecting. *IEEE Int. Conf. on Radar 77, 25 to 28th October 1977.*

25. CHAN / MOFFAT / PETERS. A Characterization of Subsurface Radar Targets. *Proc. IEEE*, vol. 67, no. 7, July 1979. pp. 991-1000.

26. CHUDOBIAK / GRAY / WIGHT. A Nanosecond Impulse X-band Radar. *Proc. IEEE letter*, vol. 66, no. 4, April 1978, pp. 523-524.

27. FELLNER-FELDEGG, H. The Measurement of Dielectrics in the Time Domain. *Jnl, Phy. Chem.* vol. 73, no. 3, March, 1969. pp. 616-623.

28. FELLNER-FELDEGG, H. Permeability, Permittivity and Conductivity Measurements with Time Domain Reflectometry. *Hewlett-Packard Application Note 153*, May 1972.

29. NICOLSON / ROSS. Measurement of the Intrinsic Properties of Materials by Time Domain Techniques. *IEEE Trans. Ins. Meas.*, vol. IM-19, no. 4, Nov. 1970. pp. 377-382.

30. COLE, R. Time Domain Spectroscopy of Dielectric Materials. *IEEE Trans. Ins. Meas.*, vol. IM-25, no. 4, Dec. 1976, pp. 371-375.

31. SUGGETT, A. Microwave dielectric measurements using time domain spectroscopy: - Note on recent technique advances. *Jnl Phys. E: Scientif Instruments*, 1975, vol. 8.

32. BENNETT / ROSS. Time Domain Electromagnetics and its Applications. *Proc. IEEE*, vol. 66, no. 3, Mar. 1978. pp. 299-318.

33. STRICKLAND, J. Time Domain Reflectometry Measurements. Tektronix Measurement Concepts Series, 1970.

34. Selected Articles on Time Domain Reflectometry Applications. *Hewlett-Packard Application Note 75.*

35. DANIELSON / GARDNER. Measurement of Liquid Layer thickness with Time Domain Reflectometry. *Hewlett Packard Jnl.* Jan 1966. pp. 7-8.

36. GERHARZ, R. Wire-guided transients as remote sensing agents for material objects. *Int. J. Electronics*, 1977, vol. 42, no. 5, pp. 449-455.

37. SKOLNIK. Radar Handbook, Chapter 16 CW and FM radar. McGraw-Hill 1970.

38. SKOLNIK. Introduction to Radar Systems, Chapter 3 CW and FM Radar. McGraw-Hill 1962.

39. ZUR HEIRDEN / OEHLEN. Radar Anticollision Warning System for Road Vehicles. *Electrical Communication*, vol. 52, no. 2, 1977.

40. CLARRICOATS, P. Portable Radar for the Detection of Buried Objects. *IEEE Int. Conf. Radar 77*, 25 to 28th Oct. 1977, pp. 547-551.

41. WADLEY, T.L. Electronic Principles of the Tellurometer. *Trans. SAIEE*, May 1958, pp. 143-172.

42. STUCKLY / HAMID / ANDRES. Microwave Surface Level Monitor. *IEEE Trans. Ind. Elec. and Cont. Ins.*, vol. IECI-18, no. 3, Aug. 1971. pp. 85-92.

43. WANTENAAR / BACON / GOODHEAD. A lecher wire system for good spatial confinment of microwaves, *Jnl. Phys. E*, pp. 714-715, 1975.

44. NILSEN / ARCHER. Depth Resolution in a synthetic aperture system of variable focal length. *UCT Research Review*, vol. 2, no. 8, Oct. 1978, pp. 299-302.

45. HORNER, F./ TAYLOR, T./DUNSMUIR, R./ LAMB. G., and JACKSON, W. Resonance Methods of Dielectric Measurement at Centimetre Wavelengths. *Jnl of IEE*, vol. 93, Part 3, no. 21, Jan. '46.

46. KUMAR, A., and SMITH, D.G. Microwave properties of liquids using a modified cavity perturbation technique. *IEE Proc.*, vol. 127, Pt.H., no. 1, Feb. 1980.

47. CAMPBELL, C.K. Free-space Permittivity Measurements on Dielectric Materials at Millimeter Wavelengths. *IE^3 Trans. Ins. Meas.*, vol. IM-27, no. 1, March 1978.

48. BUSSEY, H.E. Measurement of RF Properties of Materials: A Survey. *Proc. IEEE*, vol. 55, no. 6, June 1967, pp. 1046-1063.

49. ELLERBRUCH, D. UHF and Microwave Phase Shift Measurements. *Proc. IEEE*, vol. 55, no. 6, June 1967, pp. 960-990.

50. The Measurement of the Dielectric Constant of a material in free space. Chapter 5 Phillips Microwave Experiments Handbook.

51 JORDAN, E, and BALMAIN, K. Electromagnetic Waves and Radiating Systems. CH 5 Part II. Prentice Hall 1968.

52. LORRAIN, P., and CORSON, D. Electromagnetic Fields and Waves. CH 11 and CH 12. Freeman 1962.

53. GOUBAU, G. Surface Waves and their application to Transmission Lines. *Jnl Applied Physics*, vol. 21, Nov. 1950. pp. 1119-1128.

54. GOUBAU, G. Single-Conductor Surface-Wave Transmission Lines. *Proc. I.R.E.*, June 1951. pp. 619-624.

55. JORDAN, E./ BALMAIN, K. Electromagnetic Waves and Radiating Systems. CH 5, Part I. Prentice Hall 1968.

56. FREDERICK WILLIAMS JNR, G. Microwave Emmissivity Measurements of Bubbles and Foam. *IEEE Trans. Geo. Elec.*, vol. GE-9, no. 4, Oct. 1971.

57. GAINES. Insoluble Monolayers at liquid-gas interfaces.(Wiley 1966)

58. ADAMSON,A.W. Physical Chemistry of Surfaces. (Wiley 1976)

59. SEBBA, F. Macrocluster Gas-Liquid and Biliquid Foams and Biological Significance. ACS Symposium Series no. 9. *Colloidal Dispersion and Micellar Behaviour.*

60. GINZBURG. The propagation of Electromagnetic Waves in plasmas. *International Series of Monographs on Electromagnetic Waves.* vol. 7, (Pergamon 1964).

61. Electric Networks - Skilling (Wiley 1974).

62. ROSS, G.F. The transient analysis of certain Tem Mode 4-part Networks. *IE^3 Trans on Microwave Theory and Techniques.* Vol. MTT-14.

63. DAVIS, F., LOEB, H.W. Time Domain Measurements for Transistor and Network characterisation up to 1 GHz. *Proc. IE^3*, pp. 1649-1650 (Oct. 1965).

64. ANDREWS. Computer Techniques in Image Processing. *Academic Press.*

65. ANDREWS, J. Automatic Network Measurements in the time domain. *Proc. IE^3*, vol. 66, no. 4. April, 1978.

66. PARISIEN, B., and STUCKLY, S. A Microprocessor-controlled Time-domain Spectrometer. *IE^3 Trans. Ins. Meas.* vol. IM-28, no. 4. Dec. 1979.

67. CHALMERS, B. Applications of Super-Resolution Techniques to Time Domain Reflectometry Systems. *Electronic Letters*, 16 Feb. 1978, no. 4.

68. RIAD, S., and NAHMAN, N. Application of the Homomorphic Deconvolution for the Seperation of TDR Signals, occurring in overlapping time windows. *IE³ Trans. Ins. Meas.* vol. IM-25 no. 4, Dec. 76.

69. BENNET, C., and ROSS, G. Time Domain Electromagnetics and Its applications. *IE³ Proc.*, vol. 66, no. 3. March 1978.

70. ELLIOT, B. High Sensitivity Time-Domain Reflectometry. *IE³ Trans. Ins. Meas.* vol. IM-25, no. 4 Dec. 76.

71. OLIVER, B.M. Time Domain Reflectometry. *Hewlett-Packard Journal*, vol. 15, no. 6. Feb. 1964.

72. Scattering Coefficients. *HP Journal.* Feb. 1967, vol. 18, no. 6.

73. IEEE Glossary of Pulse Terms and Definition. *IEEE Standard 194.*

74. IEC Pulse techniques and apparatus, Part 1: Pulse terms and definitions. *Publication 469-1. 1st edition*, International Electrochemical Commission, Geneva, Switzerland, 1974.

75. MATICK. Transmission lines for Digital and Communication Networks. (McGraw-Hill 1969)

76. NAHMAN, N.S. A discussion on the Transient Analysis of Coaxial Cables considering High Frequency Losses. *IRE Trans. Circuit Theory*, June 1962.

77. NAHMAN, N.S., and WIGINGTON, R.L. Transient Analysis of Coaxial Cables considering Skin Effect. *Proc. IRE*, vol. 45, no. 2. Feb. 1957.

78. KIRSTEN, F.W. Pulse Response of Coaxial Cables. Lawrence Radiation Laboratory. *Counting Note no. CC2-1A.*

79. Tektronix Sampling Oscilloscope Handbook. Tektronix Measurement Concepts Series. *Tektronix Inc.*

80. Motorola High Speed Transistor Switching Handbook. pp. 285-304. *Motorola Inc.*

81. D'YAKONOV, V.P. Nanosecond Pulse Generators Based on Avalanche Transistors with Low-Voltage Power Supply. Translated *Pribory i Tekhnika Eksperimenta* no. 2, pp. 126-127. March-April, 1978.

82. D'YAKONOV, V.P. Nanosecond Delayed Pulse Generator Based on an Avalanche Transistor. Translated *Pribory i Tekhnika Eksperimenta*, no. 2, pp. 127-128. March-April, 1978.

83. D'YAKONOV, V.P. Generator for Rectangular Nanosecond Pulses using Avalanche and SHF Transistor. Translated *Pribory i Tekhnika Eksperimenta* no. 3, pp. 129-130, May-June, 1978.

84. D'YAKONOV, V.P. Generator of Coded Series of SMF Picosecond Pulses Based on Avalanche Transistors. Translated *Pribory i Tekhnika Eksperimenta* no. 3, pp. 131-132, May-June, 1978.

85. D'YAKONOV, V.P., and PROFATILOV, A.I. Nanosecond Pulse Shapers Based on Avalanche Transistors and Powerful SMH Transistors. Translated *Pribory i Tekhnika Eksperimenta* no. 3, pp. 134-136, May-June, 1978.

86. LARIN, I.G./LATUSHKIN, S.T./REZVOV, V.A./YUDIN, L.I. Multichannel Generator of Nanosecond Pulses. Translated *Pribory i Tekhnika Eksperimenta* no. 3, pp. 132-134, May-June, 1978.

87. SOMMERFELD, A. *Ann. Phys. Chemie (Neue Folge) 67-1, 1899.* J.A. Stratton gives sufficient information about this reference in his book 'Electromagnetic Theory' - McGraw-Hill, N.Y., 1941.

88. RUTHROFF, C.L. Some Broadband Transformers. *Proc. IRE*, August 1959, pp. 1337-1342.

89. WINNINGSTAD, C.N. Nanosecond Pulse Transformers. *IRE Trans. Nucl. Sci.*, March 1959, pp. 26-31.

90. MATICK, R.E. Transmission Line Pulse Transformers - Theory and Applications. *Proc. IE*^{3}, vol. 56, no. 1, Jan. 1968, pp. 47-62.

91. CRONSON, H.M. A wideband directional coupler for Time-Domain Measurements. *IEEE Trans. Ins. Meas.*, vol. 25, no. 1, Mar. 1976. pp. 15-17

92. MATTHAEI, G.L./YOUNG, L./JONES, G.M.T. Microwave filters, Impedance-Matching Networks and Coupling Structures. *CH13*, pp. 775-780. McGraw-Hill 1964

93. COEKIN, J.A. High Speed Pulse Techniques CH8(Pergamon 1975).

94. JÄGER, D/RABUS, W. Bias-dependent Phase Delay of Schottky contact Microstrip Line. *Electronics Letters*, 17th May, 1973, vol. 9, no. 10, pp. 201-203.

95. ADAM, J.D./DANIEL, M.R./SCHROEDER, D.K. Magnetostatic-wave devices move microwave design into the Gigahertz Realm *Electronics*, May 8, 1980, pp. 123-128.

96. GROVE, W.M. A DC to 12.4 GHz Feed through Sampler for Oscilloscope and other RF Systems. *Hewlett Packard Journal*, Oct. 1966.

97. BOCKRISS, J., and REDDY, A. Modern electrochemistry: An introduction to an interdisciplicary area. MacDonald 1970.

98. VANDRE, R. An ultrafast Avalanche transistor pulser circuit. *Electronic Engineering* Mid October 1977. p. 19.

99. POLDEN, J.R. Hybrid Technology comes of age. *The Electronics Engineer*, 20th March, 1980.

100. GUNSTON, M.A.R/WEALE, J.R. The Transmission Characteristics of Microstrip. *The Marconi Review*, vol. 32, no. 174, Third Quarter 1969. pp. 226-243.

101 LAIRD, D.T./KENDING, P.M. Attenuation of Sound in water containing bubbles. *Jnl. Ac. Soc. Am.*, vol. 24, no. 1, Jan. 1952.

102 McPHESON, J.D. The Effect of Gas Bubbles on Sound Propagation in Water. *Phys. Soc. Proc.*, vol. B70, no. 1, 1957.

103 VALITOV, V.M./FEL'DMAN , Y.D./ZUEV, Y.F. Time Domain Spectroscopy of Dielectrics (Survey) . Translated *Pribory i Tekhnika Eksperimenta*, vol. 22, no. 3, Part 1. pp. 611-629.

LIST OF FIGURES

LIST OF APPENDICES

APPENDICES

APPENDIX A

AN INTRODUCTION TO FROTH FLOTATION

The froth flotation process is the most widely used and most complex of all ore concentration methods in use by the mining industry today.

It is a physico-chemical method of concentrating the desired mineral content of finely ground ores. The process involves the chemical treatment of the ore pulp (a mixture of crushed ore and water) to create conditions favourable for the attachment of certain mineral particles to air bubbles. These air bubbles carry the selected minerals to the surface of the pulp and form a stabilised froth, which is skimmed off, while the other unwanted minerals and waste rock remain submerged in the pulp.

Particles ranging in size from 850 to a few microns are responsive to this process.

THE PROCESS

Essentially, flotation involves the attachment of mineral particles to air bubbles so that the particles can be carried to the surface of the ore pulp where they are removed.

The process can be broken down into a number of steps as follows:

1) Grinding the ore to a size sufficiently fine to liberate the valuable minerals from the adhering waste rock (gangue).
   For optimum flotation results these minerals should be completely separated from the gangue in the grinding step. In practice this is seldom economically feasible and it is necessary to find the best compromise between particle size (grinding time and cost) and percentage recovered mineral.

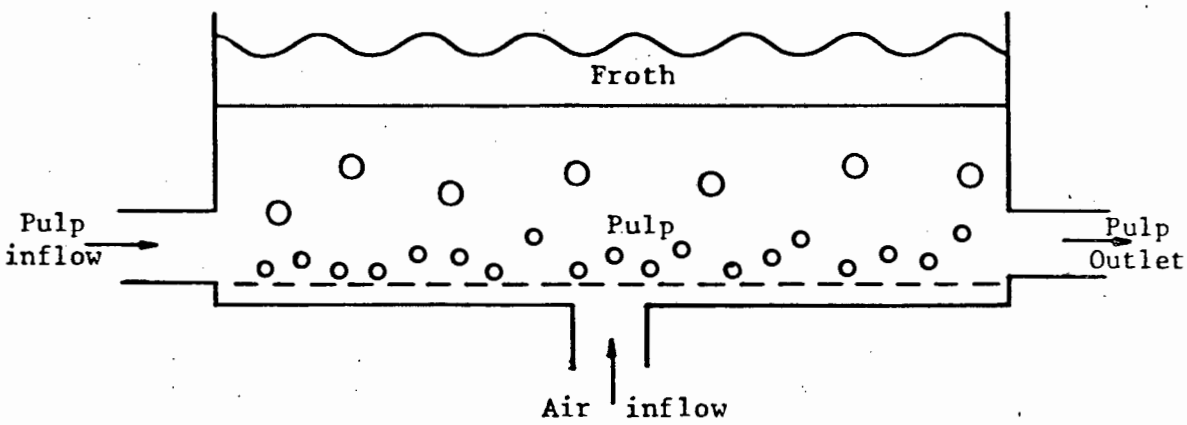

FIGURE A1 A PNEUMATIC FORM OF FLOTATION CELL

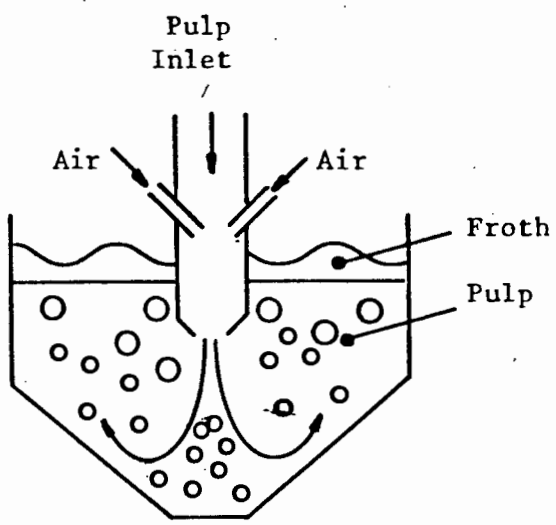

FIGURE A2 A CASCADE FORM OF FLOTATION CELL

2) Providing favourable conditions for the adherence of the desired mineral to air bubbles.

In order to obtain these conditions a hydrophobic surface film must be formed on the particles to be floated and a hydrophilic or wettable one on all others. Reagents called collectors and modifiers are used to ensure that this is so.

3) Creating a rising current of air bubbles in the ore pulp.

This is accomplished by using a flotation cell that injects air into the bottom of the pulp mixture. Further details of flotation cell construction appear elsewhere in this appendix.

4) Forming a mineral laden froth on the surface of the ore pulp.

Addition of a suitable frothing agent to the pulp ensures the formation of a stable froth.

5) Removal of the mineral laden froth.

Careful flotation cell construction must incorporate some means for the froth retrieval. This is normally done by using some form of scoop or sluice gate, or some combination of both.

FLOTATION CELL CONSTRUCTION

There are three basic classes of flotation cell, as follows:

1) Pneumatic Flotation Cells (Fig. A1)

In its' simplest form the pneumatic cell consists of a trough with some form of air supply in its' bottom. The air is bubbled through the pulp as it passes through the tank and the froth is scooped off.

2) Cascade Flotation Cells (Fig. A2).

The cascade cell utilizes the pulp inlet flow to inject air into the pulp. The action of the pulp flowing through the delivery nozzle sucks air into the stream.

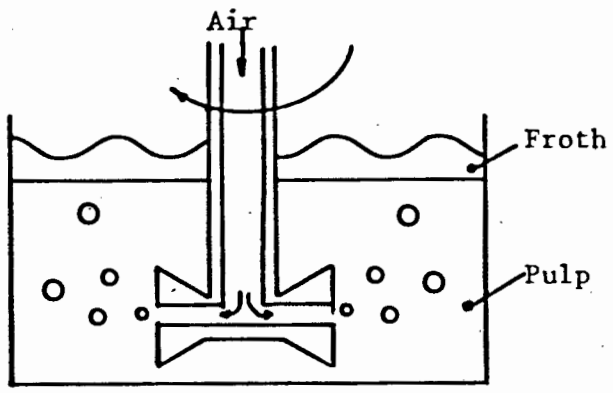

FIGURE A3 A SUB-AERATION FORM OF FLOTATION CELL WITH A HOLLOW IMPELLER SHAFT

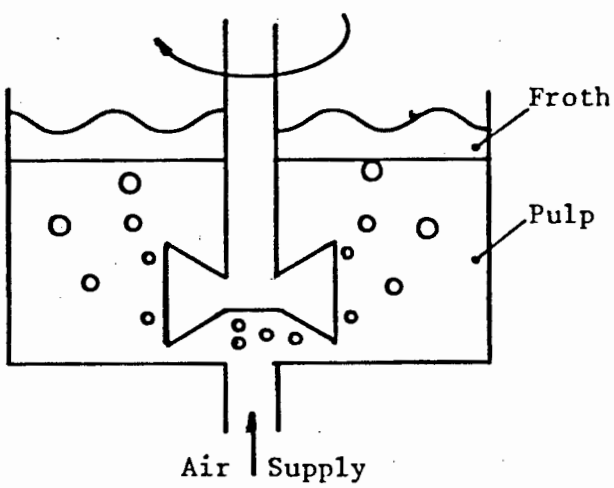

FIGURE A4 A SUB-AERATION FORM OF FLOTATION CELL WITH A SEPERATE AIR SUPPLY

3) Sub-aeration Flotation Cells.

The sub-aeration machines can be further divided into 2 groups distinguished by the manner of air introduction into them.

In the first group (Fig. A3) the impeller acts as a centrifugal air pump submerged in the pulp with its suction pipe, usually a hollow impeller shaft, passing from the surface of the pulp to the impeller zone.

In the second group (Fig. A4), however, air is pumped in at a point directly under the impeller by an external air pump. This arragement gives an additional degree of control over the process.

Of the three classes the sub-aeration system using the centrifugal air pump is the most popular and widely used.

REAGENTS

1) Collectors

The collector is the heart of the flotation process since it is the reagent which produces the hydrophobic film on the mineral particles. Most of the collectors in current use are heteropolar (i.e. they contain both a polar (charged) and non-polar (uncharged) groups). When attached to a mineral particle these molecules are so orientated that the non-polar or hydrocarbon group is extended outward. Such orientation results in the formation of a hydrophobic hydrocarbon film on the mineral surface. Fig. (A5) shows an air bubble/mineral surface contact with and without a collector. It is evident that in the absence of the collector the air bubble makes only negligible contact with the mineral surface making flotation impossible. With the collector on the other hand a 60^{o} contact angle is obtained enabling flotation to take place.

Collectors in use today are usually members of the xanthate family although other hetero-polar compounds are sometimes also used.

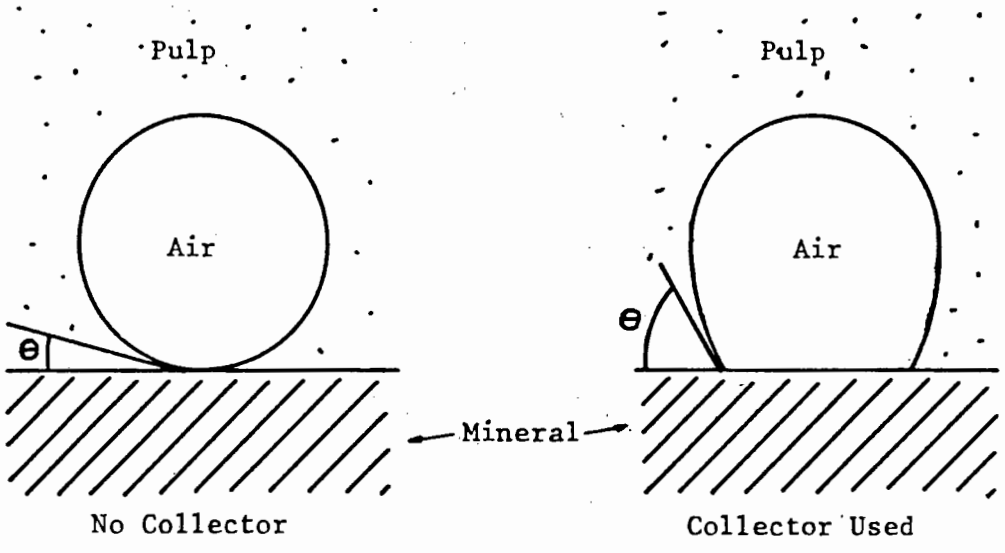

FIGURE A5

THE EFFECT OF USING A COLLECTOR

2) Frothers

The main purpose of a frothing agent is the creation of a froth capable of carrying the mineral laden bubbles until they can be removed from the flotation cell.

This objective is accomplished by imparting temporary toughness to the covering film of the bubble. The life of the individual bubbles is thus prolonged until it can be further stabilised by the adherence of mineral particles and joined with other bubbles at the pulp surface to form a froth.

All frothers in use are organic heteropolar compounds and have the ability to lower the surface tension of the water. The non-polar organic radical, like that of the flotation collector molecule, repels water while the polar portion attracts water.

The distribution of these molecules in the bubble air/water interface gives the rising bubbles the required elasticity to burst through the top layer of water and emerge at the air/water interface intact and unbroken.

Frothers in common usage are Amyl Alcohol, Cresylic Acid and Pine Oil.

3) Modifiers

All reagents whose principal function is neither collecting nor frothing are called modifiers. They may act as depressants, activators, pH regulator or dispersants.

A depressant is any reagent which inhibits the adsorption of a collector by a mineral particle and therefore prevents its' flotation. Activators on the other hand, enhance the adsorption of the collector, making the flotation of certain minerals more efficient. Singly or in combination, activators and depressants find their major usage in the differential flotation of a number of different minerals from a single ore.

The effectiveness of all classes of flotation agents depends to a large extent on the degree of alkalinity or acidity of the pulp solution. Therefore one of the primary objectives of flotation testing is to

discover the optimum pH value for a given reagent combination and ore. Alkalinity regulators most commonly used are lime and soda ash while acid pH control is usually obtained with sulphuric acid because of its' low cost.

Another problem encountered is the adherence of very fine gangue particles to the desired mineral particles. This interferes with the collector's hydrophobic action and prevents flotation of the mineral particles in the normal manner. Addition of dispersants such as Sodium Silicate to the pulp changes its' ionic balance in such a way as prevent this happening.

APPENDIX B

DEPTH RESOLUTION IN A SYNTHETIC APERTURE SYSTEM OF VARIABLE FOCAL LENGTH.

A reprint of an article that appeared in *Uct Research Review*, vol.2, no.8, Oct.1978, pp.299-302. by C.Nilsen and M.Archer.

DEPTH RESOLUTION IN A SYNTHETIC APERTURE SYSTEM OF VARIABLE FOCAL LENGTH.

C.Nilsen/M.Archer.

INTRODUCTION

There has recently been some interest in the application of electromagnetic radiation in the microwave region to the measurement of the position of liquid/air and/or liquid/froth/air interfaces in an industrial mineral processing environment.

The most obvious advantage of a microwave depth probe is its non-contacting nature, since existing analogue capacitive and resistive depth probes are prone to fouling in the extremely dirty conditions experienced.

The requirement of a resolution in depth of, say, 20mm would require in a conventional pulsed radar-like device a pulse length of not more than 133 pS. (1 pS = 10^{12} s) Such a pulse would require no less than 15 GHz total bandwidth for faithful reproduction, and the construction of the electronic elements required to generate such pulse lengths is not a task lightly undertaken.

The situation is hardly improved if, instead of a pulse system, a swept frequency (FM radar) probe is mooted. It turns out that FM radars require similar bandwidth to pulsed radar if they are to offer similar depth or range resolution.

One other characteristic of electromagnetic radiation not yet considered is its ability to be focussed (by a variety of techniques) at different distances.

One may therefore envisage a depth probe consisting of a variable focal length aperture and using continuous monofrequency microwave illumination of the surfaces below it.

Such a system is described in the literature (1) and was developed by a Canadian group for the purposes of gauging sea-ice thickness in their polar regions.

It is the object of this article to examine the resolution available to variable focal length systems whose aperture is formed by synthesis.

SIMULATION AND RECONSTRUCTION

A block diagram of a depth measuring system is illustrated in Fig. 1.

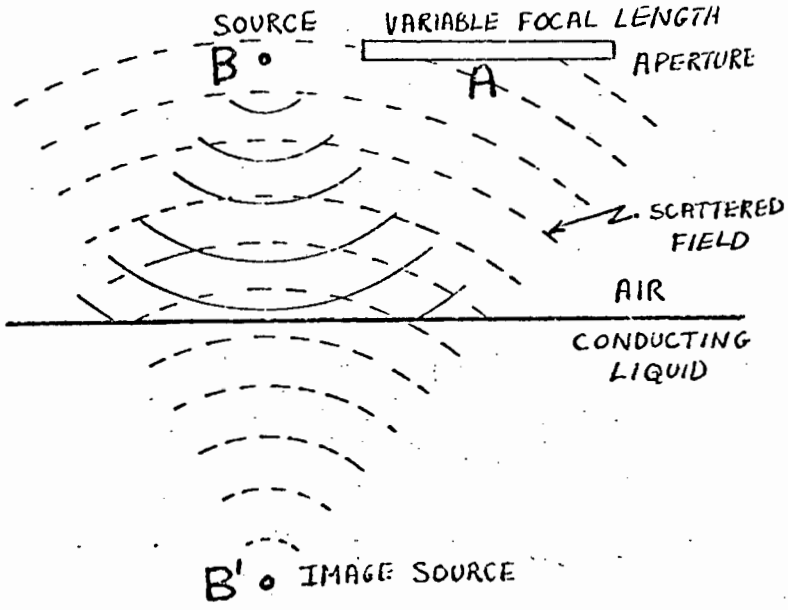

FIGURE B1

A quasi-isotropic source B illuminates a flat liquid/air interface below it; an image source can be considered to be at B' if the surface is reasonably smooth and conducting. The phase of the field scattered from the surface is measured across the aperture A.

The linear resolution attainable in axes both parallel and normal to the aperture can be estimated by a reconstruction process, (2) operating on the measured phase data, which seeks to "image" the source B'. The reconstruction process can be thought of as a matched filter operation, in as much as a complex function equal to the conjugate of the complex measured field is sought which best matches the curvature of the field incident on aperture A.

Such a system has been simulated, and the results of the reconstruction are shown below in Figures 2 and 3. This has been performed at the optimum range of 1 metre, since the data had originally a focal length or "curvature" of 1 metre.

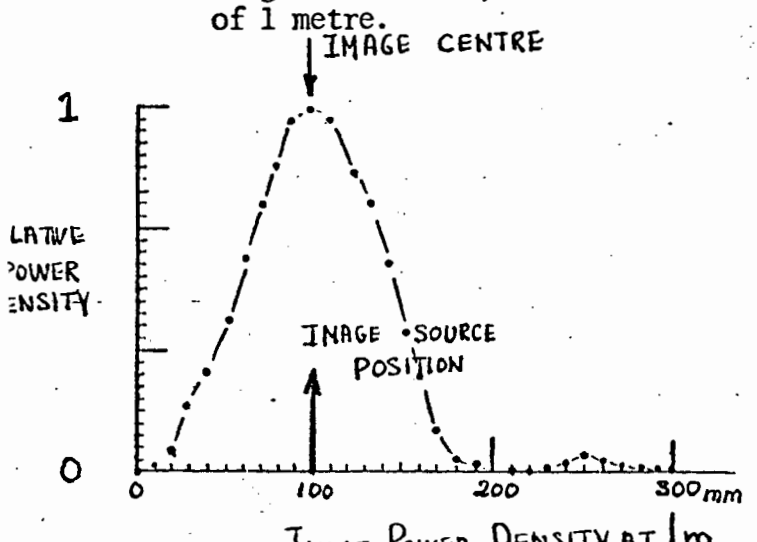

FIGURE B2 IMAGE POWER DENSITY AT 1m.

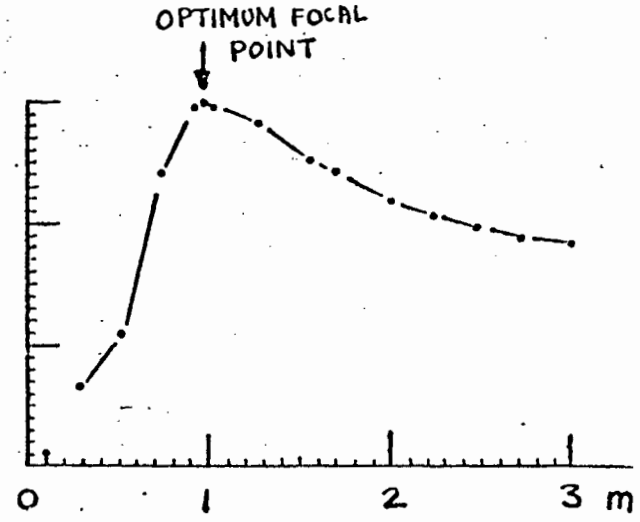

FIGURE B3 IMAGE POWER DENSITY VS. FOCAL LENGTH.

The location of the image maximum in the axis parallel to the aperture is accurately found, and the image half-power width is, as usual, diffraction limited to its theoretical value of $\frac{\lambda R}{D}$ = 101 mm. (Fig.2).

Having located the image maximum, it is a simple matter to "scan" the reconstruction process through different focal distance values. The results are shown in Fig.3; notice that the resolution is considerably poorer in this co-ordinate.

RECONSTRUCTION USING REAL PHASE DATA.

An experiment has been performed to verify the above simulation and the layout is shown in Fig.4.

A phase and amplitude receiver is available (3) which operates at 9,9GHz. (λ = 30,3mm). A continuous wave 9,9 GHz. source illuminates, inter alia, a co-operative target. The field scattered by this co-operative target is modulated at a low frequency to which the phase and amplitude receiver will alone respond. Field components scattered from other objects in the vicinity are not so modulated and are, to within second order, ignored by the receiver. A synthetic aperture 300mm long is formed by a quasi-isotropic antenna probe connected by a low loss flexible cable to the phase and amplitude receiver. A reference sample of the 9,9 GHz. source field is also connected to the receiver. The antenna probe is stepped in 10mm intervals across the aperture and the phase of the field is recorded at each point.

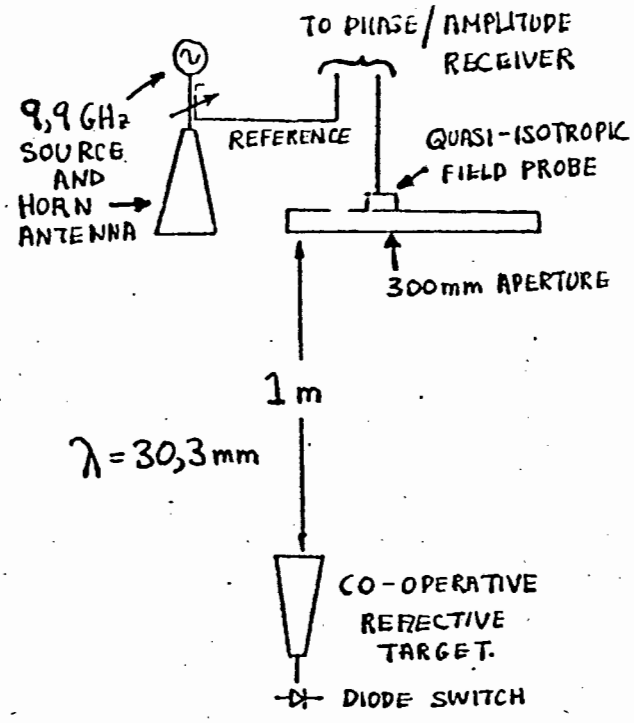

FIGURE B4 EXPERIMENT BLOCK DIAGRAM

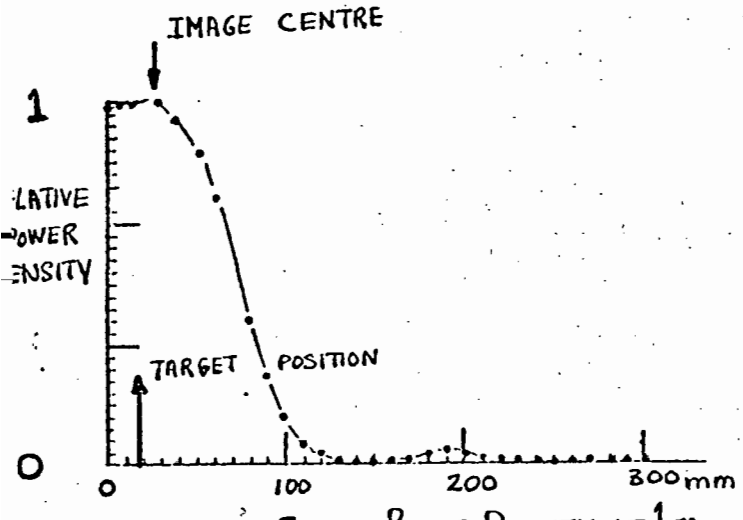

FIGURE B5 IMAGE POWER DENSITY AT 1m.

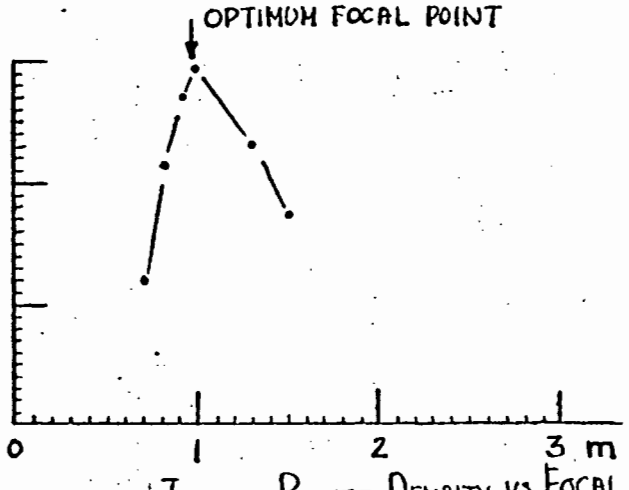

FIGURE B6 IMAGE POWER DENSITY VS FOCAL LENGTH

Fig.5 shows the reconstructed x-axis image distribution at the optimum focal length of 1 metre. The "target" (reflective co-operative target) position in the axis parallel to the aperture is correct to within 13mm at this focal length.

However, if the peak image intensity is sought at different focal lengths but at the same aperture-axis co-ordinate, then the variation with range is found to be more pronounced than was the case using simulated data (Fig.6). The reason for the improved depth resolution lies in the nature of the target. The reflective horn is not an isotropic scatterer, and in

fact the image maximum lies not along an axis normal to the aperture (as was the case in Fig.3) but at an angle to it - this angle is complementary to the angle subtended by the source and target. The locus of the image maxima are plotted in Fig.7.

This suggests that improved depth resolution may be had if the synthetic aperture is used to "look" not normal to its axis, but to one side.

There is a limit to the angle that the target may subtend with the normal to the aperture. As this angle increases the simple algorithm for reconstruction fails to describe accurately the curvature of the scattered field, and image linear resolution suffers.

CONCLUSION

It has been demonstrated that high depth resolution is not an intrinsic property of a microwave imaging system, but given a suitable choice of illuminating function, the situation may be improved. It is felt that a trade-off of depth resolution against aperture axis resolution can be made, and future experiments will be planned with this point in mind.

REFERENCES

(1) "A Hologram Matrix Radar," K. Iizuka, H. Ogura, J.L. Yen, V.K. Nguyen, and J.R. Weedmark, Proc. IEEE, pp 1482 - 1503, Vol. 64, Oct. 1976.

(2) Research Review, Vol. 1, No. 3, June 1977, pp 7 - 9.

(3) Research Review, Vol. 1, No. 1, April 1977, pp 37 - 39.

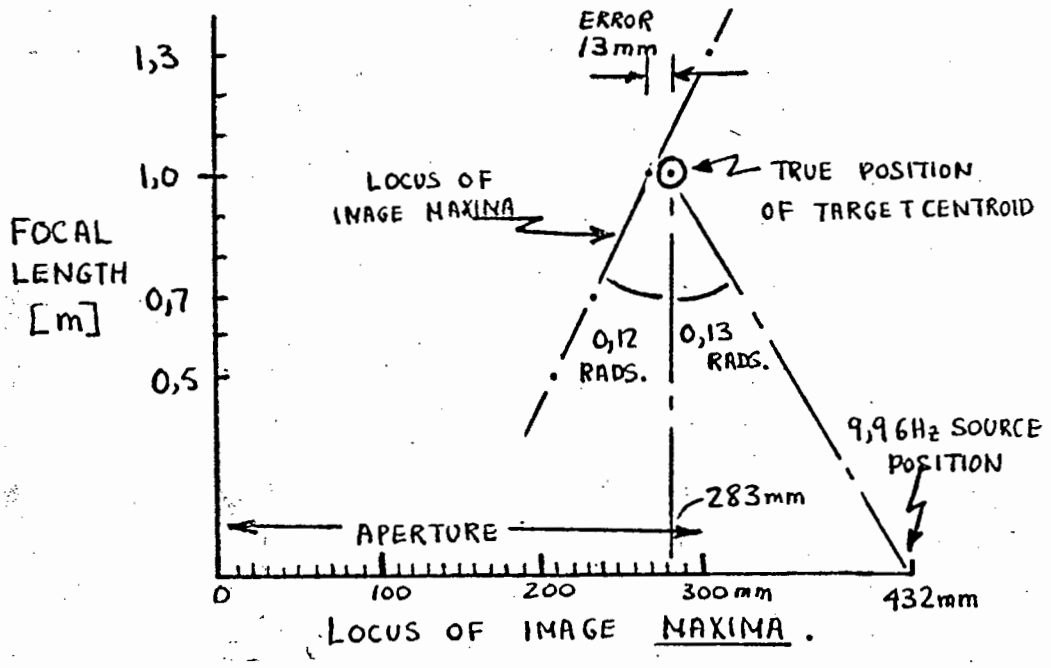

FIGURE B7

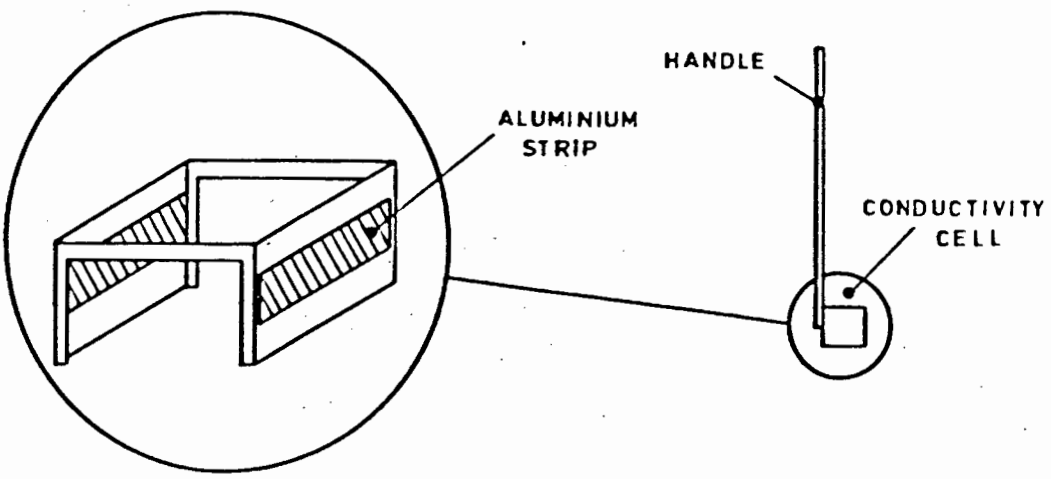

FIGURE C1 CONDUCTIVITY CELL CONSTRUCTION

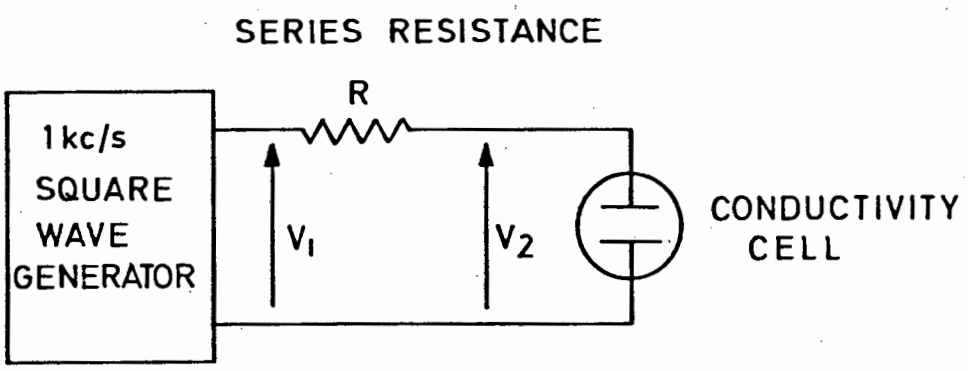

FIGURE C 2 CONDUCTIVITY APPARATUS

A P P E N D I X C

CONSTRUCTION AND CALIBRATION OF THE CONDUCTIVITY MEASURING APPARATUS

The conductivity cell was of an open construction to allow free flow of froth between its plates (Figure C1).

For calibration purposes a 0.1 Molar solution of Potassium Chloride was prepared. From tables in Bockriss and Reddy [97] the equivalent conductance Λ for the solution was found to be

$$\Lambda = 128{,}9 \text{ mho cm}^2/\text{eq}$$

From this specific conductivity $\sigma = \Lambda c z$, where

c = concentration in moles/cc

z = number of charge carriers/ion = 1

Substitution gives a theoretical specific conductivity (at 25°C)

$$\sigma = (128{,}9)(0{,}1)/1000$$
$$= 1{,}289 \times 10^{-2} \text{ mhos/cm}$$
$$= 1{,}289 \text{ mhos/m}$$

Measurement of the conductance, of the above solution, with a laboratory conductivity meter yielded a conductance of (1,27/90Ω) x 100 = 1,411 mhos/m.

This value differs from the theoretical value by only 9%, a difference easily explainable by temperature effects and the use of de-ionised water rather than distilled water for the KCℓ solution.

The resistance of the solution was measured again using the measurement system shown in Figure C2.

Cell resistance = $R V_2/(V_1-V_2)$

With a series resistance R = 220 Ω the resistance of the liquid was found to be 110 Ω. Comparing this to the previous reading (90/1.27) and correcting gives a cell constant of 1,55 for the conductivity cell.

In order to give the correct values, all measured values of conductivity must be multiplied by 1.55.

As the cell measures resistance R, it is necessary to calculate specific conductivity from

$$= \left(\frac{1.55}{R}\right) \times 100 \text{ mhos/m}$$

where the factor of 100 converts from mhos/cm to mhos/m.

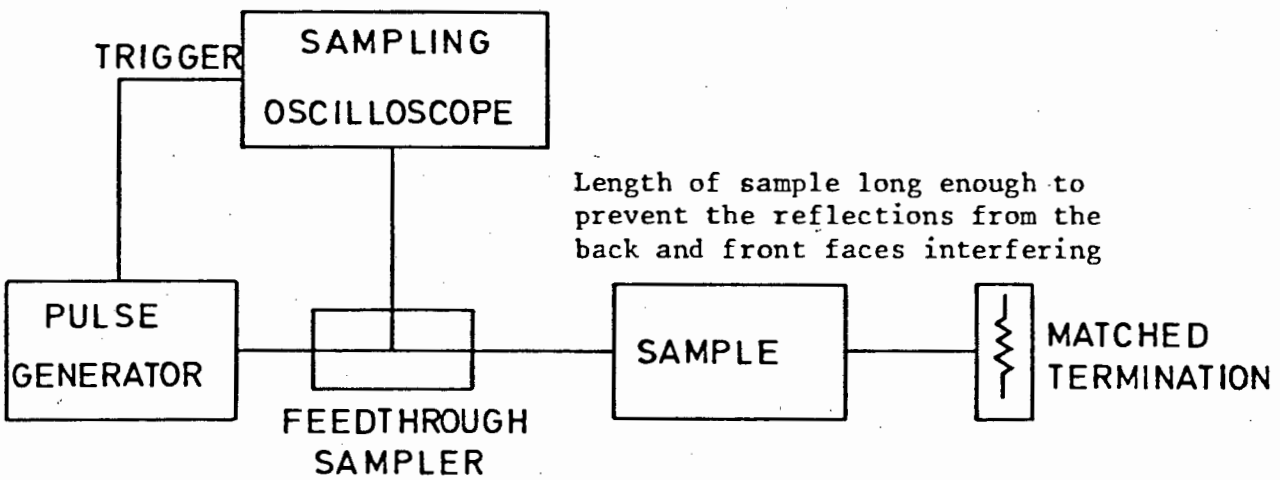

FIGURE D1 SINGLE REFLECTION APPARATUS.

A P P E N D I X D

A SUMMARY OF TIME DOMAIN SPECTROSCOPY METHODS AND A DISCUSSION OF THEIR APPLICATION TO REMOTE SENSING OF FLOTATION FROTH PROPERTIES

Until recently information on the dielectric properties of materials was obtained by measuring their complex permittivity $\epsilon(\omega) = \epsilon'(\omega) - i\epsilon''(\omega)$ over the frequency range of interest. Since the frequency range of electromagnetic radiation stretches from a few Hertz to many Giga Hertz, using this method of permittivity measurement involved a whole range of expensive instruments and time consuming processing of results.

By taking measurements in the time domain, rather than the frequency domain, it is possible to obtain the same permittivity information in only a fraction of a second. This method, called Time Domain Spectroscopy (TDS), utilises very short pulses with very fast risetimes, containing all the frequencies of interest, to perform the permittivity measurement at all these frequencies simultaneously.

Tunnel diode pulse generators (risetimes ≈25ps) and modern wideband sampling ascilloscopes allow this measurement method to be used right up into the microwave region, where savings in time and cost are most effective. The present state of the art in TDS measurements is a frequency range from 50 kHz to something slightly in excess of 15 GHz.

The Single Reflection Method [27]

Most TDS systems mentioned in the literature involve the propagation of a step voltage pulse in an air-filled coaxial line system and the monitoring of the change in the pulse characteristics after reflection from or transmission through a length of this coaxial line filled with the sample of material under test (Figure D1). The simplest TDS case involves the

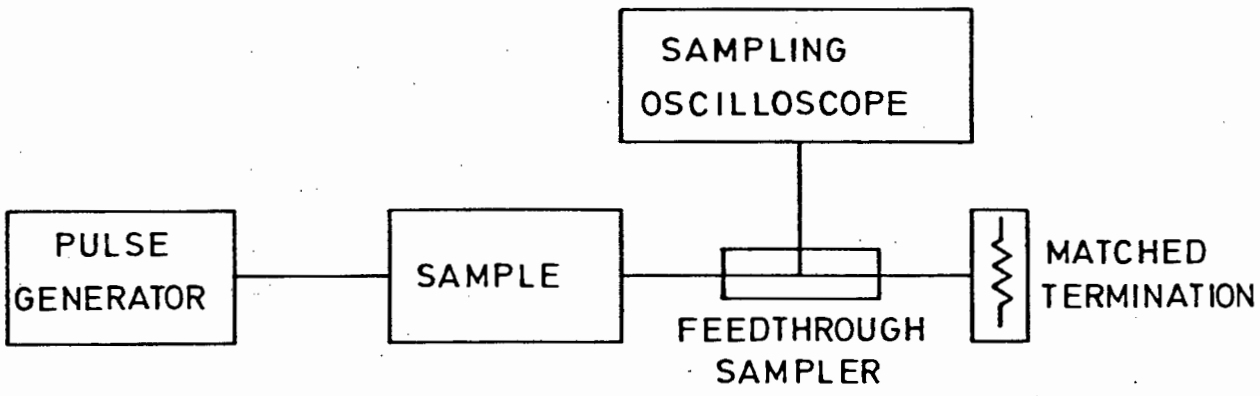

FIGURE D2 DIRECT TRANSMISSION MEASUREMENT APPARATUS

reflection of the input pulse from the first air/dielectric interface only, giving a complex reflection coefficient

$$\rho(i\omega) = \frac{1 - [\varepsilon(i\omega)]^{\frac{1}{2}}}{1 + [\varepsilon(i\omega)]^{\frac{1}{2}}}$$

The reflection coefficient $\rho(i\omega)$ is obtained from the ratio of the Fourier transform of the pulse reflected from the air/dielectric interface to that of the pulse reflected from a short circuit placed at a position equivalent to that of the air/dielectric interface.

Of all the TDS methods to be mentioned in this article, direct reflection TDS offers the highest frequency capabilities.

The Direct Transmission Method [103]

A system for measuring permittivities using the direct transmission method appears in Figure D2. The difference between this and the previous method is that the sample under test is placed between the pulse generator and sampling head. With this configuration it is no longer possible to regard the sample as infinite and some provision must be made to accommodate its finite length in the expression for the transmission coefficient. The resulting expression is

$$S_{21}(i\omega) = \frac{4\sqrt{\varepsilon(i\omega)}}{\left[1 + \sqrt{(i\omega)}\right]^2} \exp\ -ik\ell$$

where ℓ is the length of the sample.

Thin Sample Time Domain Spectroscopy [28]

By going to the extreme of using very thin samples terminated by a 50Ω load it is possible to obtain a linear relationship between signal and

permittivity. The impulse response of the dielectric and the step response of its conductivity can be measured directly, simplifying the interpretation of data and the transformation between time and frequency domains.

The relevant equations describing the behaviour of the reflected pulse in the time and frequency domain are described by Fellner-Feldegg in the above reference and are too numerous and involved to go into here.

The main advantages of this system are that very small amounts of the sample material are needed for analysis and that data processing is minimised.

The Multiple Reflection Method [29]

The multiple reflection method is one of the most widely used and well developed TDS methods used at present.

This method is similar to single reflection method already described in that it uses the same measurement setup as that shown in Figure D1. The incident pulse suffers multiple reflections at both air/dielectric interfaces of the sample (length ℓ), but in this case the time interval over which the reflected signal is recorded is such that it records the sum of all the multiple reflections.

A feature of the measurement cell used for this method is that it must allow samples of various lengths to be tested. This complicates the construction of the test line and extends the time necessary for each measurement.

The main advantage of this method is that it allows small amounts of material to be used for each investigation, and is well documented.

Analysis of TDS Data

One of the main drawbacks of TDS methods of investigation is that they require Laplace or Fourier analysis of their results to provide the necessary information about the dielectric properties of the materials investigated. This analysis usually requires the use of a computer.

More advanced processing techniques have allowed these calculations to be speeded up considerably. Various computational techniques, some involving the deconvolution of unwanted signals to increase system resolution [68], have also been developed. The present trend in VLSI circuit design promises to relieve much of the burden of TDS data analysis, as a number of maufacturers are working on circuit blocks that will implement fast Fourier transforms speedily.

It should also be mentioned here that the thin sample method of TDS measurement is the only one of those described that does not require lengthy computation to provide information about the sample under test. Unfortunately this method does not lend itself to the measurement of flotation froth properties.

TDS applied to Flotation Cells

All the methods described above use air filled coaxial lines in their measurement systems. As previously mentioned (Section 2.1.8) such a measurement system is not feasible for investigating flotation froth properties. The Goubau line offers a solution to the problem but presents a few problems of its own.

It is a far from perfect transmission line, owing to radiation effects causing a certain amount of the pulse energy to be lost. This is manifested in the pulse returns and must be accounted for theoretically before any analysis of the effects of the froth itself can be investigated. Another way of looking at it is that the impulse response of the transmission line must be separated from the impulse response of the froth.

Work by Ross and Bennett [32] in this area shows that material characterisation is feasible using a Goubau line, and future work will concentrate in this area.

A P P E N D I X E

RESULTS OF THE CONDUCTIVITY VERSUS DISPLACEMENT MEASUREMENTS (Section 2.2.1)

The resistance of the foam was measured using the conductivity cell measurement technique described in Appendix C.

Resistance R was then converted to specific conductivity using

$$\sigma = \left(\frac{155}{R}\right) \text{ mhos/m}$$

Distance from the top of the froth (cm)	Measured resistance (kΩ)	Specific conductivity (mhos/m)x10^3	
0	∞	0	
1,5	14,13	10,1	
3	8,19	18,9	
4,5	6,36	24,4	
6	5,32	29,1	R = 10kΩ
7,5	5,25	29,5	
9	5,18	29,9	
10,5	4,80	32,3	
12	4,62	33,5	
13,5	4,54	34,2	
15	4,32	35,9	
16,5	4,11	37,7	
18	3,71	41,8	
19,5	3,38	45,9	
21	3,27	47,4	
22,5	2,85	54,4	
24	2,44	63,4	R = 2,2kΩ
25,5	2,04	76,0	
27	1,80	85,9	
28,5	965	161	
30	0,721	215	
31,5	0,626	247	
33	0,603	257	

The series resistance R in the measurement apparatus was changed from 10kΩ to 2.2kΩ to improve the measurement accuracy at lower froth resistances.

A P P E N D I X F

RESULTS OF THE FREE SPACE ATTENUATION VERSUS FROTH CONDUCTIVITY MEASUREMENT

Froth resistance (kΩ)	Transmitted power (dBm)	Conductivity (mhos/m)x10^{-3}	Theoretical attentuation dB/0.1m	Actual attenuation dB/0.1m
∞	-12	0		
5,7	-55	27,2	4.44	43
6.3	-42	24.6	4.02	30
6.7	-40	23.1	3.78	28
7.0	-38	22.1	3.62	26
7.5	-35	20.7	3.38	23
8.0	-32	19.4	3.16	20
8.4	-30	18.5	3.01	18
8.8	-28	17.6	2.88	16
9.1	-26	17.0	2.78	14
9.4	-25	16.5	2.69	13
9.9	-23	15.7	2.56	11
10.4	-21	14.9	2.43	9
11.4	-19	13.6	2.22	7
12.4	-17	12.5	2.04	5
13.4	-16	11.6	1.89	4
14.4	-14	10.8	1.76	2
15.4	-10	10.1	1.64	-2
16.9	-9	9.17	1.50	-3
17.4	-8	8.91	1.46	-4
18.4	-7	8.42	1.38	-5
19.4	-7	7.99	1.31	-5
22.4	-6	6.92	1.13	-6
29.4	-6	5.27	0.86	-6
39.4	-8	3.93	0.64	-4

Theoretical Attenuation was calculated from the equation in Section 2.2.2, using a dielectric constant of 1. The calculated values were converted from Np/m to dB/m and divided by 10 to give the theoretical attenuation in dB/0.1m.

Resistance was converted to conductivity as described in Appendix C, using the relation

$$\sigma = \frac{155}{R} \text{ mhos/m}$$

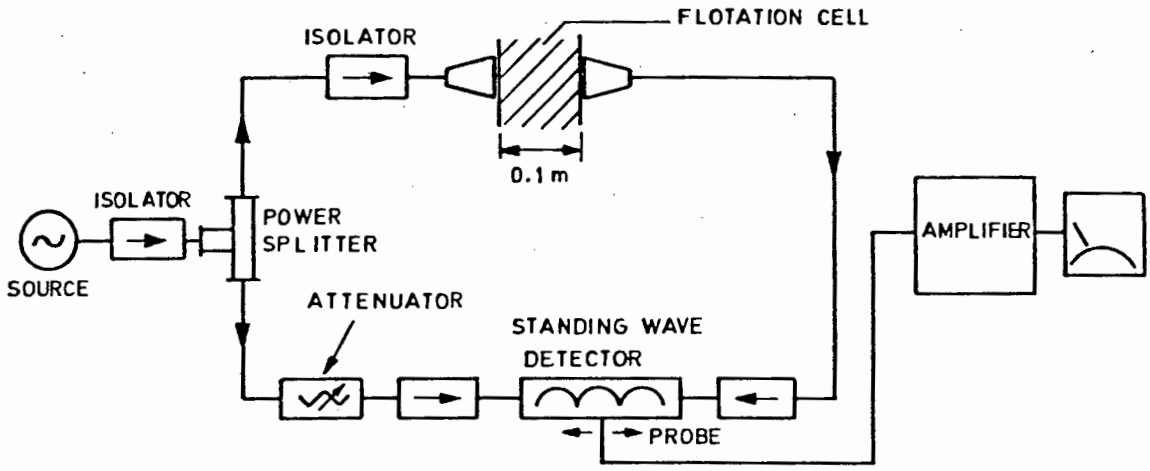

FIGURE G1 DIELECTRIC CONSTANT MEASUREMENT

A P P E N D I X G

DIELECTRIC CONSTANT MEASUREMENT - Theory and Results

A diagram of the measurement system used to measure the dielectric constant of the froth is shown in Figure G1.

The microwave energy from the 10 GHz source is split into two equal parts. One half is fed directly into one side of a slotted standing wave detector line while the other half is first fed through a free space link before being fed into the other side of the standing wave line.

Placing a dielectric material in the path between the two horns causes the standing pattern in the detector line to shift an amount determined by the thickness of the material and its dielectric constant.

By comparing the two observed standing wave patterns, one with the tank in position empty and one with it full of froth, it was possible to obtain an idea of the dielectric constant of the froth.

Theory

Propagation velocity of a signal is slower in a dielectric than in free space. A consequence of this is that its wavelength in free space is greater than in a dielectric,

$$\text{i.e.} \quad \lambda_a > \lambda_\varepsilon \qquad\qquad \lambda_\varepsilon = (\lambda_a/\sqrt{k})$$

where λ_a is the free-space wavelength

λ_ε is the wavelength in the dielectric

k is the dielectric constant

The amount that a single wavelength will change by on moving from free-space to a dielectric medium is given by:

$$d_\lambda = \lambda_a - \lambda_\varepsilon = \lambda_a - \frac{\lambda_a}{\sqrt{k}}$$

$$= \lambda_a \left(1 - \frac{1}{\sqrt{k}}\right) \quad \text{millimetres}$$

where λ_a is in millimetres.

Generalising for a dielectric layer of thickness "L" gives a total shift of

$$d_a = \left(\frac{L}{\lambda_a}\right)\lambda_a\left(1 - \frac{1}{\sqrt{k}}\right)$$

$$= L\left(1-\frac{1}{\sqrt{k}}\right) \quad \text{millimetres}$$

where L is in millimetres.

In the waveguide the change in wavelength is multiplied by a factor related to the guide wavelength λ_g:

$$d_g = d_a\left(\frac{\lambda_g}{\lambda_a}\right)$$

$$= \frac{\lambda_g L}{\lambda_a}\left(1-\frac{1}{\sqrt{k}}\right) \quad \text{millimetres}$$

where λ_g is in millimetres.

A practical consideration is that the minima of the standing wave pattern are used for measurement purposes as they are more clearly defined than the maxima. The distance between two minima will change only half as much as for a whole wavelength.

The observed distance change between two minima in the guide will be given by:

$$d = \tfrac{1}{2} d_g = \frac{\lambda_g L}{2\lambda_a}\left(1 - \frac{1}{\sqrt{k}}\right) \text{ millimetres}$$

Standard Manipulation gives this equation terms of the dielectric constant

$$k = \left(1 - \frac{2d\lambda_a}{\lambda_g L}\right)^{-2}$$

where d, λ_a, λ_g and L are in millimetres.

Results

As previously mentioned, the high attenuation in the froth made accurate measurement of the phase shift in the froth difficult. Another problem was that the continuous movement of the froth made the position of the minima in the standing wave pattern oscillate about a mean position.

Readings obtained for "d" varied over a range from 3 to 8 mm, corresponding to a range of dielectric constant from 1.1 to 1.3, respectively.

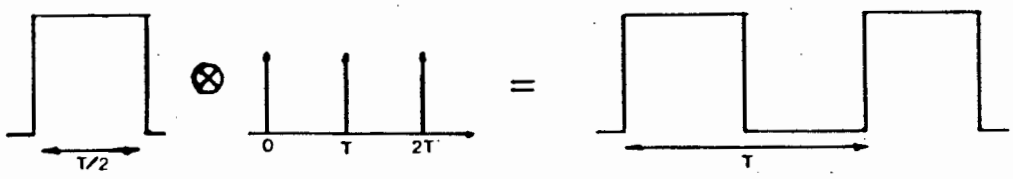

FIGURE H1 THE TIME DOMAIN REPRESENTATION OF A PERIODIC SIGNAL

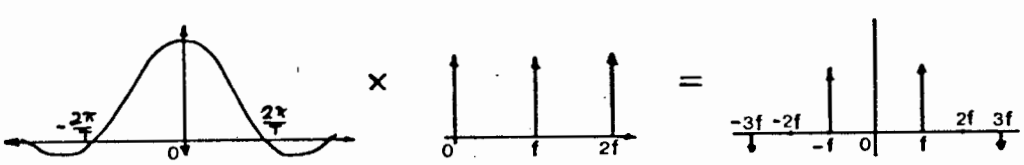

FIGURE H2 THE FREQUENCY DOMAIN REPRESENTATION OF A PERIODIC SIGNAL

APPENDIX H

FREQUENCY SPECTRUM OF A PERIODIC SIGNAL

In order to determine the spectral components of a periodic signal (e.g. a pulse train), it is necessary to compute the Fourier series of that signal. One form of the Fourier series is:

$$f(t) = A_o + \sum_{n=1}^{\infty} A_N \cos \frac{2\pi nt}{T_o} + \sum_{N=1}^{\infty} B_N \sin \frac{2\pi nt}{T_o}$$

where A_o is the average value of f(t) given by

$$A_o = \frac{1}{T_o} \int_{-T_o/2}^{+T_o/2} f(t)\, dt$$

while A_N and B_N are given by

$$A_N = \frac{2}{T_o} \int_{-T_o/2}^{+T_o/2} f(t) \cos \frac{2\pi nt}{T_o}\, dt$$

$$B_N = \frac{2}{T_o} \int_{-T_o/2}^{+T_o/2} f(t) \sin \frac{2\pi nt}{T_o}\, dt$$

It can be seen that the Fourier series consists of a summation of harmonics of a fundamental frequency $f_o = (1/T_o)$.

Using the process of convolution it is possible to show this more clearly. A repetitive (or periodic) signal can be represented by the convolution of a single cycle of its signal convolved with a Dirac function "comb" with spacing equal to the period of the signal (Figure H1).

Moving from the time domain to the frequency domain produces the spread of frequency components shown in figure H2.

The Fourier transform of the single cycle (a square pulse in the example shown) gives a continuous spectrum with a sinc function envelope. Multiplying this by the Dirac comb in the frequency domain gives the spectral components of the periodic signal.

Changing the form of the periodic function will merely change the shape of the spectral envelope obtained from a single cycle. Multiplying this by the Dirac comb in the frequency domain will once again give a discrete frequency spectrum related to the frequency of the periodic waveform.

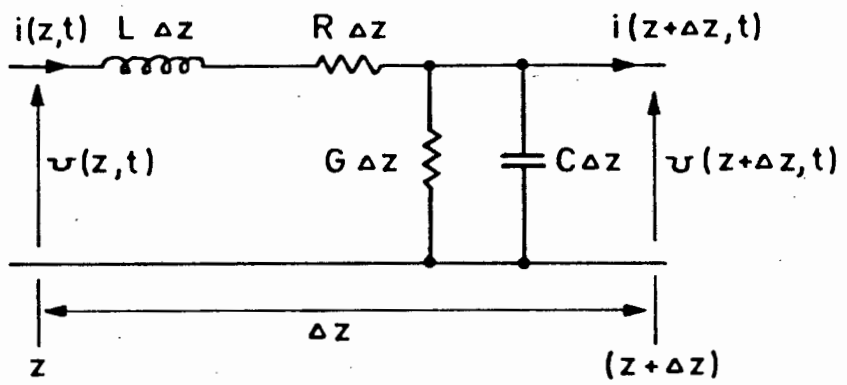

FIGURE 11 A SMALL SECTION OF LINE

APPENDIX I

SOLUTIONS TO THE DIFFERENTIAL EQUATIONS OF THE UNIFORM TRANSMISSION LINE

The differential equations for a uniform transmission line are found by looking at an infinitesimal section of line Δz, located at a point z on the line, remote from the line's termination (Fig.I1).

This line section has total series resistance $R\Delta z$, series inductance $L\Delta z$, shunt capacitance $C\Delta z$ and shunt conductance $G\Delta z$. The output voltage differs from the input voltage because of the series voltages across the resistance and inductance elements, while the output current differs from the input current because of the shunt currents through the conductance and capacitance elements.

Using the instantaneous quantities in Fig. I1 the following equations were derived using Kirchhoff's Laws.

$$v(z+\Delta z,t) - v(z,t) = \Delta v(z,t) = -R\Delta z\, i(z,t) - L\Delta z \frac{\partial i(z,t)}{\partial t} \qquad -(1)$$

$$i(z+\Delta z,t) - i(z,t) = \Delta i(z,t) = -G\Delta z\, v(z,t) - C\Delta z \frac{\partial v(z,t)}{\partial t} \qquad -(2)$$

Rewriting (1) and (2) in frequency domain form gives:

$$V(z+\Delta z) - V(z) = \Delta V(z) = -R\Delta z\, I(z) - j\omega L\Delta z\, I(z) \qquad -(3)$$

$$I(z+\Delta z) - I(z) = \Delta I(z) = -G\Delta z\, V(z) - j\omega C\Delta z\, V(z) \qquad -(4)$$

Each term of these equations is implicitly a harmonic function of time at angular frequency ω radius per second. Convenient choices for this reference may be the source voltage phasor, or the voltage phasor at the input end or the terminal load end of the line.

Dividing (3) and (4) by Δz and letting Δz tend to zero leads to the differential equations.

$$\frac{d}{dz} V(z) = -(R+j\omega L)I(z) \qquad -(5)$$

$$\frac{d}{dz} I(z) = -(G + j\omega C)V(z) \qquad -(6)$$

These are not written as partial differential equations, since V and I are explicitly functions of only the single variable z. It is not even necessary to be reminded that V and I are functions of z. Rewriting gives:

$$\frac{d}{dz} V = -(R + j\omega L)I \qquad -(7)$$

$$\frac{d}{dz} I = -(G + j\omega C)V \qquad -(8)$$

Solving these simultaneous linear first order ordinary differential equations with constant coefficients for seperate equations in V and I produces two second order equations.

$$\frac{d^2V}{dz^2} = (R + j\omega L)\ (G + j\omega C)V \qquad -(9)$$

$$\frac{d^2I}{dz^2} = (R + j\omega L)\ (G + j\omega C)I \qquad -(10)$$

In order to solve (9) and (10) it is necessary to first obtain their characteristic equations, which are identical.

$$F(D) = (D^2-\gamma^2) = (D-\gamma)(D+\gamma) \text{ where } \gamma^2 = (R+j\omega L)(G+j\omega C) \qquad -(11)$$

Using this characteristic equation a general solution for differential equations of the form of (9) and (10), is found.

$$y = C_1e^{-\gamma z} + C_2e^{\gamma z} \qquad -(12)$$

Substituting voltage and current boundary conditions leaves the solutions

$$V(z) = V_1e^{-\gamma z} + V_2e^{\gamma z} \qquad -(13)$$

$$I(z) = I_1e^{-\gamma z} + I_2e^{\gamma z} \qquad -(14)$$

where $\gamma^2 = (R+j\omega L)(G + j\omega C)$ $\qquad -(15)$

Equations (13) and (14) have been derived by straightforward mathematical processes, and in order to appreciate their physical implications it is best to seperate the magnitude and phase aspects of $e^{-\gamma z}$ and $e^{\gamma z}$, and reintroduce the harmonic time variation term $e^{j\omega t}$.

Defining the real and imaginary parts of γ by $\gamma = \alpha + j\beta$ allows (13) to be rewritten as

$$v(z,t) = |\hat{V}_1|e^{-\alpha z}\mathrm{Re}\{e^{j(\omega t-\beta z+\varepsilon_1)}\} + |\hat{V}_2|e^{\alpha z}\mathrm{Re}\{e^{j(\omega t+\beta z+\varepsilon_2)}\}$$

where $|\hat{V}_1|$ and $|\hat{V}_2|$ are the peak amplitudes of the arbitrary phase coefficients V_1 and V_2.

$e^{-\alpha z}$ and $e^{\alpha z}$ are real numbers to the attenuation of the line.

ε_1 and ε_2 are the respective phase angles of the arbitrary phasors V_1 and V_2.

$\mathrm{Re}\{e^{j(\omega t-\beta z+\varepsilon_1)}\}$ and $\mathrm{Re}\{e^{j(\omega t+\beta z+\varepsilon_2)}\}$ are numbers varying harmonically in time and with distance along the time with a peak value of unity and with values at t = z=0 determined by ε_1 and ε_2 .

Equation (12) can be rewritten in a similar manner as an equation in instantaneous currents.

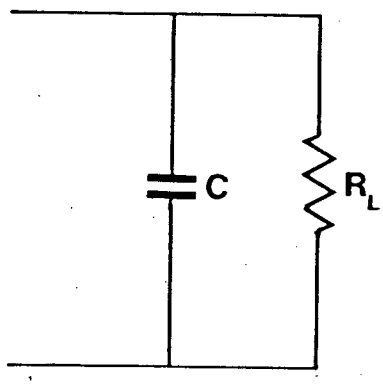

FIGURE J1

A TYPICAL TERMINATION

APPENDIX J

THE EFFECT OF REACTIVE TERMINATIONS ON THE REFLECTIONS ON A TRANSMISSION LINE

In practice, purely resistive terminations are hardly ever encountered. There are usually additional reactive components such as series inductance and shunt capacitance present.

In these cases it is necessary to use the complex form of the reflection coefficient to determine the reflection coefficient and solve using the Laplace transform method.

The reflected voltage

$$V_2(s) = V_1(s)\,\rho(s) \tag{1}$$

where $V_1(s)$ = the incident voltage

$V_2(s)$ = the reflected voltage

$\rho(s)$ = the complex reflection coefficient

$$= (Z_R(s) - Z_o)/(Z_R(s) + Z_o) \tag{2}$$

In order to demonstrate a practical application of this formula, an example using the termination shown in Figure J1, will be worked through.

The Laplace transform of the termination in Figure J1 is

$$Z_R(s) = R_L/(1 + sCR_L) \tag{3}$$

Combining equations (2) and (3) gives the reflection coefficient

$$\rho(s) = -(s-a_1)/(s+a_2) \tag{4}$$

where $a_1 = (R_L - Z_o)/CR_LZ_o$

$a_2 = (R_L + Z_o)/CR_LZ_o$

Assuming a step function input, V, from a matched source gives an initial voltage

$$V_1(s) = V/2s.$$

Substituting in equation (1) and manipulating with equation (4) gives the reflection

$$V_2(s) = \frac{V}{2}\left[\frac{a_1}{a_2} - \left(\frac{a_1+a_2}{a_2}\right)\exp(-a_2t_1)\right]$$

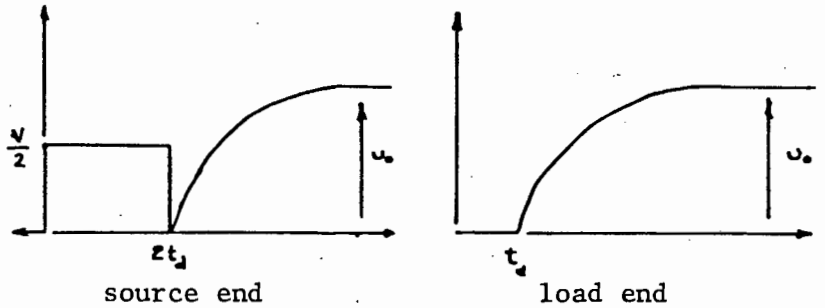

FIGURE J2 THE SIGNALS SEEN AT BOTH ENDS OF A LINE WITH A MISMATCHED TERMINATION CONTAINING SHUNT CAPACITANCE.

The total voltage at the output end is $(V_1(s) + V_2(s))$

or

$$v_o = \frac{V}{2}\left[\frac{a_1+a_2}{a_2}\right] \quad (1 - \exp(-a_2 t_1))$$

The signals seen at the source and load ends of the line are shown in Figure J2.

The effect of the capacitance is to introduce a risetime into the signal with a time constant

$$\tau = (CR_L Z_o)/(R_L+Z_o)$$

A similar treatment can be applied to series and shunt inductive circuits. The results for various reactive terminations appear in Figure (4.21).